รายงานการวิจัย

ระบบนิเวศวิทยาเชิงคณิตศาสตร์ Mathematical Ecology

ยงค์วิมล เลณบุรี ภาควิชาคณิตศาสตร์ คณะวิทยาศาสตร์ มหาวิทยาลัยมหิดล

รายงานการวิจัย

ระบบนิเวศวิทยาเชิงคณิตศาสตร์ Mathematical Ecology

วันที่	
เลขทะเบียน	****
เมพเรียกหนังสือ	PUG 39
a	CCC1

ยงค์วิมล เลณบุรี

ภาควิชาคณิตศาสตร์ คณะวิทยาศาสตร์

มหาวิทยาลัยมหิชิชิ (สถว.) สำนักงานกองทุ้นสนาสามุสทาราชิชิ (สถว.) ชั้น 14 อาคาร เอส เค็ม ทาวเวคร์ เลขที่ 979/17-21 ถบบพหลายชิบ แพวงสามเสนใน เพลงสหมาให กรุงเทพา 10400 โทร.298-0455 โกรสาร 298-0476 Home page: http://www.urfor.th E-mail: trf-infogutfor.th



กิตติกรรมประกาศ

โครงการวิจัยได้รับทุนอุคหนุนการวิจัยจากสำนักงานกองทุนสนับสนุนการวิจัย

ประเภท ทุนพัฒนานักวิจัย

ประจำปี 2538 - 2540 (รอบที่ 1)

ปีที่พิมพ์ 2540

บทคัดย่อ

แบบจำลองทางคณิตศาสตร์ของระบบนิเวศน์ของสิ่งมีชีวิตประเภทเดียว (single species) หรือสองประเภทในลักษณะของผู้ล่าและเหยื่อ (predator-prey) ได้ถูกนำมาดัดแปลง เพื่อคำนึงถึง ผลกระทบของแฟกเตอร์ดัวที่สาม เช่น ผลกระทบจากการแปรเปลี่ยนของสนามแม่เหล็กโลกต่อความ สามารถในการส่งผ่านสารอาหารของเนื้อเยื่อเซล หรือผลกระทบจากพยาชิต่อความสามารถในการลำ เหยื่อ หรือผลกระทบจากสารพิษต่อความสามารถในการสืบพันธุ์ และคำรงชีวิตอยู่ของสิ่งมีชีวิตใน สิ่งแวดล้อมปิด

แบบจำลองที่ได้เป็นสมการเชิงอนุพันธ์ไม่เชิงเส้น 3 สมการ โดยการวิจัยแบ่งเป็นสี่ขั้นตอน คือ ขั้นตอนแรก คำนึงถึงการเปลี่ยนแปลงในแฟกเตอร์ที่สามเมื่อเวลาเปลี่ยนแปลงไป จึงมีสมการ อนุพันธ์ของแฟกเตอร์ที่สามรวมอยู่ด้วย เป็นหนึ่งในสามสมการ ซึ่งประกอบขึ้นเป็นแบบจำลอง

ขั้นตอนที่สอง ไม่มีสมการของการเปลี่ยนแปลงในแฟกเตอร์ที่สาม แต่เบ่งกลุ่มของเหยื่อออก เป็นสองกลุ่ม คือ กลุ่มของ susceptible prey กับกลุ่มของ infective prey

ขั้นตอนที่สาม ไม่มีสมการของการเปลี่ยนแปลงในแฟกเตอร์ที่สาม แต่แบ่งกลุ่มของผู้ล่าออก เป็นสองกลุ่ม คือ กลุ่มของ susceptible predator กับกลุ่มของ infective predator

ขั้นตอนที่สี่ คำนึงถึงการเปลี่ยนแปลงของแฟกเตอร์ตัวที่สาม ซึ่งเป็นปริมาณของสารพิษ โดย แบ่งออกเป็นสองกลุ่ม คือ ปริมาณของสารพิษในสิ่งแวดล้อม กับปริมาณของสารพิษในประชากร

การวิเคราะห์กระทำโดยใช้ทฤษฎีทาง bifurcation และเทคนิคของ singular perturbation ซึ่ง ทำให้เราสามารถเข้าใจการทำงานของระบบที่กำลังศึกษาได้ดีขึ้น ทั้งเพิ่มความสามารถในการควบคุม ดูเล และจัดการระบบนั้น ๆ ให้ดำเนินไปตามที่เราต้องการ ผลของการวิจัยจึงจะสามารถมีประโยชน์ อย่างมากในเชิงสิ่งแวคล้อม

Abstract

Mathematical models of ecosystems involving single species or two species, namely a predator-prey system, are modified to incorporate the effect of an external force or a third factor. This can be the effect of the geomagnetic field variation on the cell membrane permeability in an activated sludge process, or the effect of parasite invasion of a predator-prey system, or the effect of toxicants on the population in a closed environment.

The resulting models consist of three nonlinear ordinary differential equations. The research project is organized into mainly 4 stages. In the first stage, variation in the third factor with time is taken under consideration in the form of one of the three differential equations which comprise the model.

In the second stage, the variation in the third factor is not taken into the model, while the prey population is divided into two groups; namely, the susceptible prey and the infective prey.

In the third stage, the variation in the third factor is still not taken into the model, while the predator population is divided into two groups; namely, the susceptible predator and the infective predator.

In the fourth and final stage, the third factor, which is the level of toxicants in this case, is divided into two groups; namely, the level of toxicant in the environment, and that in the population.

Analysis of the models are carried out using either the bifurcation theory or the singular perturbation technique. The study allows us to better understand the systems under study as well as learn how to manage and control them more efficiently. The results of our study should therefore yield valuable insights which has far reaching repercussions on the environmental problems we are facing today.

สารบัญเรื่อง

		หน้า
กิตติกรรมประกา ศ		fì
บทคัดย่อ (ภาษาไทย)		ข
บทคัดย่อ (ภาษาอังกฤษ)		PI
สารบัญเรื่อง		1
สารบัญภาพ		3
บทนำ		4
รายละเอียดและผลการวิจัย		12
การวิจัยช่วงที่ 1 ผลงานที่ได้ตีพิมพ์เรื่อง D	Dynamic Behavior of a Membrane Permeability Sensitive	13
	Model for a Continuous Bio-Reactor Exhibiting Culture Chythmicity	17
	Bifurcation and Chaos in a Membrane Permeability Sensitive Model for a Continuous Bioreactor	21
·	ามเรื่อง A Singular Perturbation Analysis of a Product	23
11	minorion model for Comminuous Dio-Keactors	23

		หน้า
ผลงานที่ submitted for p	publication (201 Modelling Effects of High Product and	
	Substrate Inhibition on Oscillatory Behavior in Continuous	
	Bioreactors	24
การวิจัยช่วงที่ 2		25
ผลงานที่ได้ตีพิมพ์เรื่อง	Singular Perturbation Analysis of a Model for a Predator-prey	
	System Invaded by a Parasite	27
ผลงานที่เสนอในการปร	ะชุมเรื่อง How Can Nonlinear Dynamics Elucidate Mechanisms	
	Relevant to Issues of Environmental Managemant and	
	Global Change	28
ผลงานที่เสนอในการปร	ะชุมเรื่อง Singular Perturbation Analysis of a Model for the	
	Effect of Toxicant in Single-Species Systems	38
ผลงานที่ได้ตีพิมพ์เรื่อง	Dynamical Modelling of the Effect of Toxicants on a	
	Single-Species Ecosystem	39
สรุปและข้อเสนอแนะ		40
สรุป Output ของโครงการ		41
บรรณานุกรม		43
ประวัตินักวิจัย		53

สารบัญภาพ

		หน้า
รูปที่ 1	คำตอบของ LV equations ซึ่งมีลักษณะกวัดแกว่ง (oscillation)และเป็นคาบ	. 9
รูปที่ 2	คำตอบของ LV equations ซึ่งมีลักษณะกวัดแกว่ง (oscillation)และเป็นคาบ	10
รูปที่ 3	คำตอบของแบบจำลองของ food web สามารถมีลักษณะของ limit cycle	
	ซึ่งมีความถี่ต่ำ และเกิด burst ของการกวัดแกว่งความถี่สูงขึ้นภายในทุก ๆ	
	รอบของความถี่ต่ำ (จาก Y. Lenbury and C. Likasiri, Mathl. Comput.	
	Modelling 20(1994) 71)	11
รูปที่ 4	คำตอบเชิงตัวเลขของระบบสมการ (5)-(7) บนระนาบ (x,y)	
	ซึ่งแสดงลู่ทาง(trajectory)ซึ่งมุ่งเข้าสู่การหมุนเวียนบนผิวของ 2-torus โดย	
	$M = 1$, $\gamma = 1$, $\beta = 1.5$, $\theta = 0.6$, $y_s = 1.5$, $d = 0.375$, $\delta = 2.1$,	
	$x_s = 7.875, \ \rho = 1.3125, \ Z_0 = 5.7, \ \omega = 1/12 \ \text{uat } \alpha = 1$	15
รูปที่ 5	แสดงคำตอบ x(t) ของระบบสมการ (5)-(7) โดย	
	$M = 1$, $\gamma = 1$, $\beta = 1.5$, $\theta = 0.6$, $y_s = 1.5$, $d = 0.375$, $\delta = 2.1$,	
	$x_s = 7.875, \ \rho = 1.3125, \ Z_0 = 5.7, \ \omega = 1/12 \ \text{uns} \ \alpha = 1$	16
รูปที่ 6	Bifurcation diagram	20
รูปที่ 7	รูปร่างของ equilibrium manifolds ของระบบสมการ (42)-(44) ใน 5 กรณี	
	ที่กล่าวไว้ในเนื้อหา	32
รูปที่ 8	คำตอบเชิงตัวเลขของระบบสมการ (42)-(44) เมื่อเลือกค่าพารามิเตอร์	
	ให้สอคคล้องกับเงื่อนไขของกรณีที่ 1	33
รูปที่ 9	คำตอบเชิงตัวเลขของระบบสมการ (42)-(44) เมื่อเลือกค่าพารามิเตอร์	
	ให้สอคคล้องกับเงื่อนไขของกรณีที่ 2	34
รูปที่ 10	คำตอบเชิงตัวเลขของระบบสมการ (42)-(44) เมื่อเลือกค่าพารามิเตอร์	
	ให้สอดคล้องกับเงื่อนไขของกรณีที่ 3	35

บทน้ำ

ความสำคัญและที่มาของปัญหาที่ทำการวิจัย

ประเทศไทยเป็นหนึ่งในหลาย ๆ ประเทศที่กำลังพยายามพัฒนาทางเศรษฐกิจและเทคโนโลยี ให้ก้าวรุคหน้าไปอย่างรวดเร็ว และต้องประสบกับปัญหาของสิ่งแวดล้อมที่กำลังจะเสื่อมลงอย่างน่า เป็นห่วง รวมทั้งปัญหาการจัดการกับปฏิกูลของเสีย (waste management) ซึ่งเป็นผลพวงของความ เจริญก้าวหน้าทางเศรษฐกิจและอุตสาหกรรม ดังที่ประเทศที่เจริญแล้วหลาย ๆ ประเทศได้ประสบมา แล้ว และต่างก็ยอมรับว่าเป็นปัญหาสำคัญที่ต้องให้ความสนใจอย่างจริงจัง ก่อนที่จะสายเกินไป

นักวิชาการย่อมประจักษ์ดีว่า เราต้องทำการวิจัยค้นคว้าในเรื่องระบบต่าง ๆ เชิงนิเวศวิทยาไป พร้อม ๆ กับการพัฒนาทางเทคโนโลยี เพื่อที่ประเทศชาติจะไม่ต้องเผชิญหน้ากับปัญหาด้านสิ่ง แวคล้อมที่ร้ายแรงในภายหน้า โดยที่ไม่มีการตระเตรียมไว้ล่วงหน้าเพื่อรับสถานการณ์คังกล่าวอย่างมี ประสิทธิภาพ เนื่องจากมิได้สนับสนุนให้มีการวิเคราะห์วิจัย เพื่อให้เกิดความเข้าใจที่คีพอเกี่ยวกับ ระบบนิเวศวิทยาต่าง ๆ ที่จะได้รับผลกระทบจากการพัฒนาด้านเทคโนโลยีและอุตสาหกรรม ทั้งมิได้ มีการค้นคว้าหาวิธีการขจัดปัญหาต่าง ๆ ที่จะเกิดขึ้นนั้นอย่างมีประสิทธิภาพ

การวิจัยด้านแบบจำลองทางคณิตศาสตร์ของระบบต่าง ๆ ในเชิงนิเวศวิทยา เป็นวิธีหนึ่งที่จะ ทำให้เราสามารถเกิดความเข้าใจที่ดีขึ้น เกี่ยวกับระบบที่เรากำลังศึกษา ทั้งยังทำให้เราได้ภาพรวมของ เหตุการณ์ และความเป็นไปได้ทั้งหมดที่อาจจะเกิดขึ้นในระบบที่กำลังศึกษาอยู่

ขบวนการที่เป็นหัวใจสำคัญขบวนการหนึ่ง ของการศึกษาด้านนิเวศวิทยา คือ ระบบซึ่งสิ่งมี ชีวิตสองชนิคล่าจับเหยื่อหรือสารอาหาร (prey) ชนิคเคียวกันเป็นอาหาร (competition) ระบบคัง กล่าวจะพบใค้ในธรรมชาติสิ่งแวคล้อมรอบตัวเราโดยทั่วไป ไม่ว่าจะเป็นเสือกับสิ่งโตที่ต่างก็ล่ากวาง เป็นเหยื่อ หรือเหยี่ยวกับนก magpie ที่ต่างก็กินหนอนและแมลงเป็นอาหาร ตัวอย่างคั้งเคิมของ competition ระหว่าง 2 species คือ feeding process ของ barnacles สองชนิค คือ Chthamalus และ Balanus (J. Connell, Ecology 42 (1961) 710) ซึ่งพบว่ามีพฤติกรรมที่น่าสนใจหลาย ๆ แบบ

แบบจำลองของ competing species นี้ มีรากฐานมาจาก model ของ feeding process ระหว่าง 2 species ซึ่งเป็นระบบผู้ล่ากับเหยื่อ (predator-prey) โดยมีกลไกของการจับกินเหยื่อที่ขึ้นอยู่กับความ หนาแน่น (density dependent) ซึ่งได้มีผู้อธิบายโดยใช้สมการซึ่งเรียกกันว่า Lotka-Volterra (LV) equations (A.J. Lotka, Essays on Growth and Form, Oxford U. Press, New York (1945)). สมการ คังกล่าวสามารถอธิบายและกำหนดเงื่อนไขที่ species หนึ่งจะสูญพันธุ์ หรือเงื่อนไขที่ทั้งสอง species

สามารถอยู่ร่วมกันได้ (persistence) นอกจากนั้น ยังสามารถหาเงื่อนไขที่สมการดังกล่าวจะมีคำ ตอบที่เป็นคาบ (limit cycle behavior)

ผลงานเกี่ยวกับระบบที่ 2 species แย่งกินเหยื่อชนิดเดียวกันเป็นอาหาร ที่สำคัญและเป็นที่อ้าง ถึงโดยทั่วไป คือผลงานของ Volterra (V. Volterra, R. Commun. Talassogratico Italiano. (1927)1-142) หากแต่ Volterra model นั้นมีขีดจำกัดหลายประการ เช่น amplitude of oscillation ของคำตอบ จะไม่แน่นอน ทั้งยังมีความไม่เสถียร (structurally unstable) อีกด้วย

ภายใต้เงื่อนไขบางประการ Hopf bifurcation จะสามารถเกิดขึ้นใน LV equations ได้ ก่อให้ เกิดเป็น limit cycles ดังที่เห็นได้ในรูปที่ 1 และรูปที่ 2 ซึ่งระบบ predator - prey นี้มักจะใช้กล่าวถึง สัตว์บก เช่น แมวป่ากับกระต่ายในประเทศแคนาดา (C. Elton and M. Nicholson, J. Anim. Ecol. 11 (1942) 215) แต่ก็สามารถใช้อธิบายปรากฏการณ์ระหว่างสัตว์น้ำกับ algae (M.L. Rosenzweig, Science 175 (1972) 564) หรือนกกับแมลง หรืออื่น ๆ อีกได้มากมาย รวมทั้งสามารถใช้อธิบายระบบ เชิงชีววิทยา ที่ใช้ในการขจัดของเสีย (สารอาหาร-แบกทีเรีย-โปรโตซัว) ซึ่งเป็นวิธีขจัดของเสียในน้ำ ทิ้ง จากโรงงานต่าง ๆ ที่มีผู้หันมานิยมใช้มากขึ้นกว่าการขจัดโดยขบวนการทางเคมี เนื่องจากการใช้ ขบวนการทางเคมีเพื่อขจัดของเสียจะทำให้เกิดปฏิกูลจากสารเคมีที่ใช้ในขบวนการนั้นเพิ่มขึ้นในสิ่ง แวดล้อม อันเป็นสิ่งที่เราไม่พึงประสงค์เป็นอย่างยิ่ง

ได้มีผู้ทำการวิจัยถึงแฟกเตอร์ตัวอื่น ๆ ที่มีผลกระทบกับระบบ predator-prey มาเป็นเวลา นานพอสมกวร เช่นผลกระทบจากยาฆ่าแมลง (insecticides) ปุ้ย (fertilizer) ซึ่งเปลี่ยนแปลงกวามทรง ตัวที่ดี (balance) ระหว่าง predator (ผู้ล่า) และ prey (เหยื่อ) ไม่นานมานี้ Freedman (H.I. Freedman, Math. Biosc. 99 (1990) 143) ได้ทำการศึกษาระบบ predator-prey โดยปรับเปลี่ยนเพื่อกิดถึงผลของ พยาธิ (parasites) ซึ่ง infect ทั้ง predator และ prey ในเวลาเดียวกัน ซึ่ง Freedman ได้ทาเงื่อนไข ซึ่ง ทำให้ประชากรทั้งหมดอยู่ร่วมกันต่อไปได้ (persistence) และเงื่อนไขที่ประชากรบาง species จะ สูญพันธุ์ (extinct) หลังจากนั้น Nhung และ Anh (T.V. Nhung and T.T. Anh, preprint IC/93/391 ICTP) นำผลของ Freedman ไปปรับเปลี่ยนโดยคิดว่าแต่ละเผ่าพันธุ์ (population) สามารถแบ่งได้เป็น 2 กลุ่ม คือ susceptible group และ infective group นั่นคือ กลุ่มที่ยังไม่โดน infect โดย parasites จะ มีความสามารถในการล่าเหยื่อ (หรือเจริญเติบโต) แตกต่างไปจากกลุ่มที่โดน infect แล้ว ดังปรากฏ ใน model system ต่อไปนี้

$$\begin{split} \dot{S}(t) &= B(X) - \frac{D(X)S(t)}{X(t)} - \left[\beta_0 + \beta_1 Y_2(t)\right] S(t) - \frac{Q_1(X)SY_1(t)}{X(t)} - \frac{P_1(X)SY_2(t)}{X(t)} \\ \dot{I} &= \left[\beta_0 + \beta_1 Y_2(t)\right] S - \frac{D(X)I(t)}{X(t)} - \frac{Q_2(X)I(t)Y_2(t)}{X(t)} - \frac{P_2(X)I(t)Y_2(t)}{X(t)} \\ \dot{Y}_1 &= -\Gamma(Y)Y_1 - \gamma_0 IY_1 - \gamma_1 Y_1 Y_2 + C \frac{Q_1 SY_1}{X} + C_1 \frac{P_1 SY_2 + Q_2 IY_1 + P_2 IY_2}{X} \\ \dot{Y}_2 &= -\Gamma(Y)Y_2 + \gamma_0 IY_1 + \gamma_1 Y_1 Y_2 + (C - C_1) \frac{P_1 SY_2 + Q_2 IY_1 + P_2 IY_2}{X} \end{split}$$

โดยที่ $S(t), I(t), X(t) = S(t) + I(t), Y_1(t), Y_2(t), Y(t) = Y_1(t) + Y_2(t)$ คือ susceptible prey, infective prey, prey ทั้งหมด, susceptible predator, infective predator, และ predator ทั้งหมด ตาม ลำดับ

Nhung และ Anh. ก็ได้กำหนดเงื่อนไขที่ทำให้เกิด persistence และ extinction ของแต่ละ กลุ่ม เช่นเดียวกัน ทั้งนี้เขากล่าวว่า model นั้นควรเหมาะสมที่จะใช้กับระบบ predator-prey ที่พบได้ ในประเทศเวียดนาม เช่น เหยี่ยว กับ magpie ซึ่งต่างก็มีพยาธิ flukes หรือ เสือกับหมูป่า ซึ่งต่างก็มี พยาธิ Tapeworms เป็นต้น ทั้งนี้ model system ของ Nhung และ Ahn ประกอบด้วยสมการของอัตรา การเปลี่ยนแปลงของ prey และ predator เท่านั้น โดยไม่ได้คิดถึงการเปลี่ยนแปลงใน factor ตัวที่สาม แต่ประการใด

ในผลงานที่กล่าวมาข้างต้นนี้ ยังไม่ได้มีการศึกษาหาความเป็นไปได้ที่จะเกิด limit cycle behavior จาก bifurcation analysis แต่อย่างใด ซึ่งการที่มีแฟกเตอร์ที่สามมาเป็นอีกแรงหนึ่งที่เปลี่ยน แปลง dynamics ของระบบ predator-prey นี้ ควรจะก่อให้เกิด limit cycle behavior ในลักษณะต่าง ๆ ที่น่าสนใจยิ่งกว่าที่พบในรูปที่ 1 และรูปที่ 2

ในผลงานขึ้นหนึ่งของผู้วิจัย ซึ่งได้รับตีพิมพ์ในวารสารนานาชาติแล้ว (Y. Lenbury and C. Likasiri, Mathematical and Computer Modelling, 20(1994)71) ผู้วิจัยได้ศึกษาระบบห่วงโซ่อาหาร ซึ่งมี species ที่สามเป็น superpredator จับกินทั้ง prey และ predator เป็นอาหาร ซึ่งมี model เป็น ระบบสมการต่อไปนี้

$$\begin{split} \dot{p} &= -\mathrm{D}p + \nu(b)p + \eta(s)p \\ \dot{b} &= -\mathrm{D}b + \mu(s)b - \frac{1}{X}\nu(b)p \\ \dot{s} &= D(s_0 - s) - \frac{1}{Y}\mu(s)b - \frac{1}{Z}\eta(s)p \end{split}$$

โดยที่ p(t), b(t), s(t) คือ superpredator, predator, และ prey ตามลำดับ

ผู้วิจัยใต้ใช้ singular preturbation method และ separation conditions หาเงื่อนไขที่คำตอบ ของแบบจำลองจะมีลักษณะเป็นคาบ โดยมีความถี่ต่ำ และหาเงื่อนไขที่คำตอบ จะมีลักษณะเป็น limit cycle ที่มีความถี่ต่ำ แต่แทรกด้วย oscillations ที่มีความถี่สูง เป็นช่วง ๆ (bursts of high frequency oscillations) คังที่เห็นได้ในรูปที่ 3 คำตอบที่มีลักษณะที่สับสนเช่นนี้ สามารถอธิบายปรากฏการณ์ ของ eco-systems ต่างๆ ที่เราต้องการศึกษาได้เป็นอย่างคี โดยมันบอกให้เราเข้าใจยิ่งขึ้นถึงการที่ใน วงจรหนึ่งจะแบ่งได้เป็น 2 ฤดู คือ rich season กับ poor season

ในระหว่าง rich season นั้น prey (เหยื่อ) มีอยู่เป็นจำนวนมาก ผู้ถ่าทั้ง predator และ superpredator สามารถล่าเหยื่อเป็นอาหารได้อย่างสะควกสบาย ทำให้มีการเพิ่มจำนวน หรือลด จำนวนลงอย่างคล่องตัว (high - frequency) เกิดเป็น oscillations ที่มีความถี่สูง จนกระทั่ง prey ลด จำนวนลงไปอย่างมาก เกิดเป็น poor season prey มีจำนวนน้อยมากและสามารถเพิ่มจำนวนขึ้นได้ อย่างเชื่องช้า (low-frequency) predator และ superpredator ก็จะลดจำนวนลงด้วย เนื่องจากขาด แคลนเหยื่อที่เป็นอาหาร เมื่อเวลาผ่านไปเหยื่อได้มีเวลา regenerate ก็จะกลับเข้าสู่ rich season และ fast dynamics อีกครั้งหนึ่ง

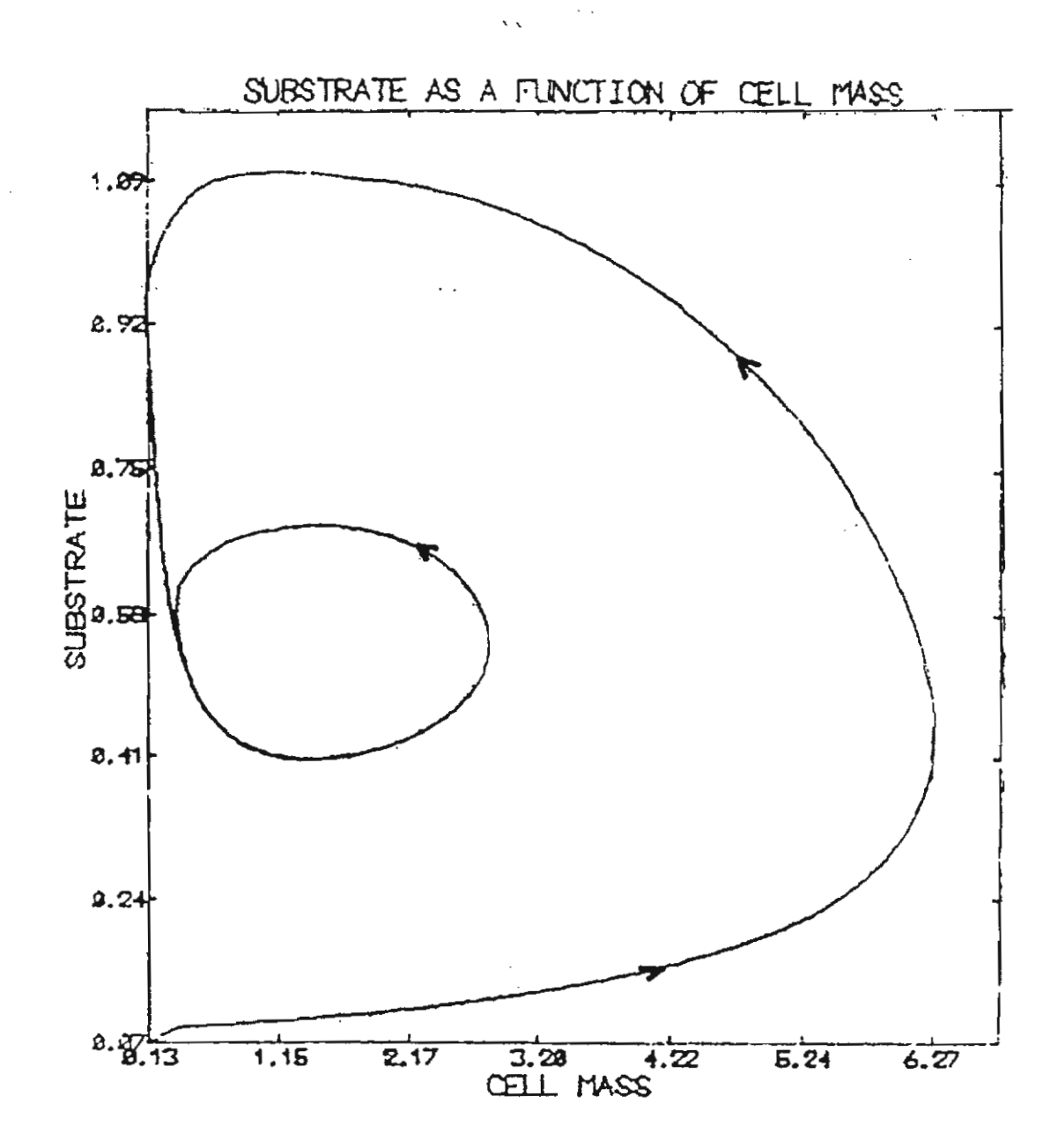
ความเข้าใจที่ได้จากการวิเคราะห์แบบจำลองทางคณิตศาสตร์เช่นนี้ มีประโยชน์ในหลาย ๆ ด้าน ถ้าเราจะสามารถคาดได้ว่า poor season นั้น จะมีขึ้นในช่วงใด เราจะสามารถทิ้งระยะการล่าเหยื่อ ในช่วงดังกล่าว เพื่ออำนวยให้ species ที่ใกล้จะสูญพันธุ์ได้มีเวลา regenerate นอกจากนั้นเรา อาจสามารถใช้กลไกของ species ที่สาม ซึ่งใช้ทั้ง prey และ predator เป็นอาหาร กับเรื่องของการ ปลูกข้าว (prey) ซึ่ง ถูกบ่อนทำลายด้วยตัวแมลง (predator) ชนิดใดชนิดหนึ่ง เราอาจจะสามารถนำ superpredator ซึ่งกินทั้งแมลงและข้าวเป็นอาหารมาช่วยขจัดแมลง โดยกำหนดเงื่อนไขให้แมลงถูก ขจัดหมดไปก่อนที่ข้าวจะถูก superpredator ใช้เป็นอาหาร จนหมดไป เช่นนี้เป็นต้น ทั้งนี้แบบจำลอง ของคลื่นอาหารที่เคยทำการศึกษาที่ผ่านมาข้างต้น ยังไม่ได้กิดถึงลักษณะที่ poputation มีการแบ่งแยก เป็น susceptible และ infective group แต่ก็จะเห็นได้ว่า การวิเคราะห์วิจัยแบบจำลองทางคณิตศาสตร์ ของระบบต่าง ๆ เช่นนี้ จะเพิ่มขีดความสามารถในการจัดการ (manage) สิ่งแวดล้อมอย่างมี ประสิทธิภาพมากขึ้น

บทพื้นฐานของ model ของ Nhung และ Anh ผู้วิจัยจึงทำการวิเคราะห์ แบบจำลองของ ระบบ predator-prey ซึ่งมีลักษณะการแบ่งแยกเป็น susceptible และ infective group โดยใช้ Singular Perturbation Method เพื่อศึกษาลักษณะคำตอบต่าง ๆ ของ model system โดยใช้ response functions ลักษณะต่าง ๆ เช่น เป็น function เชิงเส้น (linear) หรือเป็นฟังก์ชัน แบบ Holling เป็นต้น เพื่อจะสามารถนำ model คั้งกล่าวไปคัดแปลงให้รวมถึงผลกระทบของการเปลี่ยนแปลงจำนวนของ factor หรือ force ตัวที่สามต่อไป

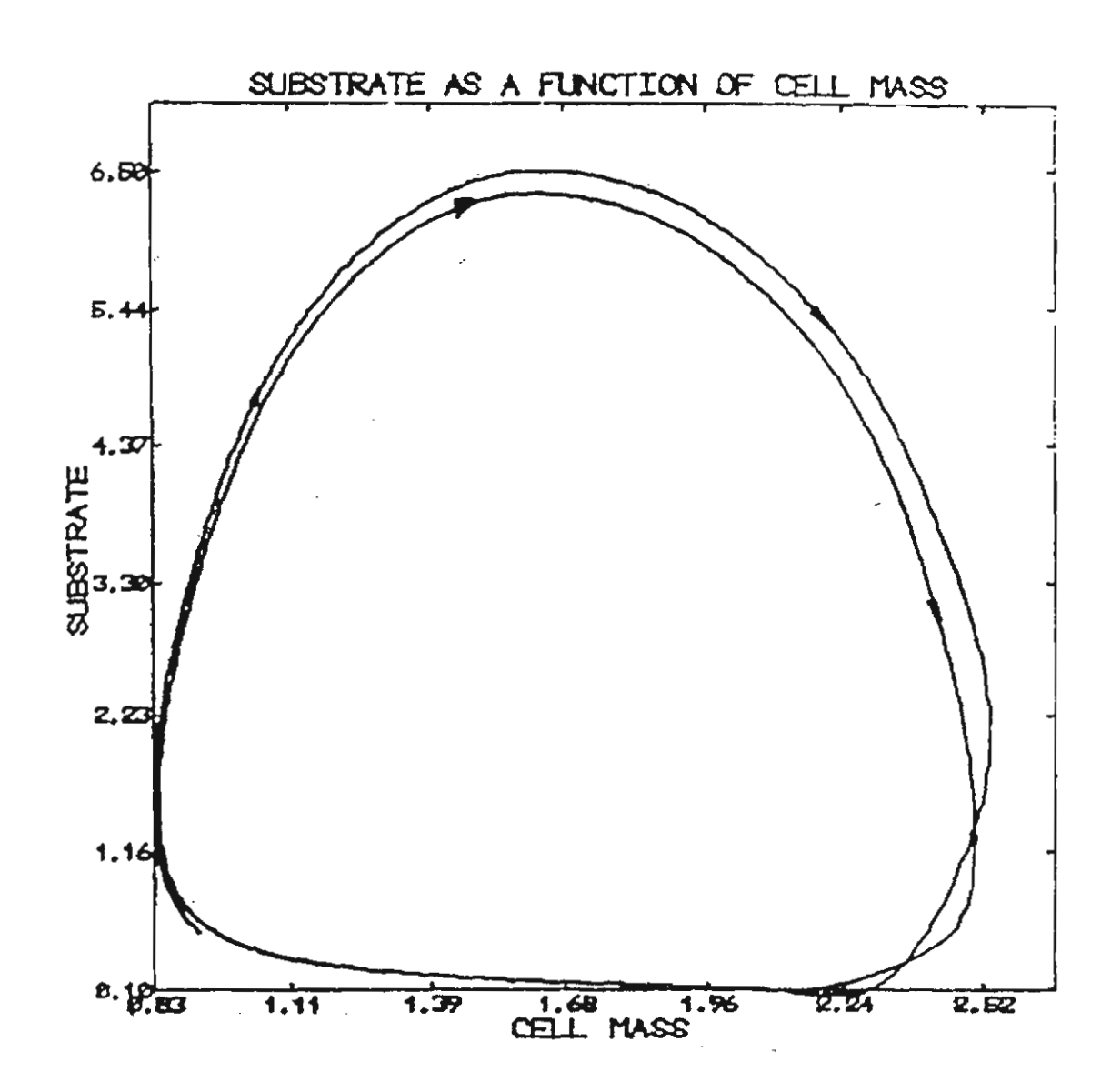
นอกจากนั้นยังได้คัดแปลง ปรับปรุง model predator-prey เพื่อรวมผลกระทบของการ เปลี่ยนแปลงใน "third force" ซึ่งอาจจะเป็น parasites หรือ พันธุ์สัตว์ชนิดที่ 3 (superpredator) หรือ third force อื่น ๆ ที่จะมีผลทำให้ขีดความสามารถในการล่าเหยื่อและการขยายพันธุ์ ของ 2 species แรกนั้นเปลี่ยนแปลงไป โดยที่ susceptible และ infective groups จะมี dynamics ที่ต่างกัน ทั้งนี้ จะ พิจารณาการ incorporate ผลจาก force ที่ 3 นี้ ในลักษณะต่าง ๆ กัน เพื่อพิจารณาสร้าง model ให้ เหมาะสมกับระบบ eco-systems ที่เราสนใจ

หลังจากนั้นจึงคำเนินการวิเคราะห์แบบจำลองที่พัฒนาขึ้น ด้วยทฤษฎีทางคณิตศาสตร์
(Theory of Differential Equations, Singular Perturbation Method, Bifurcation Theory) เพื่อหา เงื่อนไขของความอยู่รอดของทุก species และเงื่อนไขที่คำตอบในลักษณะต่าง ๆ จะเกิดขึ้นได้

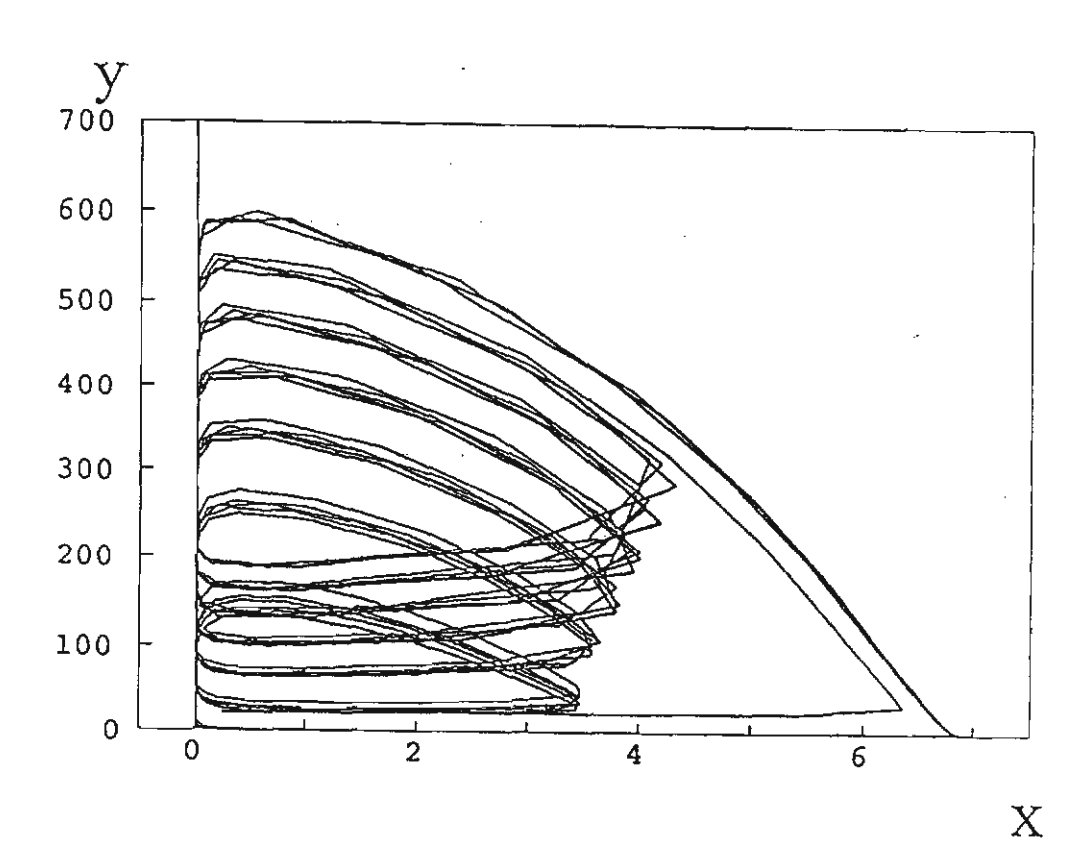
ในขั้นสุดท้ายจึงหาคำตอบเชิงตัวเลข (numerical simulation) ของแบบจำลอง เพื่อทคสอบ ผลการวิจัยทางทฤษฎีว่าถูกต้องหรือไม่ แล้วนำผลการวิเคราะห์ทางทฤษฎีไปแปลผลเพื่ออธิบาย eco-systems ที่ทำการศึกษา



รูปที่ 1 คำตอบของ LV equations ซึ่งมีลักษณะกวัดแกว่ง (oscillation)และเป็นคาบ



รูปที่ 2 คำตอบของ LV equations ซึ่งมีลักษณะกวัดแกว่ง (oscillation)และเป็นคาบ



รูปที่ 3 คำตอบของแบบจำลองของ food web สามารถมีลักษณะของ limit cycle ซึ่งมีความถี่ต่ำ และเกิด burst ของการกวัดแกว่งความถี่สูงขึ้นภายในทุก ๆ รอบของความถี่ต่ำ (จาก Y. Lenbury and C. Likasiri, Mathl. Comput.

Modelling 20(1994) 71)

รายละเอียดและผลการวิจัย

โครงการวิจัยนี้แบ่งออกเป็น 4 ช่วงย่อย ช่วงละประมาณ 9 เคือน โดยงานวิจัยในแต่ละช่วง เริ่มจากรากฐานของแบบจำลองทางคณิตศาสตร์ของระบบการแพร่พันธุ์ของสิ่งมีชีวิตหรือประชากร (population growth) อย่างง่าย ๆ ดังนี้

$$\frac{\mathrm{dx}}{\mathrm{dt}} = \mu \,\mathbf{x} - \mathbf{D}\,\mathbf{x} \tag{1}$$

โดยที่ x(t) คือ จำนวนประชากร ณ เวลา t ใด ๆ

μ คือ อัตราการเจริญเติบโตสัมพัทธ์ของประชากร x

D คือ อัตราการตายของประชากร x

ถ้าเราคิดถึงระบบของผู้ล่ากับเหยื่อ (predator-prey systems) และให้ S(t) เป็นปริมาณของ เหยื่อ หรือสารอาหรที่ x จับกินเป็นอาหาร ก็อาจจะเขียนแบบจำลองของระบบคังกล่าวได้คังนี้

$$\frac{dS}{dt} = D(S_F - S) - \frac{\mu(S)x}{v}$$
 (2)

$$\frac{\mathrm{d}x}{\mathrm{d}t} = \mu(S)x - Dx \tag{3}$$

โดย S_F คือความเข้มข้นหรือความหนาแน่นของ S ที่นำมาเพิ่มให้กับระบบที่กำลังศึกษาด้วย อัตราที่คงที่ ซึ่งอาจคิดได้ว่าเป็นอัตราการเคลื่อนย้าย (migration) ของ S เข้าสู่สังคมนิเวศน์ที่กำลังทำ การศึกษา

Monod เป็นผู้มีชื่อเสียงในการเสนอให้ specific growth rate μ(S) เป็นฟังก์ชันต่อไปนี้

$$\mu(S) = \frac{\mu_{\rm m} S}{K + S} \tag{4}$$

โดยที่ µm คือ maximum specific growth rate

K คือ Monod constant

Y คือ yield coefficient ซึ่งเท่ากับอัตราการลดลงของ S ต่ออัตราการเพิ่มขึ้นของ x

ผู้วิจัยได้นำสมการ (1) หรือสมการ (2) และ (3) มาปรับปรุงเพิ่มเติมในลักษณะต่าง ๆ เพื่อ กิดถึงผลกระทบของแฟกเตอร์ภายนอก หรือแฟกเตอร์ตัวที่สาม โดยได้แบ่งการวิจัยเป็น 4 ช่วง ดังกล่าวแล้วข้างต้น ดังต่อไปนี้ การวิจัยช่วงที่ 1

1.1 ในช่วงนี้ผู้วิจัยได้นำแบบจำลองต้นแบบ (2) และ (3) มาปรับเปลี่ยนเพื่อคำนึงถึง ผลกระทบของ external force เช่น การแปรเปลี่ยนของ geomagnetic field ซึ่งมีผลทำให้ permeability P ความสามารถในการส่งผ่านสารอาหารผ่านผิวของเซล เปลี่ยนแปลงไปตามเวลา t และจะมีผลค่อ การใช้สารอาหาร S เพื่อการเจริญเติบโตของเซล x ทำให้ได้เป็นสมการอนุพันธ์ไม่เชิงเส้น 3 สมการ ดังนี้

$$\frac{dS}{dt} = -\frac{(c_1 x P + c_2)S}{(S + K_m)y} - D(S_F - S)$$
 (5)

$$\frac{\mathrm{dx}}{\mathrm{dt}} = \frac{(c_1 x P + c_2)S}{S + K_m} - Dx \tag{6}$$

$$\frac{dP}{dt} = -\gamma \cos(w_0 t) P - \frac{(\gamma_2 - P)(c_1 x P + c_2) S}{S + K_m}$$
 (7)

โดยที่ เทอมแรกในสมการ (7) เป็นอัตราการเปลี่ยนแปลงของ P ในลักษณะเป็นคาบ ซึ่ง derive ได้ จากการสังเกตความสัมพันธ์ระหว่าง P กับการเปลี่ยนแปลงใน geomagnetic field (Yerushalmi et al.,

โดยใช้ bifurcation analysis ผู้วิจัยสามารถพิสูจน์ทฤษฎีบทต่อไปนี้ได้ ทฤษฎีบทที่ เ ถ้า

$$\gamma > 0$$
 (8)

$$\beta \ge 1$$
 (9)

$$\frac{1}{\beta} > \theta > \frac{1 - \sqrt{\frac{\gamma}{\gamma + 1}}}{\beta} \tag{10}$$

$$\gamma > M > \frac{1 - \theta}{\theta} \tag{11}$$

โดยที่

$$\gamma = \frac{(z_S + d) M}{z_S^2 - M d}$$

$$\beta = \frac{\gamma_2 c_1}{D}$$

$$\theta = \frac{z_{S}}{M + z_{S}}$$

$$M = k_m$$

และ z_S คือค่าของ S ที่ steady state แล้วระบบสมการ (5)-(7) จะมีคำตอบเป็นคาบ ซึ่ง bifurcate จาก non-washout steady state สำหรับค่าของ δ ในช่วง (δ_c , δ_c + ϵ) โดยที่

$$\delta = \frac{(\beta x_S + \rho) M}{(M + z_S)^2} \tag{12}$$

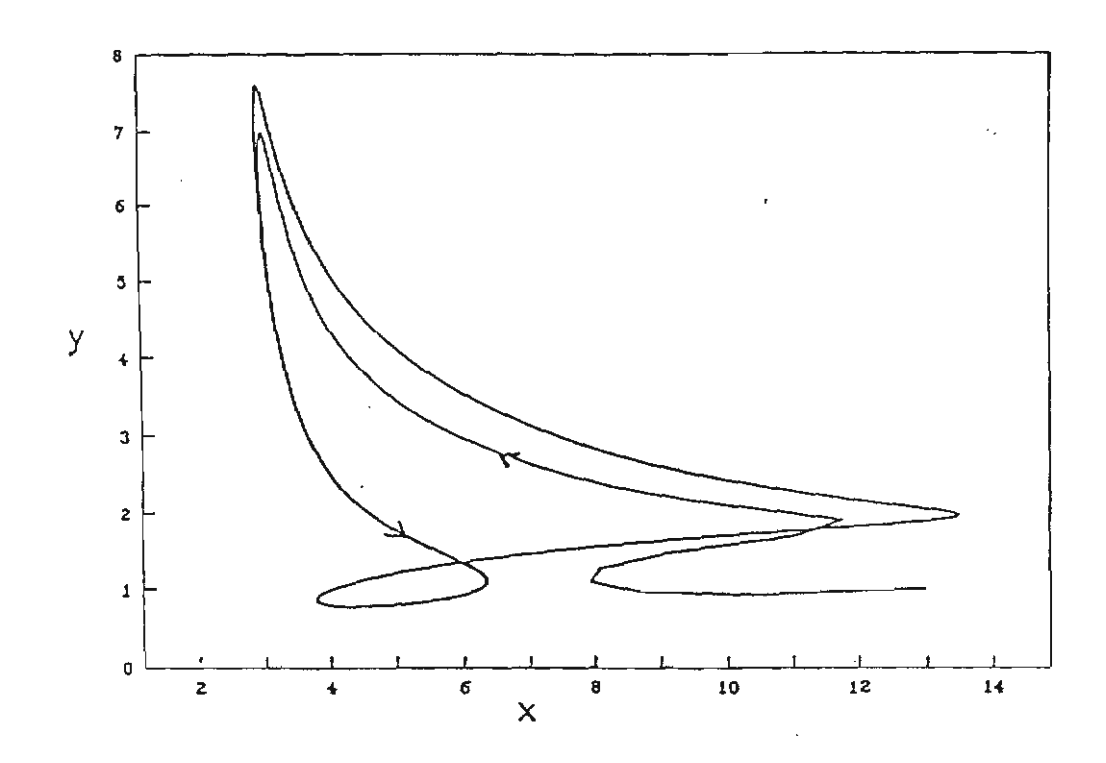
$$\delta_{c} = (2 - \beta \theta)(z_{S} + d)\gamma \tag{13}$$

$$\rho = \frac{c_2}{a D_2} \tag{14}$$

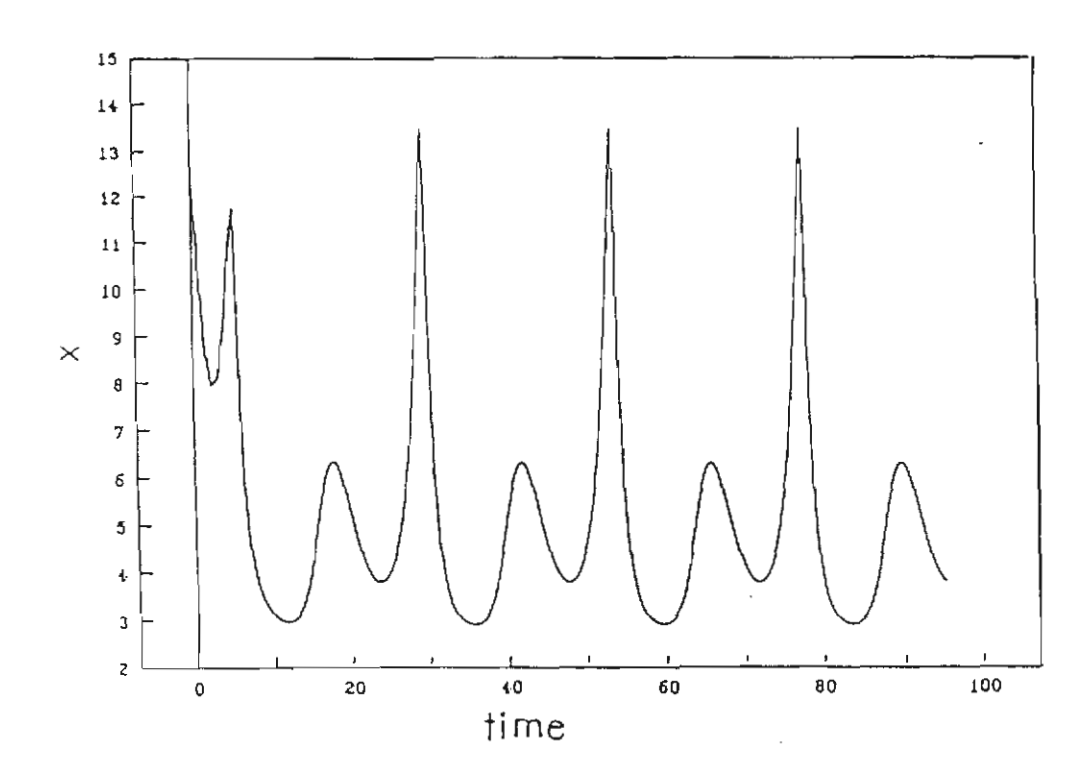
โดย bifurcation ที่เกิดขึ้นนี้จะซ้อนกับ periodic solution ที่ได้จาก eigenvalues $\pm w_0$ i ที่เกิดจากการ ที่ geomagnetic field มีการเปลี่ยนแปลงอย่างเป็นคาบอยู่แล้ว จึงจะได้คำตอบของระบบสมการ (5)- (7) เป็น periodic solution บนผิวของ 2-torus ดังที่แสดงในรูปที่ 4 และ 5 ซึ่งเทียบกับข้อมูลจากห้อง ทดลองแล้วมีลักษณะใกล้เคียงกันมาก แสดงว่าแบบจำลองที่ทำการวิจัยสามารถจำลองสิ่งที่เกิดขึ้นจริง ได้เป็นอย่างดี

การวิเคราะห์ด้วยทฤษฎีบทของ Hopf และผลของการหาคำตอบเชิงตัวเลขทำให้เราสามารถ
บอกได้ว่า operating zone ใด เราจึงจะสามารถคำเนินงานปฏิกรณ์ (reactor) ได้อย่างปลอดภัย และ
หลีกเลี่ยงบริเวณที่จะมีคำตอบแบบยุ่งเหยิงสับสนซึ่งไม่เป็นที่ต้องการได้ ทั้งนี้ reactor ในปฏิกรณ์ขจัด
ของเสียซึ่งเป็นสารพิษมีอันตรายต่อสิ่งมีชีวิตได้เป็นอย่างมาก ทำให้ผลการวิเคราะห์วิจัยในลักษณะนี้
มีประโยชน์มากในการ monitor และ control ปฏิกิริยาใน reactor ให้คำเนินการไปอย่างปลอดภัยและ
มีประสิทธิภาพมากที่สุด

ผู้วิจัยได้นำผลงานวิจัยระบบสมการ (5), (6) และ (7) เขียนขึ้นเป็น paper และได้รับ published เรียบร้อยแล้วใน *J. Sci. Soc. Thailand* ซึ่งจะสามารถอ่านรายละเอียดของการวิจัยได้ใน manuscript ที่แนบมาด้วยต่อไปนี้



รูปที่ 4 คำตอบของระบบสมการ (5) - (7) บนระนาบ (x,y) ซึ่งแสดงลู่ท่าง (trajectory) ซึ่งมุ่งเข้าสู่การหมุนเวียนบนผิวของ 2-torus โดย $M=1,\ \gamma=1,\ \beta=1.5,$ $\theta=0.6,\ y_s=1.5,\ d=0.375,\ \delta=2.1,\ x_s=7.875,\ \rho=1.3125,\ Z_0=5.7,$ $\omega=1/12$ และ $\alpha=1$



รูปที่ 5 แสดงคำตอบ x(t) ของระบบสมการ (5)-(7) โดย M = 1, γ = 1, β = 1.5, θ = 0.6, y_s = 1.5, d = 0.375, δ = 2.1, x_s = 7.875, ρ = 1.3125, Z_0 = 5.7, ω = 1/12 และ α = 1

Dynamic Behavior of a Membrane Permeability Sensitive Model for a Continuous Bio-Reactor Exhibiting Culture Rhythmicity

DYNAMIC BEHAVIOR OF A MEMBRANE PERMEABILITY SENSITIVE MODEL FOR A CONTINUOUS BIO-REACTOR EXHIBITING CULTURE RHYTHMICITY

YONGWIMON LENBURY, SOMSAK ORANKITJAROEN

Department of Mathematics, Faculty of Science, Mahidol University, Rama 6 Rd., Bangkok 10400, Thailand.

(Received April 3, 1995)

ABSTRACT

A modified Monod model of a continuous microbial culture in which the yield term depends linearly on the substrate concentration is extended to incorporate the effect of external forces on the cell membrane permeability. Bifurcation analysis of the new mathematical model, which consists of three non-linear ordinary differential equations, shows that the model can simulate the oscillatory behavior observed in experimental data for certain ranges of the system parameters. Computer simulation of the model is presented in support of our theoretical predictions.

INTRODUCTION

Sustained oscillations in the patterns of microbial growth and product formation have been frequently observed in continuous cultures when the feed conditions and the culture conditions remain constant [1, 2]. According to Yerushalmi et al. [2], these oscillations are even more pronounced in the long term fermentations or in the cell-retention fermentations where the cells stay in the bio-reactor for long periods of time.

Although the mechanism for these oscillations is not yet fully understood, it is clear that occurrence of such oscillatory behavior has adverse effects on the efforts to optimize the operation of continuous bio-reactors. It also effects productivity of the process and complicates its proper design. It is therefore most important to investigate in depth the factors that cause such rhythmicities, the explanations for which range from experimental errors to the changing microbial physiological behavior often attributed to changes in the cellular metabolic pathway under certain conditions. Recent studies of the parameter affecting the cell physiology of *C. acetobutylicum* showed a high sensitivity of growth and solvent production to the cytoplasmic membrane permeability [2]. A high permeability of the cytoplasmic membrane promotes the growth of the microbial culture, the utilization of the substrate and the biosynthesis of the solvents. The opposite result is obtained with a low permeability of the cell membrane.

The controlling action of the cellular membrane permeability on the activities in many anaerobic processes has been frequently observed. Examples include the influence of plasma-membrane lipid composition and membrane fluidity on growth and solute accumulation by S. cerevisiae [3], growth of Clostridium thermocellum [4], and growth and production of ethanol and glycerol by yeast cultures [5].

In this paper, we consider a mathematical model which incorporates this sensitivity to the cellular membrane permeability, the specific rate of change of which is assumed to vary in a sinusoidal fashion. One physical controlling factor which has been proposed to exert its biological effect on the cytoplasmic membrane permeability is the geomagnetic field variation. This concept has been extensively investigated and is well supported by experimental evidence [6, 7]. Attempts to incorporate such effects into a model of the continuous microbial culture was carried out by Yerushalmi et al. [2]. We consider a modification of their model based on an adaptation of the Monod model in which the yield term is assumed to vary linearly with the substrate concentration. Through bifurcation analysis, the model is shown to simulate different oscillatory behavior observed in experimental data.

SYSTEM MODEL

Basically, microbial kinetics have varied in diverse ways from a model due to Monod fashioned after Michaelis-Menten kinetics for single enzyme-substrate reactions. This simple but valuable model views microbial growth as conversion of a fixed amount of substrate (or nutrient) to biomass occurring autocatalytically in the presence of preexisting biomass [8]. The yield coefficient Y in the Monod's model is constant. The most obvious departure of the predictions of Monod's model, apparently, is in the variation of the stoichiometric coefficient Y. Theoretical studies of models in which the yield term varies linearly with the substrate concentration can be found in the work of Agrawal et al. [8] and that of Lenbury et al. [9]. In [8], Agrawal et al. carried out an extensive theoretical investigation of the dynamic behavior of isothermal continuous stirred tank biological reactors modelled by the following mass balance equations on cells and the limiting substrate:

$$\frac{dS}{dt} = -\sigma(S)X + D(S_0 - S) \tag{1}$$

$$\frac{dX}{dt} = \mu(S)X - DX \tag{2}$$

where X denotes the cells concentration; S the substrate concentration; $\mu(S)$ the specific growth rate; $\sigma(S)$ the specific substrate consumption rate; S_0 the feed substrate concentration; and D the dilution rate.

In their work, the function $\sigma(S)$ was assumed to have the form

$$\sigma(S) \equiv \frac{\mu(S)}{Y(S)} \equiv \frac{\mu_{m}S}{(K_{m}+S)Y(S)}$$
(3)

where μ_m is the maximum specific growth rate and $-K_m$ is the Monod constant while the yield term $-Y(-S_0)$ has the form

สำนักงานกองทุนสนับสนุนการวิจัย (สกว.)

ชั้น 14 อาการ เอก เกีย การเราคร์ เลชที่ 979/17-21 กรมเพทกโยชีม แขวงสามเสนใน เขตพฤปไท กรุษเกพจ 10400 โทร.298-0455 โภรสาร 298-0476 Home page : bun//www.trforth

Home page: http://www.trf.or.th E-mail: trf-info(a trf.or.th



$$Y(S) = \frac{\text{amount of blomass formed}}{\text{amount of substrate consumer}} = aS + b$$
 (4)

which reflects the increase in the yield in response to an increase in the substrate concentration S. This also includes the case of constant yield when a = 0.

The model equations (1) and (2) do not take into account the variation of the membrane permeability with time. Since studies have confirmed high sensitivity of culture growth and production to membrane permeability, it is suggested in [2] that the influence is incorporated into the system model so that the mass balance equation on the limiting substrate is given by

$$\frac{dS}{dt} = -\frac{n'SX}{S+K_m} + D(S_0 - S)$$
 (5)

where n' = kn, with k a proportionality constant, and n the number of active nutrient transport sites. According to Yerushalmi et al. [2], permeation dynamics is the major factor responsible for the formation of the active sugar (nutrient) transport sites, especially in the aging cells. This is in turns due to the accumulation of the non-active deposits in the cytoplasm which make the permeation control the incorporation of the protein in the lipid skeleton of the cytoplasmic membrane. This relationship may be described by the equation:

$$\frac{d}{dt}(nX) = k_p \frac{d}{dt}(PX) \tag{6}$$

where P measures the membrane permeability and k_p is a constant of variation. Integrating equation (6), we obtain the relation

$$nX = k_p XP + k_1 \tag{7}$$

where k₁ is a constant of integration.

Using (7), equation (5) may be cast in the following form:

$$\frac{dS}{dt} = -\frac{(C_1 XP + C_2)S}{(S + K_m)Y} + D(S_0 - S)$$
 (8)

where $C_1 = kk_p Y$ and $C_2 = kk_1 Y$ are constants. In other words, assuming that the yield term is constant, the specific growth rate has the form

$$\mu = \frac{(C_1 P + C_2 / X)S}{(S + K_m)}$$
 (9)

so that the mass balance equation for X becomes

$$\frac{dX}{dt} = \frac{(C_1XP + C_2)S}{(S + K_m)} - DX$$
 (10)

in which the effect of permeability variation has been taken into account. On the other hand, it is reasonable to expect the yield coefficient Y to reflect the varying amount of nutrient mass required to produce a unit of biomass, as has been argued in [8] and [9] for example. We therefore combine both effects by letting Y assume the form in (4) so that the mass balance equation for S becomes

$$\frac{dS}{dt} = -\frac{(C_1XP + C_2)S}{(S + K_m)(aS + b)} + D(S_0 - S)$$
 (11)

Experimental evidence has shown that external forces such as electrical or magnetic fields can contribute to permeability by introducing an 'order' in the composition of the cytoplasmic membrane (see [2] for more detail). As a result, the cellular membrane permeability can follow an oscillatory pattern which can be described by the following equation:

$$\frac{dP}{dt} = -K\cos(\omega_0 t)P \qquad (12)$$

where K is a proportionality constant. Equation (12) describes the periodic changes in the cytoplasmic membrane permeability when there is no cells growth. If there is cells growth, the newly formed cells posses thin cell membrane with high permeability which contributes to an increase in the apparent permeability of the cells population. In the case of influence from the geomagnetic field variations, the period is found to be approximately 24 hours, so that $\omega_0 = 2/24$. However, to include other factors which may effect membrane permeability in the similar manner, we let ω_0 be an arbitrary constant frequency of oscillation of the applied field.

Thus, the variation in the permeability of the cells population, based on the overall cells mass, can be described by the following equation:

J.Sci.Soc.Thailand, 21(1995)

$$\frac{d}{dt}(PX) = -\gamma_1 \cos(\omega_0 t) PX + \gamma_2 \frac{dX}{dt}$$

in which the first term on the right was directly obtained from equation (12), describing the periodic changes in the membrane permeability, while the second term describes the increase in the apparent permeability of the cells population due to the growth of the culture and the formation of new cells, assuming that the inhibitory effect of other factors such as the butanol level is neglegible.

Eliminating X from both sides of the above equation results in the following expression:

$$\frac{dP}{dt} = -\gamma_{1}\cos(\omega_{0}t)P + (\gamma_{2} - P)\mu \qquad (13)$$

where μ is given by equation (9).

Therefore, our system model consists of equations (10), (11), and (14) with (9). We are interested in the dynamic behavior and, in particular, the existence of different types of oscillatory behavior in the system described by these three equations.

BIFURCATION ANALYSIS

For the following analysis, it is convenient to introduce new variables. Namely: we define T=Dt, x=X/a, $y=PC_1/D$, z=S, $\rho=C_2/aD$, $M=k_m$, d=b/a, $z_0=S_0$, $\alpha=1/D$, $\beta=\gamma_2C_1/D$, $u=\cos(\omega_0 t)$, $v=\gamma_1\sin(\omega_0 t)$, and $\omega=\omega_0/D$.

In these variables, our model equations becomes

$$\frac{dx}{dT} = (xy + \rho) \frac{z}{M + z} - x \tag{14}$$

$$\frac{dy}{dT} = -\alpha uy + (\beta - y) \left[y + \frac{\rho}{x} \right] \frac{z}{M + z}$$
 (15)

$$\frac{dz}{dT} = -(xy + \rho) \frac{z}{(M+z)(z+d)} + (z_0 - z) \quad (16)$$

$$\frac{du}{dT} = -\omega v \tag{17}$$

$$\frac{dv}{dT} = \omega u \tag{18}$$

The above system has a steady state solution $(x_s, y_s, z_s, u_s, v_s)$ obtained from equating the right sides of equations (14) - (18) to zero, namely

$$y_s = \beta \qquad (19)$$

$$-(\beta x_s + \rho) \frac{z_s}{(M + z_s)(z_s + d)} + (z_0 - z_s) = 0$$
 (20)

$$x_s = (z_s+d) (z_0-z_s)$$
 (21)

and

$$u_{s} = 0, \quad v_{s} = 0 \quad (22)$$

If we let

$$\theta = \frac{z_s}{M + z_s} \tag{23}$$

$$\delta = \frac{(\beta x_s + \rho)M}{(M + z_s)^2}$$
 (24)

then the Jacobian matrix J of the system of equations (14) - (18) evaluated at the steady state (x_s , y_s , z_s , u_s , v_s) can be written as

$$J = \begin{bmatrix} \beta\theta - 1 & \theta x_{s} & \delta & 0 & 0 \\ 0 & -1 & 0 & -\alpha y_{s} & 0 \\ \frac{-\theta\beta}{z_{s} + d} & \frac{-x_{s}\theta}{z_{s} + d} & \frac{\delta(z_{s}^{2} - Md)}{M(z_{s} + d)^{2}} - 1 & 0 & 0 \\ 0 & 0 & 0 & 0 & -\omega \\ 0 & 0 & 0 & \omega & 0 \end{bmatrix}$$

The 5 eigenvalues of 1 are found to be

$$\lambda_{1,2} = \frac{1}{2}\Gamma(\delta) \pm \frac{1}{2}\Lambda^{1/2}(\delta)$$
 (25)

$$\lambda_3 = -1$$

$$\lambda_{4.5} = \pm i\omega$$

where

$$\Gamma(\delta) = \beta\theta + \frac{\delta(z_s^2 - Md)}{M(z_s + d)^2} - 2$$
 (26)

$$\Lambda(\delta) = \Gamma^{2}(\delta) - 4\{(\beta\theta - 1)\left[\frac{\delta(z_{s}^{2} - Md)}{M(z_{s} + d)^{2}} - 1\right] + \frac{\theta\beta\delta}{z_{s} + d}\}$$
 (27)

Due to the complex conjugate eigenvalues \pm iw, therefore, the model will have a periodic solution for appropriate parametric values. In particular, by the theory of ordinary differential equations, if the parametric values are such that all ligenvalues other that $\alpha_{4,5}$ have negative real parts, then the simulated solution trajectories close to the steady state will approach a closed cycle surrounding the critical point (x_s , y_s , z_s , u_s , v_s) in the five dimensional phase space. In this case the profile of x(T) will be periodic with time closely resembling the regular rhythmicity found in many experimental data. However, such closed cycles lying on a plane in the phase space cannot simulate more irregular oscillatory patterns also observed in other data, such as that taken from the work of Paruleka et al.[10] presented in Figure 1. Here, alternatively low and high peaks can be observed in the growth pattern. Such characteristics appear in all their runs under different operating parameters.

To investigate the possibility of such higher dimensional oscillations in our model, we consider the system of equations (14) - (16) with $\alpha = 0$, and let

$$\delta_{\rm b} = (\beta \theta - 1)^2 (z + d) / \beta \theta \tag{28}$$

$$\delta_{\rm c} = (2 - \beta \theta)(z_{\rm s} + d) \gamma \tag{29}$$

where

$$\gamma = \frac{(z_s + d)M}{z_s^2 - Md} \tag{30}$$

According to Hopf bifurcation theory [11], if a value δ_c can be found such that

- i) Re $\lambda_1(\delta_c) = 0$,
- ii) $\lambda_1(\delta_c)$ and $\lambda_2(\delta_c)$ are complex conjugates,
- iii) Im $\lambda_1(\delta_c) \neq 0$,
- iv) Re $\lambda'_1(\delta_c) \neq 0$, where λ' denotes the derivative of λ ,
- all other eigenvalues have negative real parts,

then the system of equations (14)-(16) with $\alpha=0$ will have a family of periodic solutions for values of δ in some open interval (δ_c , $\delta_c+\epsilon$). The result is stated in the following theorem.

Theorem If

$$\gamma > 0 \tag{31}$$

$$\beta \geq 1$$
 (32)

$$1/\beta > \theta > \frac{1-\sqrt{Y/(Y+1)}}{\beta}$$
 (33)

and

$$\gamma > M > \frac{1-\theta}{\theta} \tag{34}$$

then the system of equations (14) - (16) with $\alpha=0$ will have periodic solutions bifurcating from a non-washout steady state for values of δ in some open interval (δ_c , $\delta_c+\epsilon$) where is given by equation (29).

Proof First, we show that with θ so chosen, $\delta_b < \delta_c$ by considering the equation

$$F(\theta) = (\beta\theta)^2 - 2(\beta\theta) + \frac{1}{\gamma + 1} = 0$$

The function $F(\theta)$ is quadratic in θ and has two real roots:

$$\theta_{1,2} = \frac{1 \pm \sqrt{\gamma/(\gamma+1)}}{\beta} \tag{35}$$

Thus, for $~\theta_1\!>\,\theta\!>\!\theta_2$, we have $~F(\theta)~<~0,$ that is

$$(\beta\theta)^2 - 2(\beta\theta) + \frac{1}{\gamma+1} < 0$$
 (36)

Rearranging (36), we find

$$(\beta\theta)^2 - 2(\beta\theta) + 1 < (2\beta\theta - \beta^2\theta^2)^{\gamma}$$
 (37)

Multipying both sides by z,+d, we have

$$\frac{(\beta\theta-1)^2(z_s+d)}{\beta\theta} < (2-\beta\theta)(z_s+d)\gamma \qquad (38)$$

That is, we have

$$\delta_{\rm b} < \delta_{\rm c}$$
 (39)

if $\theta_1 > \theta > \theta_2$. However,

$$\theta_1 = \frac{1 + \sqrt{\gamma / \gamma + 1}}{\beta} > 1/\beta$$

so that if θ satisfies inequality (33) then

$$\theta_1 > 1/\beta > \theta > \theta_2$$

which implies (39) as claimed,

Now, we observe that

$$\Gamma (\delta_c) = 0 \qquad (40)$$

and
$$\Lambda(\delta_c) = -4\left[-(\beta\theta - 1)^2 + \frac{\theta\beta\delta_c}{z_s + d}\right]$$
 (41)

which is negative because of inequality (39). Thus,

Re
$$\lambda_1(\delta_c) = \Gamma(\delta_c)/2 = 0$$

and λ_1 (δ_c) and λ_2 (δ_c) are complex conjugates. Also, since we have strict inequality in (39),

$$\operatorname{Im} \lambda_1(\delta_c) = \frac{1}{2} \left[-\Lambda(\delta_c) \right]^{1/2} \neq 0$$

These are requirements i), ii), and iii), respectively.

Moreover, from (26) we have

$$\Gamma'(\delta_c) = \frac{(z_s^2 - Md)}{M(z_s + d)^2} = \frac{1}{\gamma(z_s + d)} \neq 0$$

and therefore Re λ'_1 (δ_c) $\neq 0$ which is requirement iv). Finally, the remaining eigenvalue is $\lambda_3 = -1 < 0$.

Thus, all requirements for Hopf bifurcation are met. For δ in some open interval $(\delta_c, \delta_c + \epsilon)$, the system of equations (14) - (16) with $\alpha = 0$ will have a periodic solution bifurcating from its steady state (x_s, y_s, z_s) . For the system of equations (14) - (18) with $\alpha \neq 0$, this means that if conditions (31) - (34) are satisfied a Hopf bifurcation occurs on top of the existing periodic solution (due to the eigenvalues $\pm i\omega$) giving rise to solution trajectory on a 2-torus in the five dimensional phase space.

With the above choice of parametric values, Hopf bifurcation occurs at a non-washout steady state (x_s , y_s , z_s), namely $y_s = \beta \ge 0$ and from (23),

$$z_s = \frac{M\theta}{1-\theta} > 0 \tag{42}$$

since $\frac{M\theta}{1-\theta} > 0$, with θ chosen to be less than $1/\beta = 1$. Then, the value of d can be determined from (30) as

$$d = \frac{\gamma z_s^2 - z_s M}{M(\gamma + 1)}$$
 (43)

Since

$$(\gamma z_s^2 - z_s M)$$
 $(M z_s^2 - z_s M) = M (z_s^2 - z_s)$

and $z_s > 1$ by the second inequality in (34), we have d > 0.

With these values of γ , β , θ , z_s , and d, the critical value δ_c can be found from (29). It is important to note that with our choice of γ ,

$$\theta < \theta_1 = \frac{1 + \sqrt{\gamma / (\gamma + 1)}}{\beta} < \frac{2}{\beta}$$

since $\frac{\gamma}{(\gamma+1)} < 1$. Therefore $2 - \theta \beta > 0$ so that the value of δ_c given by (29) will be positive.

The parametric value $\delta>0$ is then chosen to be in the interval (δ_c , $\delta_c+\epsilon$) for some small $\epsilon>0$ so that Hopf bifurcation may occur. Then, x_s can be determined from (20) and (24) as

$$x_{c} = \delta (\Lambda + z_{c}) z_{c}/M > 0$$
 (44)

Then, from (20) and (21) we find that

$$\rho = \frac{x_s(M + z_s)}{z_s} - \beta x_s$$

That is,

$$\rho = x_{\epsilon} (1 - \theta \beta) / \theta \qquad (45)$$

which is positive since $\theta < 1/\beta$.

Finally, from (21), we have

$$z_0 = \frac{x_s}{z_s + d} + z_s > 0$$
 (46)

using the values of x_s, y_s, z_s and d found previously

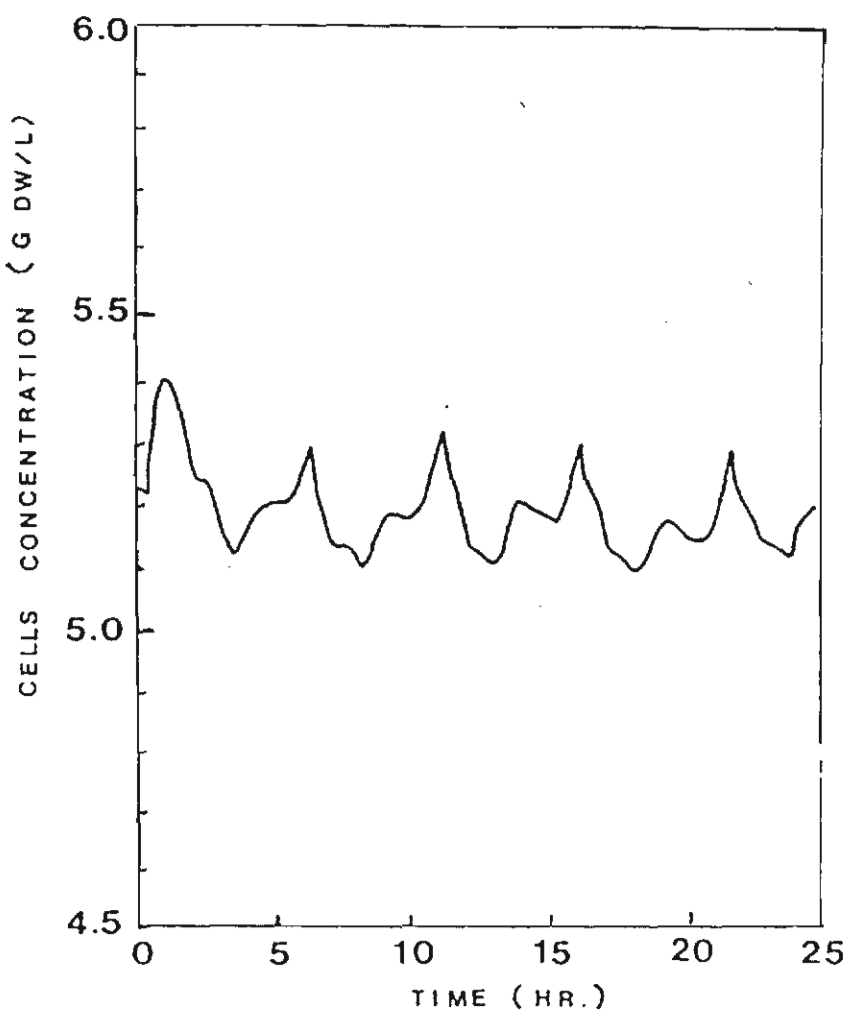


Fig. 1. Alternatively low and high peaks can be observed in the profile of cells concentration (x), for which the data points have been taken from reference [10] of continuous culture with fixed dilution rate: D=0.2 hr¹, pH = 5.5, Temp = 30° C

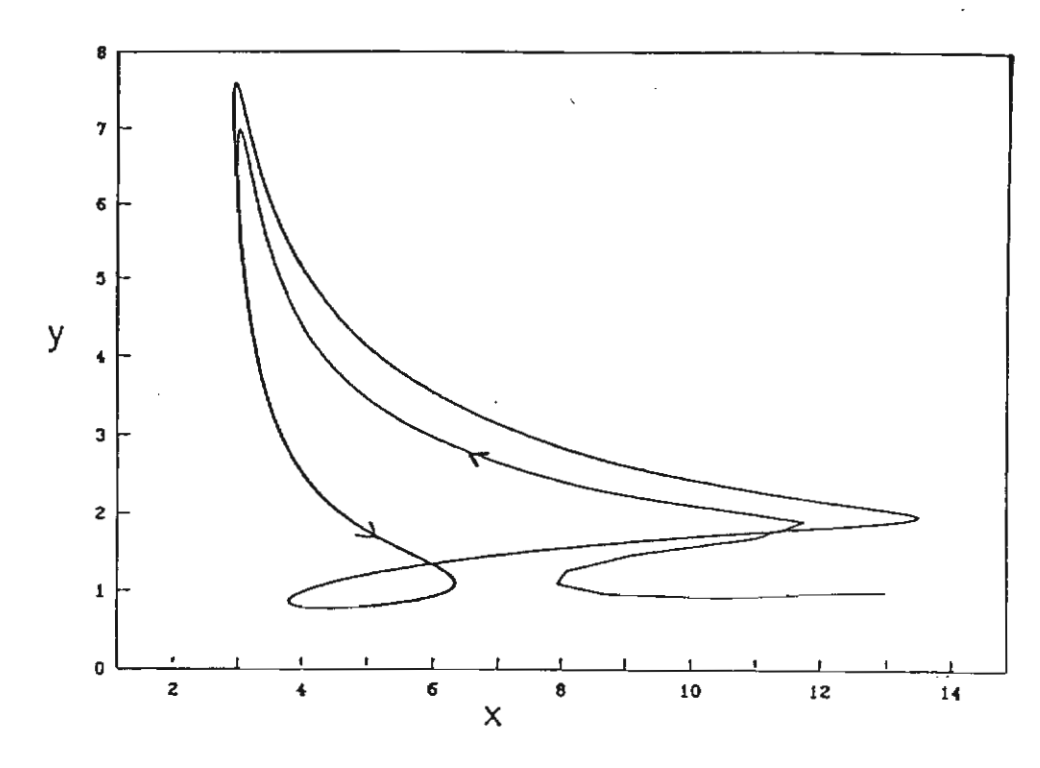


Fig. 2. Computer simulation of the model system of equations (14) - (18) with parametric values chosen so that bifurcation occurs: M=1, $\gamma=1$, $\beta=1.5$, $\theta=0.6$, $y_s=1.5$, d=0.375, $\delta=2.1$, $x_s=7.875$, $\rho=1.3125$, $Z_0=5.7$, $\omega=/12$ and $\alpha=1$. The solution trajectory, projected onto the (x, y)-plane, is seen to approach the closed curve on a torus surrounding the steady state (x_s, y_s, z_s, u_s, v_s) = (7.875, 1.5, 1.5, 0.0)

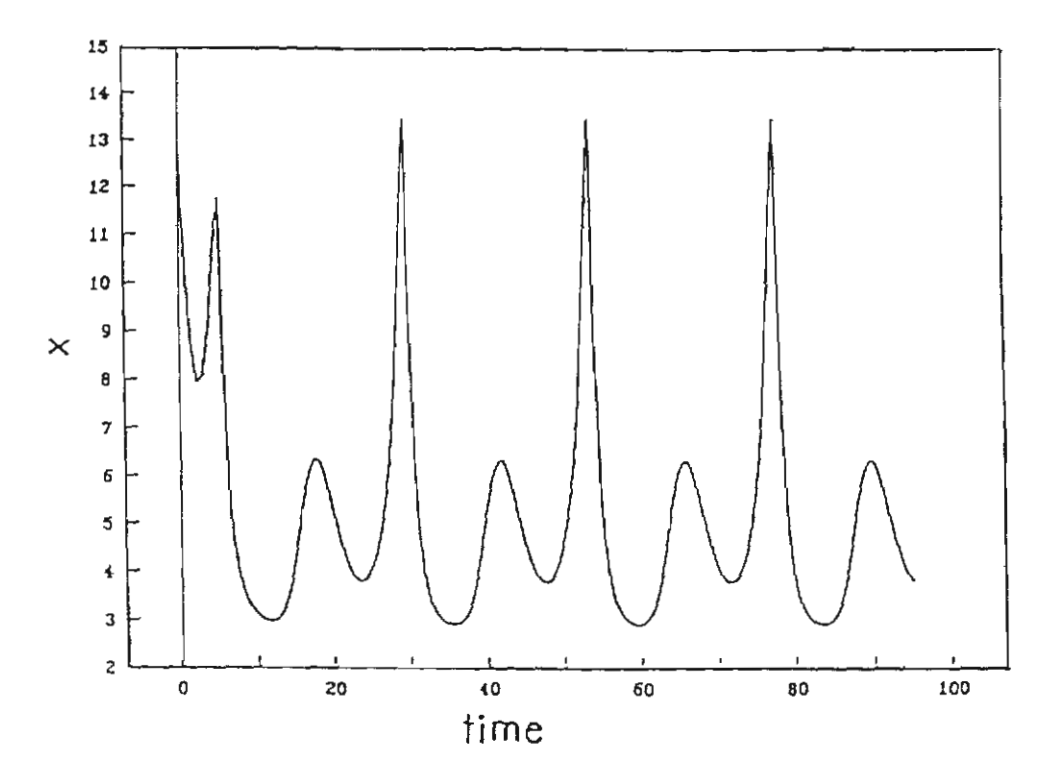


Fig. 3. The simulated time course of cells concentration | x | of Fig. 3 exhibiting alternatively low and high peaks resembling those observed in experimental data.

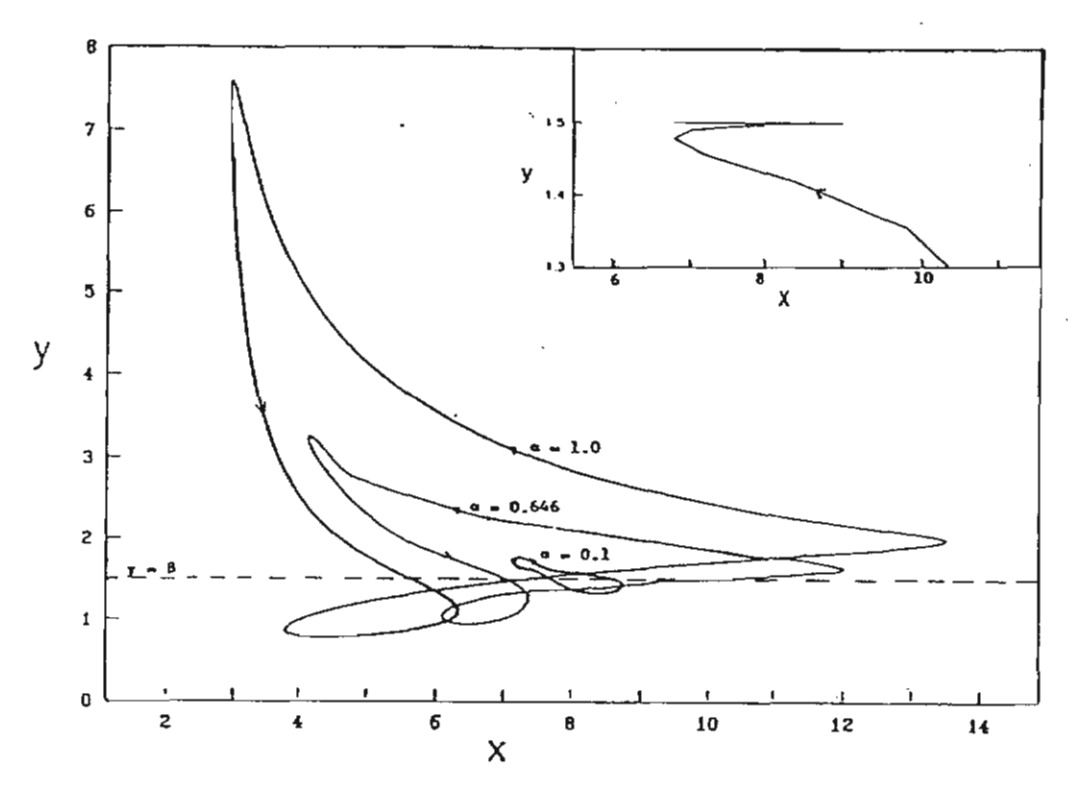


Fig. \Rightarrow . The effect of varying the field density constant α . In the inset, where $\alpha = 0$, the solution trajectory is seen to approach and lie on the plane $y = \beta$ as time progresses.

In Figure 2, we present a computer simulation of the model equations (14) - (18) with $\alpha \neq 0$ and parametric values chosen to satisfy the bifurcation requirements (31) - (34). The solution trajectory is seen to approach the closed curve on the surface of a 2-torus surrounding the steady state $(x_s, y_s, z_s, u_s, v_s) = (7.875, 1.5, 1.5, 0, 0)$ in the 5-dimensional phase space, seen here projected onto the (x, y) - plane. The time course of cells concentration is shown in Figure 3 exhibiting alternatively low and high peaks which compares well with experimental data mentioned earlier (Figure 1). When different parametric values were tried, we have been able to generate different oscillatory patterns resembling those observed in experimental data of continuous cultures under different operating parameters [1, 10].

ASYMPTOTIC BEHAVIOR AND STABILITY ANALYSIS

On multiplying equation (14) by y, equation (15) by x, and adding, we obtain the equation

$$\frac{dw}{dT} = (\alpha u - 1)w + \beta(w + \rho)\frac{z}{M + z}$$
 (47)

where w = xy. We see that equations (16) and (47) involve only the two variables w and z, and therefore can be solved without the help of equation (14). Letting (\hat{w} (T), \hat{z} (T)) be the solution to equations (16) and (47), equation (14) may then be written as

$$\frac{dx}{dT} = F(T) - x \tag{48}$$

where $F(T) = (\widehat{w}(T) + \rho) \frac{\widehat{\xi}T}{M + \widehat{\xi}T}$ is a known function of T. Equation (48) can be solved directly for the solution $x = \widehat{x}(T)$.

Moreover, on substituting z = 0 in (16), we find that

$$\frac{dz}{dT}\Big|_{z=0} = z_0 > 0$$

which means that

$$z(T) \ge 0$$
 for all $T \ge 0$ (49)

Considering equation (47) with w = 0, we also have

$$\frac{dw}{dT}\Big|_{w=0} = \frac{\beta \rho z}{M+z} \ge 0$$

for positive parametric values. Thus,

$$x (T)y(T) \ge 0$$
 for all $T \ge 0$ (50)

Using (49) and (50) in (48), we again have

$$x(T) \ge 0$$
 for all $T \ge 0$ (51)

Therefore, we conclude that all solutions to our system model remain in the positive octant of the (x, y, z) space.

Further, with (49), (50) and (51), equation (15) can be written as

$$\frac{dy}{dT} = -\alpha u(y - \beta) - (y - \beta)G(T) - \alpha\beta u \qquad (52)$$

where G (T) = $\frac{(\hat{x}(T)\hat{y}(T) + p)\hat{z}(T)}{(M + \hat{z}(T))\hat{x}(T)}$ is a known function which satisfies

$$C(T) \ge 0 \text{ for } z! \mid T \ge 0$$
 (53)

Using the Liebnitz' formula to solve equation (52), we obtain

$$y(T) - \beta = e^{-\alpha v(T) - h(T)} \left\{ c - \alpha \beta \int_{0}^{T} e^{\alpha v(\tau) + h(\tau)} u(\tau) d\tau \right\}$$
 (54)

where $h(T) = \int_0^{G(r)dr} and c$ is a constant of integration. Since (53) holds h(T) is increasing with T. Also, $e^{\pm cv(T)} \le e^{\alpha}$ since $-1 \le v(T) \le 1$. Thus, we have

$$\left| e^{-h(T)} \int_{0}^{T} e^{h(\tau)} u(\tau) d\tau \right| \leq e^{2\alpha - h(T)} e^{h(T)} \left| \int_{0}^{T} u(\tau) d\tau \right| \leq e^{2\alpha}$$

Thus, letting $T \rightarrow \infty$ in (54) we find

y(T) -
$$\beta \rightarrow \alpha \beta e^{2\alpha} y_p$$
 (T) as T $\rightarrow \infty$

where $y_p(T)$ is a bounded function. In other words, with $\alpha = 0$, all solutions to the system of equations (14)-(16) approach and lie, as time passes, on the plane $y = \beta$ in the (x, y, z) space.

Figure 4 shows the effect of varying the field density constant α on the position and shape of the solution trajectory. The solution trajectories for smaller α are closer to the plane $y = \beta$

With regards to the stability of these periodic solutions, one can apply various stability criteria (see, for example, [11]) on the system of equations (16) and (47) with $\alpha=0$ which describes the solution curve ($\widehat{w}(T)$, $\widehat{z}(T)$). It turns out to be very laborous calculation if one allows complete generality for the system parameters. However, for the case $\rho=0$ and $\beta=1$, equations (16) and (47) may be written as

$$\frac{dx_1}{dT} = \Pi(x_2)x_1 - x_1 \tag{55}$$

$$\frac{dx_2}{dT} = -\Sigma(x_2)x_1 + x_2 \tag{56}$$

where $x_1 = \frac{W}{z_0}$, $x_2 = 1 - \frac{z}{z_0}$,

$$\Pi(x_2) = \frac{(1-x_2)}{1+\phi-x_2}$$
 (57)

and

$$\Sigma(x_2) = \frac{\Pi(x_2)}{1 + \Psi - x_2} \tag{58}$$

with $\phi = \frac{M}{z_0}$, and $\psi = \frac{d}{z_0}$

By making use of the Poincare's criterion and Friedrichs' bifurcation theory, the following condition for orbitally stable periodic solution of equations (55) and (56) can be found [8]:

$$3\Sigma'''(x_{2s}^*) x_{2s}^* < \Sigma''(x_{2s}^*) \left[1 + \frac{4\Pi''(x_{2s}^*) x_{2s}^*}{3\Pi'(x_{2s}^*)} \right]$$
 (59)

where x_{2s}^* is the value of $x_{2s} = 1 - \frac{z_s}{z_0}$ at the critical value δ_c of δ . That is, from (24) and (29),

$$x_{s2}^{\bullet} = 1 - \frac{1}{z_0} \left[\frac{\delta}{\gamma(2-\theta)} - d \right]$$

Using (57) and (58) in (59), we find that the bifurcated periodic solution will be stable if

$$F(\phi, \psi) = \left[1 - x_{2s}^* - \phi\theta(1 + \theta)\right] \left\{9 \frac{x_{2s}^*}{\theta} - 1 - \frac{\theta}{3} x_{2s}^*\right\} - 9\phi x_{2s}^* \theta^2 < 0$$
 (60)

where

$$\theta = \frac{(1 + \Psi - x_{2s}^*)}{(1 + \Phi - x_{2s}^*)}$$

Therefore, the bifurcation originating at the critical value δ_c of δ is stable if F<0 and unstable if F>0. Moreover, it can be shown that a stable bifurcated periodic solution surrounds an unstable critical point. If it surrounds a stable critical point, it is unstable.

CONCLUSIONS

A model of three ordinary differential equations is used to describe, under certain simplifying hypotheses, a membrane permeability sensitive chemostat system. Depending on the values of the system parameters, the model system may exhibit sustained regular oscillation in the form of a one frequency limit cycle, or a more irregular oscillation in the form of a solution trajectory on the surface of a torus surrounding a non-washout steady state. Thus, by incorporating the effect of membrane permeability variation, the model is shown to be capable of exhibiting oscillatory behavior which compares well with observed experimental data. A stability investigation shows that if the quantity $F(\phi, \psi)$ has positive value then the bifurcated solutions are repelling and if it is negative then the solutions are attracting.

Factors such as electric and magnetic forces have been proposed to have significant effects on cytoplasmic membrane permeability inducing oscillatory pattern in permeability which in turn causes the rhythmicity in the microbial growth patterns. Some investigations have been carried out in that direction [2, 7]. Nontheless, relatively little efforts have been made, up to date, to model such effects of rhythmic variation in membrane permeability

on microbial culture, in order that their biochemical impact may be better understood and appreciated. More in depth studies of the causes and mechanism of the rhythmicities are clearly needed, the repercussions of these kind of studies in the large scale fermentation industry being significant indeed.

ACKNOWLEDGEMENT

Appreciation is rendered to the National Research Council and the Thailand Research
Fund for their financial support.

REFERENCES

- 1. Borzani, W., Gregori, R.E., and Vairo, M.L.R., Some observations on oscillatory changes in the growth rate of Saccharamyces cerevisiae inaerobic continuous undisturbed culture. Biotech. Biotech. Biotech. 19, 1363-1374 (1979).
- 2. Yerushalmi, L., Volesky, B., Votruba, J., and Molnar, L., Circadian rhythicity in a fermentation process. Appl. Microbiol. Biotechnol., 30, 460-474 (1989).
- 3. Thomas, D.S., and Rose, A. H., Inhibitory effect of ethanol on growth and solute accumulation by Saccharomyces cerevisiae as affected by plasma-membrane lipid composition. Arch. Microbiol., 122, 49 (1979).
- 4 Herrero, A.A., and Comez, R.F., Development of ethanol tolerance in Chstridium thermocellum., 40, 571 (1980).
- 5. Panchal, C.J., and Stewart, G.G., Regulatory factors in alcohol fermentations. Proc. Int. Yeast Symp., 5, 9 (1981).
- 6. Hong, F.T., Photoelectric and magneto-orientation effects in pigmented biological membranes. J. Colloid and Interface Sci., 58, 471 (1977).
- 7. Dubrov, A.P., The Geomagnetic Field and Life, Plenum Press, New-York (1974), p. 20.
- 8. Agrawal, P., Lee, C., Lim, H.C., and Ramkrishna, D., Theoretical Investigations of Dynamic Behavior of Isothermal Continuous Stirred Tank Biological Reactors. *Chemical Engineering Science*, 37(3), 453-462 (1982).
- 9. Lenbury, Y., Novaprateep, B., and Wiwatpataphee, B., Dynamic behavior classification of a continuous bio-reactor subject to product inhibition. *Mathematical and Computer Medelling*, 19, 107-117 (1994).
- 10 Paruleka, S. J., Semones, G.B., Rolf, M. J., Levense, J.C., and Lim. H.C., Induction and Elimination of Oscillations in Continuous Cultures of Saccharemyces cerevisiae. Biorech. Biorech. Biorech. 28 (5),700-710 (1986).
- 11 Hassard, B.D., Kazarinoff, N.D., and Wan, Y.H., Theory and Applications of Hopf Bifurcation, Cambridge University Press, Cambridge (1981), p. 16

1.2 ผู้วิจัยยังได้ทคลองปรับปรุงแบบจำลอง เพื่อพิจารณาผลกระทบของ geomagnatic field variation ที่มีต่อ permeability ต่อไป โดยคิดให้ specific growth rate เป็นฟังก์ชันของ Monod โดยตลอด และการเปลี่ยนแปลงใน premeability นั้นให้มีผลกระทบต่อ yield coefficient เพียงอย่าง เดียว จึงได้แบบจำลองเป็นสมการ 3 สมการ ต่อไปนี้

$$\frac{dS}{dt} = -\frac{(c_1 x P + c_2)S}{(S + K_m)y} - D(S_F - S)$$
 (15)

$$\frac{\mathrm{dx}}{\mathrm{dt}} = \frac{\mu_{\mathrm{m}} \, \mathrm{S} \, \mathrm{x}}{\mathrm{S} + \mathrm{K}_{\mathrm{m}}} - \dot{\mathrm{D}} \, \mathrm{x} \tag{16}$$

$$\frac{dP}{dt} = -\gamma \cos(w_0 t) P - \frac{(\gamma_2 - P) \mu_m S}{S + K_m}$$
(17)

ผู้วิจัยสามารถพิสูจน์ทฤษฎีบทต่อไปนี้ได้

ทฤษฎีบทที่ 2 ถ้า

$$\eta > 1 \tag{18}$$

$$\rho > \beta x_{S} > 0 \tag{19}$$

โดยที่

$$\eta = \frac{\mu_m}{D}$$

$$\rho = -\frac{c_2}{\mu_m}$$

$$\beta = \frac{\gamma_2 c_1}{\mu_m}$$

และ x_S คือค่าของ x ที่ steady state แล้วระบบสมการ (15)-(17) จะมีคำตอบเป็นคาบ ซึ่ง bifurcate จาก non-washout steady state สำหรับค่าของ δ ในช่วง ($\delta_c, \delta_c + \epsilon$) โดยที่

$$\delta = \frac{x_{S}}{z_{S} + K_{m}} \tag{20}$$

$$\delta_{c} = \frac{x_{S}}{(\rho - \beta x_{S})(\eta - 1)} \tag{21}$$

ยิ่งไปกว่านั้น ผู้วิจัยได้สร้าง bifurcation diagram โดย plot ค่าของ

$$H_n = \xi_n - \frac{M_{\alpha} + m_{\alpha}}{2}$$
, $n = 1, 2, ..., 40$

โดยที่

$$M_{\alpha} = \max_{n} \, \xi_{n}$$

$$m_\alpha = \underset{n}{mix} \; \xi_n$$

$$\xi_{\alpha} = \log z(T_n)$$
, $n = 1, 2, ..., 40$

4

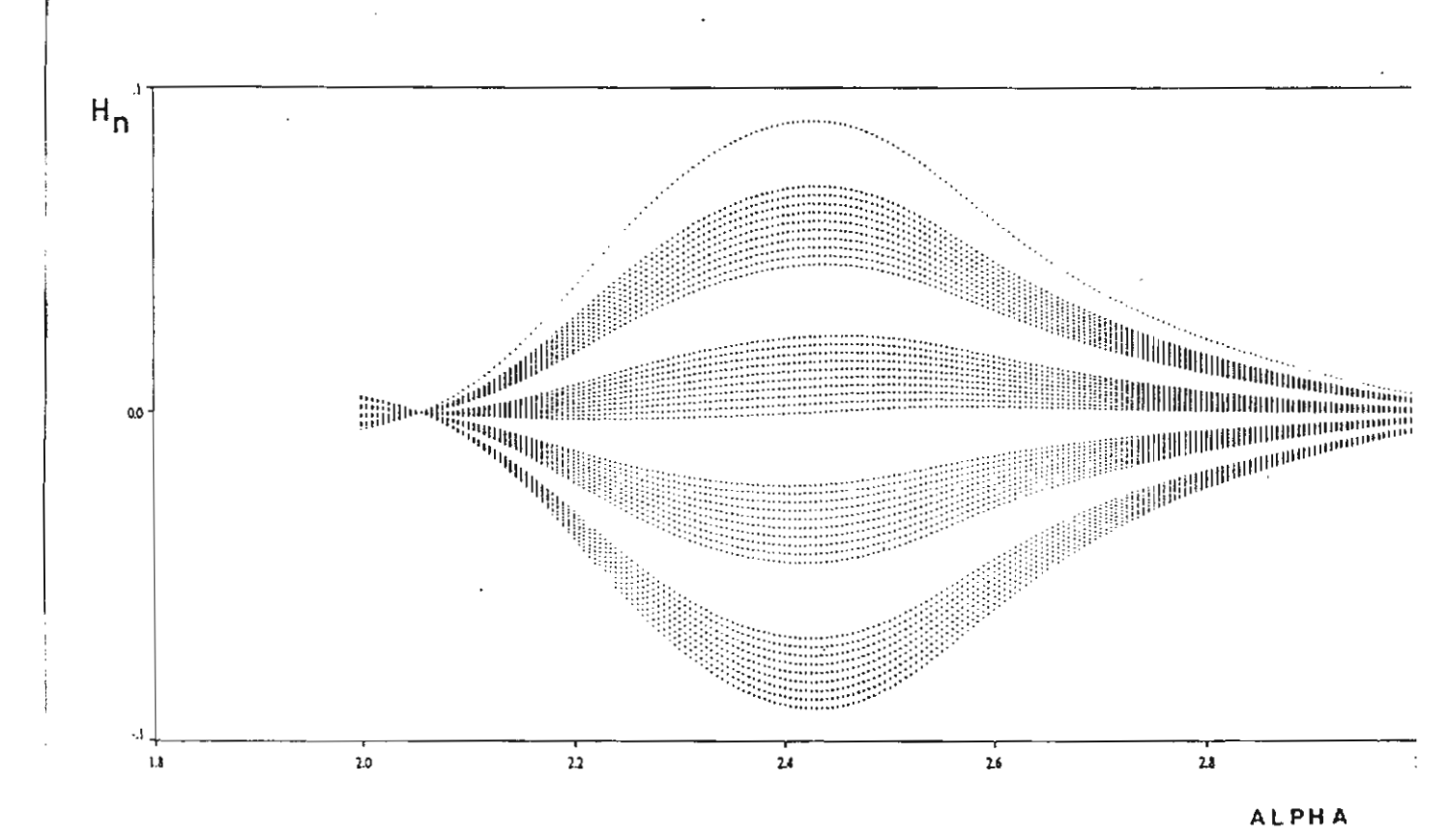
$$T_n = T_0 + \frac{2 n \pi}{w}$$
, $n = 1, 2, ..., 40$

สำหรับค่า α หนึ่งค่า จะได้ว่า H_n 40 ค่า ซึ่งผู้วิจัยใช้ค่า α ในช่วง [0,3] ได้เป็น bifurcation diagram ดังที่แสดงในรูปที่ 6 แสดงว่าเมื่อ α มีค่าอยู่ในช่วง

$$2.1 < \alpha < 3$$

จุด 40 จุด จะ scatter ออกเป็น 5 กลุ่ม แสดงว่าคำตอบของระบบสมการ (15)-(17) มีคำตอบ ที่สับสนเป็น chaotic region ซึ่งควรจะหลีกเลี่ยงในการควบคุมปฏิกรณ์การขจัดสารพิษจากโรงงาน อุตสาหกรรมต่าง ๆ

ผู้วิจัยได้นำผลงานวิจัยแบบจำลองซึ่งประกอบด้วย สมการ (15), (16) และ (17) ที่กล่าวข้าง ด้นเขียนเป็น paper และได้รับ published แล้วในวารสาร Mathematical and Computer Modelling ดังที่ได้แนบ manuscript ดังกล่าวมาด้วยต่อไปนี้



รูปที่ 6 Bifurcation diagram

Bifurcation and Chaos in a Membrane Permeability Sensitive

Model for a Continuous Bioreactor



Mathl. Comput. Modelling Vol. 24, No. 9, pp. 37-48, 1996
Copyright©1996 Elsevier Science Ltd
Printed in Great Britain. All rights reserved
0895-7177/96 \$15.00 + 0.00

PII: S0895-7177(96)00152-5

Bifurcation and Chaos in a Membrane Permeability Sensitive Model for a Continuous Bioreactor

Y. LENBURY*, B. SUKPRASONG AND B. NOVAPRATEEP
Department of Mathematics, Faculty of Science
Mahidol University, Bangkok, Thailand

(Received February 1995; accepted November 1995)

Abstract—In this paper, we investigate the dynamic behavior of a continuous stirred tank reactor modelled by cells and substrate balance equations which have been extended to incorporate the effect of external forces on the cell membrane permeability. Bifurcation analysis done on the system of three ordinary nonlinear differential equations which comprises the model shows that it can simulate oscillatory behavior and more complex dynamic behavior which have been frequently observed in experimental data. Investigation is carried out to identify parametric ranges for which we can expect undesirable complex situations that can compromise the quality of the effluent.

Keywords—Bifurcation, Limit cycles, Continuous bioreactor, Membrane permeability, Chaotic behavior.

NOMENCLATURE

C_1	Proportionality constant, hr^{-1}
C_2	Constant of integration, g/ℓ
D	Dilution rate, $h\tau^{-1}$
K_m, k 's	Constants, g/ℓ
n	Number of active transport sites, hr^{-1}
P	Measure of membrane permeability
\boldsymbol{S}	Substrate concentration in the fermentation vessel, g/ℓ
$S_{f F}$	Substrate concentration in the feeding solution, g/ℓ
t.	Time, hr
X	Cell concentration in the fermentation vessel, g/ℓ
Y	Yield coefficient for cell formation from the limiting substrate
γ 's	Proportionality constants, hr^{-1}
μ	Specific growth rate, hr^{-1}
μ_m	Maximum specific growth rate for the Monod model, hr^{-1}
ω_0	External force field frequency, $h\tau^{-1}$

1. INTRODUCTION

Continuous stirred tank reactors (CSTRs) are often used in wastewater treatment and biological technologies, since they represent one of the simplest approaches to continuous processes [1].

Appreciation is rendered to the Thailand Research Fund and The National Research Council of Thailand for their financial support.

^{*}Author to whom all correspondence should be addressed.

Activated sludge processes and the oxidation of some dangerous compounds usually take place in well-mixed continuous reactors at ambient temperature. Most of these biological reactions, described with Michaelis-Menton kinetics, exhibit chaotic behavior as shown by Agrawal et al. [2] in their work on the theoretical investigations of isothermal continuous stirred tank biological reactors. The appearances of limit cycles which can degenerate to chaos for certain values of the control parameters of CSTRs have been more recently reported and discussed in [1,3]. Although the mechanisms for this oscillatory behavior are not yet fully understood, it is clear that such behavior affects the performance of the process and complicates its proper design and optimization. Not only are these phenomena undesirable from the point of view of process control, they can also give rise to potentially dangerous situations in the case of toxic compound treatment. It is, therefore, necessary to investigate in depth the factors that cause such rythmicities in order to better understand the underlying mechanisms and learn how best to avoid this undesirable dynamic behavior.

Basically, microbial kinetics have varied in diverse ways from a model due to Monod fashioned after Michaelis-Menton kinetics for single enzyme-substrate reactions [1]. This model portrays microbial growth as conversion of a fixed amount of substrate (or nutrient) to biomass occurring autocatalytically in the presence of pre-existing biomass. The yield coefficient, determined by the amount of fresh biomass produced per unit mass of nutrient, remains fixed during the growth process. The mass balance equations on cells and the limiting substrate can be expressed as

$$\frac{dX}{dt} = -DX + \mu(S)X,\tag{1}$$

$$\frac{dX}{dt} = -DX + \mu(S)X,$$

$$\frac{dS}{dt} = D(S_F - S) - \frac{\mu(S)}{Y}X,$$
(2)

where X denotes the concentration of cells, S the substrate concentration, $\mu(S)$ the specific growth rate, S_F the feed substrate, and D denotes the dilution rate. Monod's model regards the yield coefficient Y as a constant and simply does not admit any periodic behavior. The most obvious departure of the predictions of the Monod's model is in the variability of the stoichiometric coefficient Y, which has led to damped as well as sustained oscillations [4]. Other workers have also theoretically studied the continuous reactor for the cases in which the specific growth rate responds with time lag to changes in pH, or the Monod's equation holds for growth limitation, and the case where growth inhibitors are formed during the process [5]. In [6], Lenbury et al. made a theoretical study on the dynamic behavior of a single-vessel continuous bioreactor subject to a growth inhibition at high concentration of the rate limitation substrate. Bifurcation and stability analysis showed oscillatory behavior and complexity in terms of steady-states multiplicity and characteristics.

Recent studies of the parameters affecting the cell physiology of C. acetobutylicum showed a high sensitivity of growth and solvent production to the cytoplasmic membrane permeability [7]. A high permeability of the cytoplasmic membrane promotes the growth of the microbial culture, the utilization of the substrate, and the biosynthesis of the solvents. The opposite result is obtained with low permeability of the cell membrane. The controlling action of the cellular membrane permeability on the activities in many continuous processes has been frequently observed. Examples include the influence of plasma-membrane lipid composition and membrane fluidity on growth and solute accumulation by S. cerevisiae [8], growth of Clostridium thermocellum [9], and growth and production of ethanol and glycerol by yeast cultures [10].

In this paper, we consider a mathematical model which incorporates this sensitivity to the cellular membrane permeability, the specific rate of change of which is assumed to vary in a sinusoidal fashion. Bifurcation analysis of the model shows that it can exhibit oscillatory behavior in the form of a closed orbit on the surface of a 2-torus for certain ranges of parametric values. Further investigation shows that chaotic behavior can result for values of a control parameter which correspond to the windows of chaos.

2. SYSTEM MODEL

One physical mechanism which has been proposed to exert its biological effect on the variability of the cytoplasmic membrane is the geomagnetic field variation [7]. Due to its crystalline structure, the performance of the cell membrane is influenced by such external forces. This concept has been extensively investigated and is well supported by experimental evidence [11,12]. Attempts to incorporate the effects of external forces on the cell membrane permeability into a model of the continuous bioreactor was carried out by Yerushalmi et al. [7] who asserted that, as a result of the influence of the geomagnetic field, the cellular membrane permeability can follow an oscillatory pattern which will in turn cause the complexed oscillatory behavior in the bioreactor.

The geomagnetic field can exert its biological effect by introducing an "order" in the composition of the cytoplasmic membrane. It is well documented [7] that the rodlike molecules in a liquid crystal can orient themselves in a magnetic field which will increase the anisotropy of the liquid crystals, making the cellular membrane more compact, resulting in a decrease in its permeability. The opposite effect is observed when the external force is not so strong.

Studying the relationship between the magnetic field strength and the anisotropy of liquid crystals, which is indirectly related to the cytoplasmic membrane permeability, it was found in [7] that the variation of the membrane permeability P with time can be described by the following equation:

$$\frac{dP}{dt} = -\gamma_1 \cos(\omega_0 t) P,\tag{3}$$

where γ_1 is a proportionality constant which is related to the intensity of the external force field that varies in a sinusoidal fashion (with a period of approximately 24 hours for the geometric field variation).

Equation (3) describes the periodic changes in the cytoplasmic membrane permeability when there is no cell growth. Growth of the cells contributes to an increase in the apparent permeability of the cell population due to the newly formed cells which possess a thin cell membrane with high permeability. Thus, the variations in the permeability of the cell population can be described by the following equation:

$$\frac{d(PX)}{dt} = -\gamma_1 \cos(\omega_0 t) PX + \gamma_2 \frac{dX}{dt},\tag{4}$$

where γ_2 is a proportionality constant. The second term in equation (4) describes the increase in the apparent permeability due to the growth of the culture and the formation of new cells.

Eliminating X from both sides of (4) results in the following equation for the dynamics of the cells membrane permeability:

$$\frac{dP}{dt} = -\gamma_1 \cos(\omega_0 t) P + (\gamma_2 - P) \mu, \tag{5}$$

where μ is the specific growth rate. More detailed discussions on the derivation of the above equations may be found in [7], where the inhibitory effect of butanol was also incorporated, but which will be considered negligible here, however.

The rate of nutrient utilization in the continuous culture is proportional to the number of active sugar transport sites which results in the following equation for nutrient uptake rate:

$$\frac{dS}{dt} = -\frac{n'S}{S + K_m}X + D(S_F - S),\tag{6}$$

where n' = kn, k being a proportionality constant, while the direct relationship between the number of active transport sites and the membrane permeability can be expressed as

$$\frac{d(nX)}{dt} = k_p \frac{d(PX)}{dt}. (7)$$

Thus, integrating (7), we find that equation (6) reduces to

$$\frac{dS}{dt} = -\frac{(C_1 X P + C_2)S}{S + K_m} + D(S_F - S), \tag{8}$$

where $C_1 = kk_P$ and C_2 is a constant of integration.

Thus, our model system consists of equations (1), (5), and (8), where the Monod model will be assumed for the specific growth rate, that is

$$\mu(S) = \frac{\mu_m S}{S + K_m}.\tag{9}$$

3. BIFURCATION ANALYSIS

For the following analysis, it is convenient to introduce new variables. Namely, we define $T=Dt, \ \alpha=\gamma_1/D, \ \beta=\gamma_2C_1/\mu_m, \ \eta=\mu_m/D, \ \omega=\omega_0/D, \ \rho=-C_2/\mu_m, \ M=K_m, \ x=X, \ y=C_1P/\mu_m, \ z=S, \ z_0=S_F, \ u=\cos(\omega_0t), \ {\rm and} \ v=\sin(\omega_0t).$

In these variables, our model equations (1), (5), and (8) become

$$\frac{dx}{dT} = \frac{\eta zx}{z+M} - x,\tag{10}$$

$$\frac{dy}{dT} = -\alpha uy + (\beta - y)\frac{\eta z}{z + M},\tag{11}$$

$$\frac{dz}{dT} = -(xy - \rho)\frac{\eta z}{z + M} + (z_0 - z),$$
(12)

$$\frac{du}{dT} = -\omega v,\tag{13}$$

$$\frac{dv}{dT} = \omega u. \tag{14}$$

The above system has a steady state solution $(x_S, y_S, z_S, u_S, v_S)$ obtained from equating the right sides of equations (10)-(14) to zero, namely

$$\frac{\eta z_S x_S}{z_S + M} - x_S = 0, \tag{15}$$

$$(\beta - y_S) \frac{\eta z_S}{z_S + M} = 0, \tag{16}$$

$$-(x_S y_S - \rho) \frac{\eta z_S}{z_S + M} + (z_0 - z_s) = 0,$$

$$u_S = 0, \qquad v_S = 0,$$
(17)

from which we obtain

$$z_S = \frac{M}{\eta - 1},\tag{18}$$

$$y_S = \beta$$
, and (19)

$$x_S = \frac{(z_0 - z_s) + \rho}{\beta}. (20)$$

If we let

$$\delta = \frac{x_S}{z_S + M},\tag{21}$$

then the Jacobian matrix J of the system of equations (10)–(14) evaluated at the steady state $(x_S, y_S, z_S, u_S, v_S)$ can be written as

$$J = \begin{bmatrix} 0 & 0 & \frac{M\eta\delta}{z_S + M} & 0 & 0 \\ 0 & -1 & 0 & -\alpha\beta & 0 \\ -\beta & -x_S & -\left(\beta - \frac{\rho}{x_S}\right) \frac{M\eta\delta}{z_S + M} - 1 & 0 & 0 \\ 0 & 0 & 0 & 0 & -\omega \\ 0 & 0 & 0 & \omega & 0 \end{bmatrix}.$$

The five eigenvalues of J are found to be

$$\lambda_{1,2} = \frac{1}{2}\Gamma(\delta) \pm \frac{1}{2}\Delta^{1/2}(\delta),$$

$$\lambda_{3} = -1,$$

$$\lambda_{4,5} = \pm i\omega,$$
(22)

where

$$\Gamma(\delta) = -\left(\beta - \frac{\rho}{x_S}\right) \frac{M\eta\delta}{z_s + M} - 1,\tag{23}$$

$$\Delta(\delta) = \Gamma^2(\delta) - 4(\eta - 1)\delta\beta. \tag{24}$$

Due to the complex conjugate eigenvalues $\pm i\omega$, the linearized model will have a periodic solution for appropriate parametric values. In particular, if the parametric values are such that the eigenvalues λ_1 and λ_2 both have negative real parts, then we will observe the solution trajectories tending toward a periodic orbit in the phase space. This is the oscillatory behavior caused by sinusoidal variation in the cellular membrane permeability due to the influence of the external force field. We can show, however, that the system also possesses a natural frequency, which when compounded with the forced frequency, can give rise to a more complicated dynamic behavior. To do this, we consider the system of equations (10)–(12) with $\omega = 0$, for which the eigenvalues are also λ_1, λ_2 , and λ_3 . Letting

$$\delta_C = \frac{x_S}{(\rho - \beta x_S)(\eta - 1)},\tag{25}$$

then, according to Hopf bifurcation theory [13], if a value δ_C can be found such that

- (i) Re $\lambda_1(\delta_C) = 0$,
- (ii) $\lambda_1(\delta_C)$ and $\lambda_2(\delta_C)$ are complex conjugates,
- (iii) $\operatorname{Im} \lambda_1(\delta_C) \neq 0$,
- (iv) Re $\lambda'_1(\delta_C) \neq 0$,
- (v) all other eigenvalues have negative real parts,

then a Hopf bifurcation occurs and the system will have a family of periodic solutions for values of δ in some open interval $(\delta_C, \delta_C + \varepsilon)$. The result can be stated as in the following theorem.

THEOREM. If

$$\eta > 1,\tag{26}$$

$$\rho > \beta x_S > 0, \tag{27}$$

then the system of equations (10)–(14) with $\omega = 0$ will have periodic solutions bifurcating from a nonwashout steady state for values of δ in some open interval $(\delta_C, \delta_C + \varepsilon)$, where δ_C is given by equation (25).

PROOF. First, we note that if η and ρ are chosen to satisfy (26) and (27), then $\delta_C > 0$. Substituting δ_C into δ in (23) and using (18), we find $\Gamma(\delta_C) = 0$, so that $\operatorname{Re} \lambda_1(\delta_C) = 0$, which is the requirement (i). Also, at $\delta = \delta_C$, we have

$$\Delta(\delta_C) = -4(\eta - 1)\delta_C \beta < 0,$$

so that $\lambda_1(\delta_C)$ and $\lambda_2(\delta_C)$ are complex conjugates, and moreover,

Im
$$\lambda_1(\delta_C) \neq 0$$
.

Differentiating Re $\lambda_1(\delta_C)$ with respect to δ , we find

$$\lambda'_1(\delta_C) = -\left(\beta - \frac{\rho}{x_S}\right) \frac{M\eta}{z_S + M} \neq 0,$$

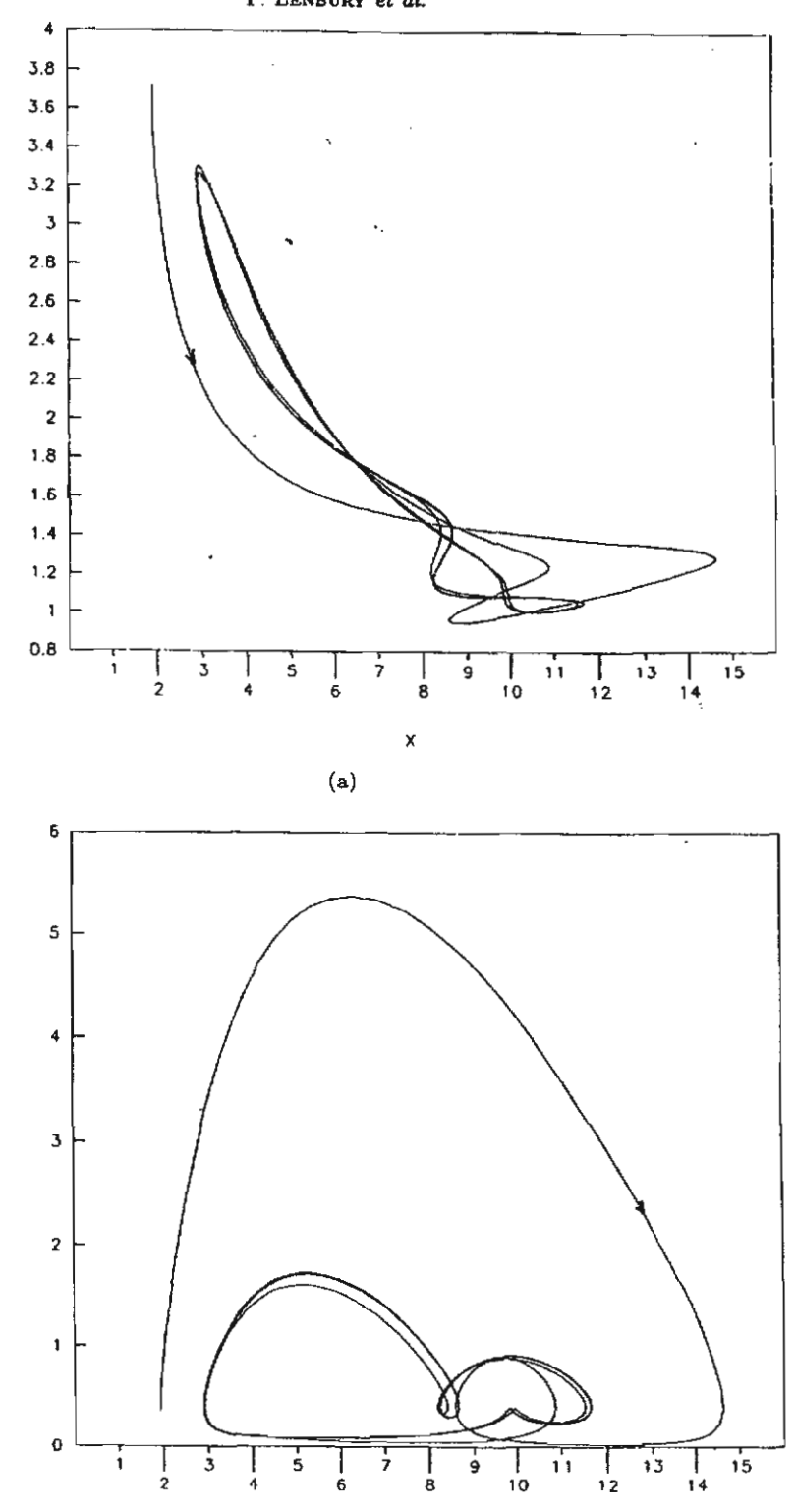


Figure 1. Computer simulation of model equations (10)–(14) with $\alpha=1.1$, $\beta=1.5$, $\rho=11$, $\eta=6$, $\delta=0.241$, M=2, $\omega=1.256$, $z_0=0.2$, $z_S=0.5$, $y_S=1.5$, and $z_S=0.05$. The solution trajectory approaches and eventually lies on a 2-torus, seen here projected onto the coordinate planes.

(b)

and finally, $\lambda_3 = -1 < 0$. Thus, all requirements for Hopf bifurcation are met. For δ in some open interval $(\delta_C, \delta_C + \varepsilon)$, the system of equations (10)-(12) with $\omega = 0$ will have a periodic solution bifurcating from its steady state (x_S, y_S, z_S) . For the system of equations (10)-(14) with $\omega \neq 0$, this means that if conditions (26) and (27) are satisfied, a Hopf bifurcation occurs on top

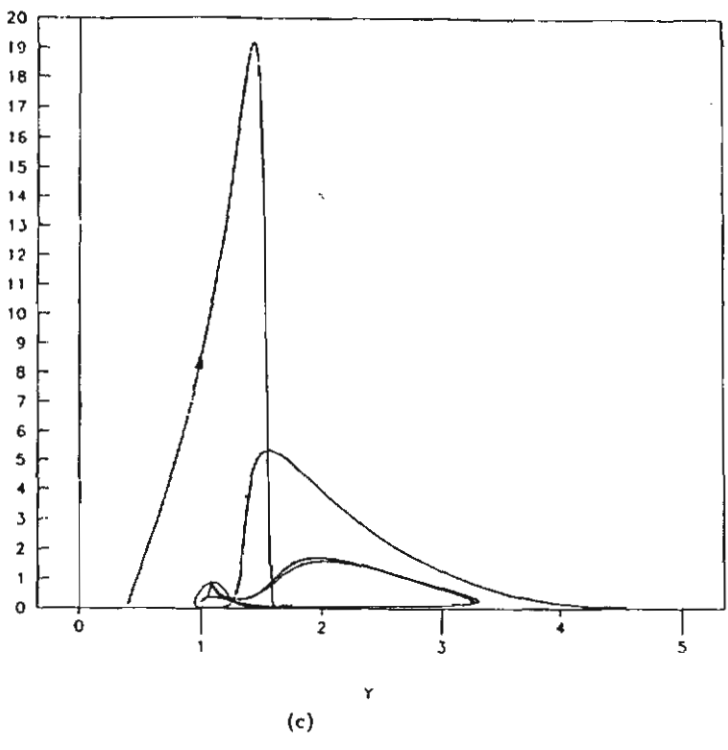


Figure 1. (cont.)

of the existing periodic solution, due to the eigenvalues $\pm i\omega$, giving rise to solution trajectories on a 2-torus in the five-dimensional phase space.

Now, with the above choice of parametric values, Hopf bifurcation occurs at a nonwashout steady state (x_S, y_S, z_S) , namely $y_S = \beta > 0$, and from (20),

$$z_S = z_0 + (\rho - \beta x_S) > 0,$$

while $x_S > 0$ by (27). In fact, the solution trajectory of the model equations (10)-(12) remains in the first octant $(x \ge 0, y \ge 0, z \ge 0)$ of the (x, y, z) space since, on substituting z = 0 into equation (12), we find

$$\frac{dz}{dT} = z_0 > 0, (28)$$

here. Also, on the (x, z) plane y = 0 so that

$$\frac{dy}{dT} = \beta > 0,$$

and on the plane x = 0, we have

$$\frac{dx}{dT} = 0,$$

so that the solution trajectory does not cross the coordinate planes.

In Figure 1, we present a computer simulation of the model equations (10)-(14) with $\omega \neq 0$ and parametric values chosen to satisfy the bifurcation requirements (26) and (27), that is, $\eta = 6$, $\beta = 1.5 = y_S$, $x_S = 0.5$, and $\rho = 11$. Then, from (25), we find

$$\delta_C = 0.125$$
.

Thus, we chose $\delta=0.241>\delta_C$, which gives $z_S=0.05$, M=2, while $\omega=1.256$, $\alpha=1.1$, and $z_0=0.2$. The solution trajectory is observed to approach the closed curve on the surface of a 2-torus surrounding the steady state $(x_S,y_S,z_S,u_S,v_S)=(0.5,1.5,0.05,0,0)$ in the 5-dimensional phase space, seen here projected onto the coordinate planes.

4. FORCE FIELD INTENSITY AND BIFURCATION DIAGRAM

We now investigate the influence of the force field intensity α on the dynamic behavior of the model system (10)-(14) by first showing that the smaller the force field intensity α , the closer to the plane $y = \beta$ will the solution trajectory on the 2-torus lie.

Letting

$$G(T) \equiv \frac{\eta z(T)}{z(T) + M},\tag{29}$$

we see by (28) that G(T) > 0 for all T. Thus, equation (12) can be written as

$$\frac{d(y-\beta)}{dT} = [-\alpha u - G(T)](y-\beta) - \alpha \beta u. \tag{30}$$

Using the Leibnitz' formula, we then find

$$y(T) - \beta = e^{\int_0^T (-\alpha u - G(\tau))d\tau} \left\{ \int_0^T e^{-\int_0^T (-\alpha u - G(u))du} (-\alpha \beta u)d\tau + C \right\}. \tag{31}$$

Letting

$$h(T) = \int_0^T G(\tau) d\tau, \tag{32}$$

it is easily seen that h(T) is an increasing function, and therefore, we have

$$y(T) - \beta = e^{-\alpha v(T) - h(T)} \left\{ C - \alpha \beta \int_0^T e^{\alpha v(\tau) + h(\tau)} u(\tau) d\tau \right\},\,$$

where $e^{-h(T)} \to 0$ as $T \to \infty$.

Since $e^{h(\tau)} \le e^{h(T)}$, $0 \le \tau \le T$, we have

$$\left| e^{-\alpha v(T) - h(T)} \int_0^T e^{\alpha v(\tau) + h(\tau)} u(\tau) d\tau \right| \leq e^{-\alpha v(T) - h(T)} e^{h(T)} \left| \int_0^T e^{\alpha v(\tau)} u(\tau) d\tau \right| = 1.$$

Therefore,

$$|y(T) - \beta| \le \alpha \beta$$
, as $T \to \infty$, (33)

which means that for small α , the time course of y(T) tends to a value close to β as time passes. In fact, if $\alpha = 0$, then we have

$$y(T) \to \beta$$
, as $T \to \infty$,

and the bifurcating solution trajectory eventually lies on the plane $y = \beta$. The expression (33), in fact, gives us a bound for the extent to which y will be perturbed from the value β .

Now, we have shown that the critical point (x_S, y_S, z_S) of the system of equations (10)-(12) with $\omega = 0$ loses its stability and a Hopf bifurcation occurs when the two complex conjugate eigenvalues λ_1 and λ_2 cross the imaginary axis. In other words, at the value δ_C of our bifurcation parameter δ , the two eigenvalues λ_1 and λ_2 have a vanishing real part. Figure 2 shows the stability region in the (x_S, δ) plane for a continuous stirred tank reactor modelled by equations (10)-(14) under the conditions $\beta = 1.5$, $\rho = 11$, and $\eta = 6$. The region is the union of two sets S_1 and S_2 , where

$$S_{1} = \{(x_{S}, \delta) \mid 0 < x_{S} < \rho \beta^{-1}, 0 < \delta < \delta_{C}\},$$

$$S_{2} = \{(x_{S}, \delta) \mid \rho \beta^{-1} < x_{S}\}.$$

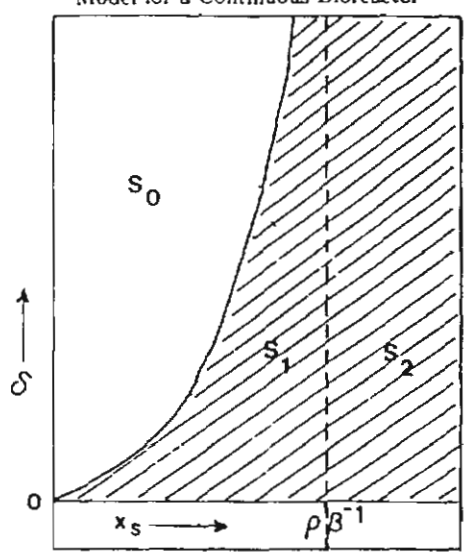


Figure 2. Stability diagram in the (x_S, δ) plane for the model system (10)-(14).

In $S_1 \cup S_2$, solution trajectories near the steady state solution $(x, y, z) = (x_S, y_S, z_S)$ remain close to that point as time passes.

On the other hand, in the instability region given by

$$S_0 = \{(x_S, \delta) \mid 0 < x_S < \rho \beta^{-1}, \delta_C < \delta < \infty\},\,$$

the reactor can exhibit bifurcation or chaotic behavior. The set is thus to be avoided from a control point of view. The transition from periodic orbits to chaos is known to occur after a cascade of period doubling, followed by the appearance of chaos windows. Following the work presented by Schaffer [14] on how nonlinear dynamics can elucidate mechanisms in ecology and epidemiology, we create a bifurcation diagram, shown in Figure 3, in the following manner. For each value of the force field intensity α , the simulation of the model equations (10)-(14), for parametric values in the region S_0 , is allowed to run for a sufficiently long period of time, then 40 data points $z(t_n)$, $n=1,2,\ldots,40$, are collected every interval of $2\pi/\omega$, the period of the external force field. That is,

$$T_n = T_0 + \frac{2n\pi}{\omega}, \qquad n = 1, 2, \dots, 40,$$

where $T_0 = 100$ in Figure 3. The values $\xi_n = \log z(T_n)$, $n = 1, 2, \ldots, 40$, are then plotted against α which ranges from 0 to 3. All other parametric values are the same in all computer simulations which generate the points in this figure. We see here that the solution is periodic for small α ; all 40 data points for each value of α apparently fall on the same spot in the (α, ξ) plane. Windows of chaos are observed for α in the approximate ranges $1.2 < \alpha < 1.9$ and $2.1 < \alpha < 3$, although the chaotic scatter of data points is more pronounced in the second range. The data points for each value of α no longer fall on the same spot, a characteristic which is markedly different from the behavior in the range where α is small.

In Figure 4, we investigate the behavior in the range $2.1 < \alpha < 3$ more closely. Here, we plot

$$H_n \equiv \xi_n - \frac{M_{\alpha} + m_{\alpha}}{2}, \qquad n = 1, 2, \dots, 40,$$

where

$$M_{\alpha} = \max_{n} \xi_{n}, \qquad m_{\alpha} = \min_{n} \xi_{n},$$

against α . We observe that at $\alpha = 2.1$, approximately, the 40 data points apparently fall on the same spot. As α increases, however, they bifurcate into two groups, one of which bifurcates

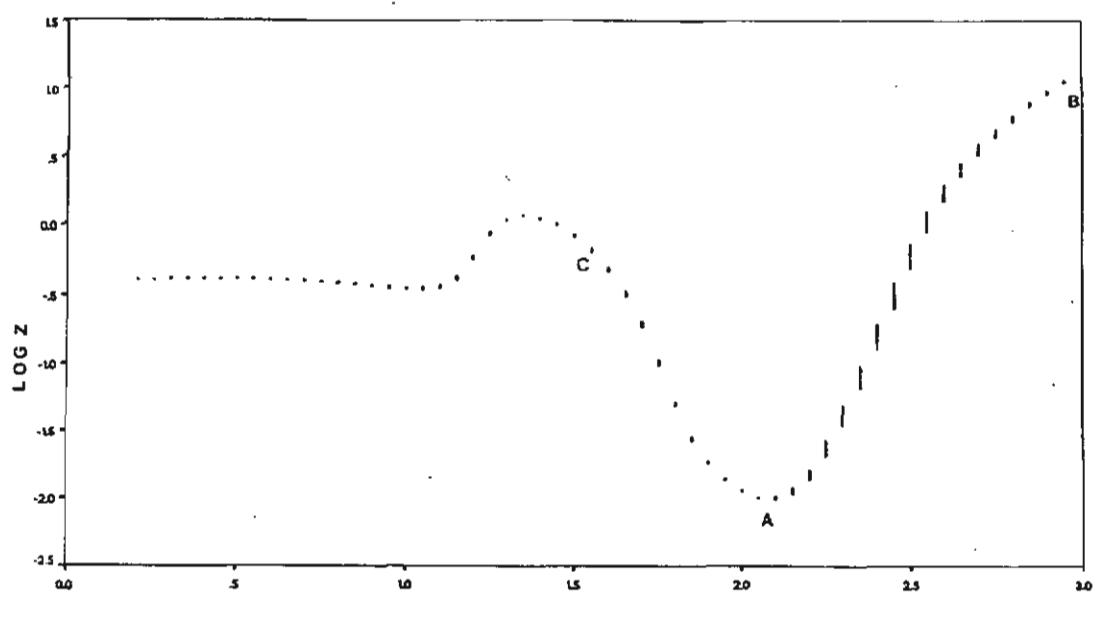


Figure 3. Bifurcation diagram of the model system (10)-(14) with parametric values in the region S_0 ; $\beta=1.5$, $\rho=11$, $\eta=6$, $\delta=0.241$, M=2, $\omega=1.256$, $z_0=0.2$, $x_S=0.5$, $y_S=1.5$, $z_S=0.05$: plot of $\log(z_n)$ versus α .

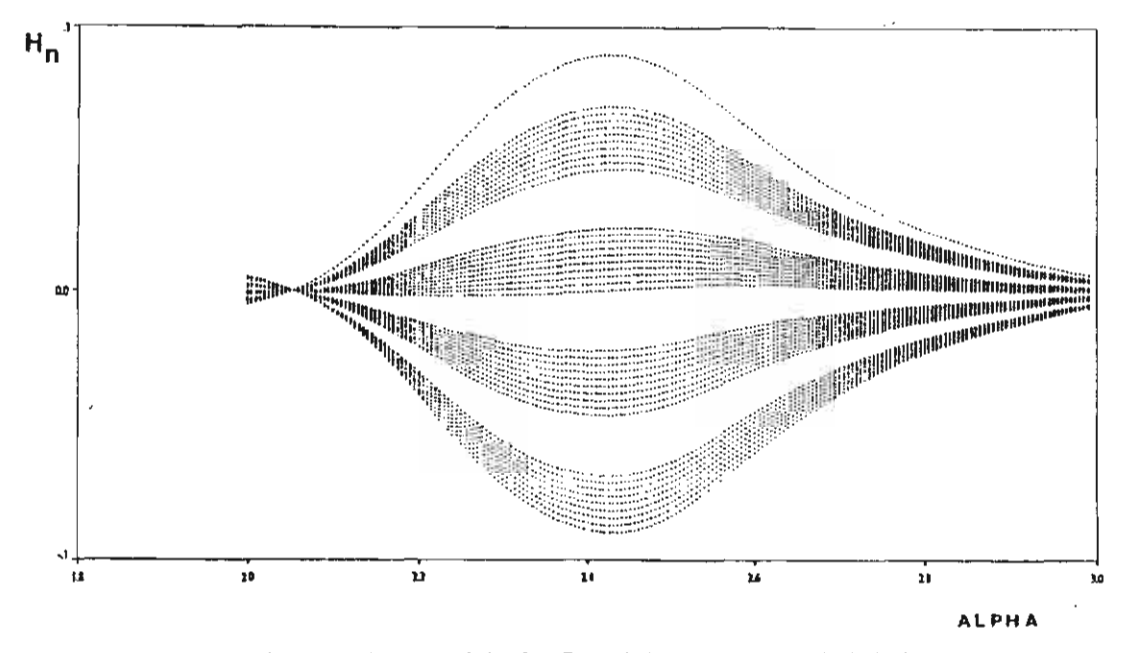


Figure 4. Bifurcation diagram of the CSTR modelled by equations (10)–(14) in the range $2 < \alpha < 3$ with parametric values of Figure 3: plot of H_n versus α .

further into four. For α around 2.45, the solution is apparently no longer periodic. We do not obtain the same value of z(T) every interval of $2\pi/\omega$. A similar chaos window can be observed for α between the values 1.2 and 1.9, approximately, although not so marked. Periodicity is recaptured, however, at α around 2.1 and 3.0 (points A and B, respectively).

Finally, Figure 5 shows the time course of z(T) for parametric values of Figure 3, but with $\alpha = 1.5$, inside the range of a chaos window (point C). The solution is no longer periodic, as is born out by the bifurcation diagram in Figure 3. Similar dynamic behavior of this type has previously been observed in a model for the spread of measles reported in [14], where an increase

Alpha

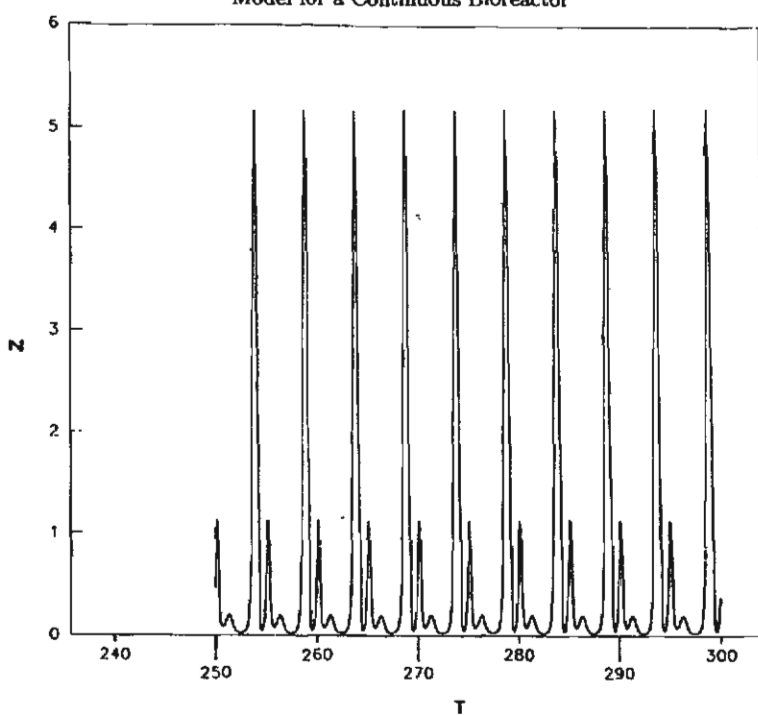


Figure 5. The time course of the simulated substrate concentration z with $\alpha = 1.5$ and other parametric values as in Figure 3.

in the amplitude of an external factor can drive the system into behaving in such an unpredictable manner.

5. CONCLUSIONS

We have investigated the dynamic behavior of a continuous stirred tank reactor modelled by cells and substrate balance equations which have been extended to incorporate the effect of external forces, such as the earth's magnetic field, on the cell membrane permeability. From considerations of the relationship between the anisotropy of the liquid crystals and the permeability of the cytoplasmic membrane, it is deduced that the membrane permeability varies with time in a sinusoidal fashion. The equation for the dynamics of variation in the permeability is then derived, taking into account also the increase in the apparent permeability due to the newly-formed cells.

The balance equation for the nutrient uptake rate is also adjusted to take into account the direct relationship between the membrane permeability and the number of active transport sites.

Bifurcation analysis done on the resulting model equations shows that, for suitable ranges of parametric values, the model system admits oscillatory behavior as a result of a Hopf bifurcation on top of the existing periodic solution due to the sinusoidal variation in the membrane permeability. Consequently, if parametric values satisfy the conditions put down in the theorem, the model system will have a solution whose phase space trajectory eventually lies on the surface of a 2-torus.

Particular attention is then devoted to the identification of the operating zones in which it is possible to carry out the continuous process while avoiding undesirable complex dynamic behavior. Owing to the importance of the process and the hazardous nature of the compounds which might be involved, we have attempted to identify the ranges of control parameters (δ and x_S , specifically) to be avoided since they correspond to the region where complex dynamic behavior is possible. The appearance of chaos windows for ranges of the external force field intensity identified in the bifurcation diagrams is not only undesirable for control and design problems, it can also give rise to potentially dangerous situations in the case where toxic compounds are involved, such as in the operation of wastewater treatment processes. Clearly, further theoret-

ical studies must be carried out to shed more light onto this complicated, but most frequently observed dynamic behavior.

REFERENCES

- O. Paladino, Transition to chaos in continuous processes: Applications to wastewater treatment reactors, Environmetics 5, 57-70 (1994).
- 2. P. Agrawal, C. Lee, H.C. Lim and D. Ramkrishna, Theoretical investigations of dynamic behavior of isothermal continuous stirred tank biological reactors, *Chemical Engineering Science* 37, 453-462 (1982).
- L. Pellegrini and G. Biardi, Chaotic behavior of a controlled CSTR, Computers and Chemical Engineering 14, 1237-1247 (1990).
- 4. J. Cheng-Fu, Existence and uniqueness of limit cycles in continuous cultures of micro-organisms with non-constant yield factor. Universita degli studi di Bari, Italy, (preprint).
- 5. T. Yano, Dynamic behavior of the chemostat subject to substrate inhibition, Biotechnology and Bioengineering 11, 130-153 (1960).
- Y. Lenbury, B. Novaprateep and B. Wiwatpataphee, Dynamic behavior classification of a model for a continuous bio-reactor subject to product inhibiton, Mathl. Comput. Modelling 19 (12), 107-117 (1994).
- L. Yerushalmi, B. Volesky, J. Votruba and L. Molnar, Circadian rhythmicity in a fermentation process, Appl. Microbiol. Biotechnol. 30, 460-474 (1989).
- D.S. Thomas and A.H. Rose, Inhibitory effect of ethanol on growth and solute accumulations by Saccharomyces cerevisiae as affected by plasma-membrane lipid composition, Arch. Microbiol. 122, 49 (1979).
- 9. A.A. Herrero and R.F. Gomez, Development of ethanal tolerance in clostridium thermorellum: Effects of growth temperature, Appl. Environ. Microbiol. 40, 571 (1980).
- C.J. Panchal and G.G. Stewart, Regulatory factors in alcohol fermentations, Proc. Int. Yeast Symp. 5, 9 (1981).
- F.T. Hong, Photoelectric and magneto-orientation effects in pigmented biological membranes, J. Colloid and Interface Sci. 58, 471 (1977).
- 12. A.P. Dubrov, The Geomagnetic Field and Life, Plenum Press, New York, pp. 20-45, (1974).
- J.E. Marsden and M. McCracken, The Hopf Bifurcation and its Applications, Springer-Verlag, New York, pp. 65-135, (1976).
- S. Schaffer and W.M. Can, Nonlinear dynamics elucidate mechanisms in ecology and epidemiology, IMA J. Math. Appl. Med. Biol. 2, 221-252 (1985).

1.3 แฟกเตอร์ที่สามที่ผู้วิจัยกำนึงถึงอีกแฟกเตอร์หนึ่งคือ ผลผลิต (product) ของขบวน การหมัก ซึ่งเมื่อ product นี้ มีปริมาณมากขึ้นก็สามารถมีผลทำให้อัตราการเพิ่มจำนวนของ x ลดลง ได้ เช่น ขบวนการในปฏิกรณ์ต่อเนื่อง (continuous bio-reactors) จะพบว่า product เป็นก๊าซ เช่น ethanol หรือเป็น cells killing products อื่น ๆ ซึ่งเป็นผลพวงของขบวนการนั้น ๆ จะสามารถ inhibit การเจริญเติบโต หรือการขยายพันธุ์ของ x ได้ ในขณะที่ระดับของเหยื่อ หรือสารอาหารที่มีสูงเกินไป ก็สามารถ inhibit การขยายพันธุ์ของ x ได้เช่นกัน

ผู้วิจัยจึงได้นำ model ต้นแบบ (2) และ (3) มาปรับเปลี่ยนเพิ่มเติมสมการที่สามซึ่งคิดถึงการ เปลี่ยนแปลงในระคับของ product P(t) และได้เป็นระบบสมการไม่เชิงเส้น 3 สมการ คังนี้

$$\frac{dS}{dt} = D(S_F - S) - \frac{\mu x}{Y}$$
 (22)

$$\frac{\mathrm{dx}}{\mathrm{dt}} = \mu \mathbf{x} - \mathbf{D}\mathbf{x} \tag{23}$$

$$\frac{\mathrm{dP}}{\mathrm{dt}} = \eta_0 \mu x - \mathrm{DP} \tag{24}$$

โดยที่

$$\mu = \frac{kSe^{-\frac{S}{K_S}}}{\left\{1 + \frac{P}{K_P}\right\}} \tag{25}$$

โดยการวิเคราะห์ด้วย singular perturbation technique เราสามารถแสดงได้ว่า ถ้าเงื่อนไข ต่อไปนี้เป็นจริง

$$a > 1 \tag{26}$$

$$\beta > 1 - \frac{1}{a} - \frac{1}{a^2} \tag{27}$$

$$e^{a} < \frac{\omega}{d_{2}} < ae \left[\frac{\varepsilon \eta d_{1}}{\gamma d_{3}} \left(1 - \frac{1}{a} \right) \left(\frac{1}{a} + \beta \right) + 1 \right]$$
 (28)

แถะ

$$\frac{\eta d_1 \beta}{\gamma d_2} > \frac{1}{ae} \tag{29}$$

ระบบสมการ (22)-(25) จะมีคำตอบที่เป็นคาบ ซึ่งผลงานในขั้นต้นนี้ได้นำเสนอในการประชุมวิชาการ นานาชาติ International Conference on Dynamical Systems and Differential Equations ที่ Southwest Missouri State University ณ ประเทศสหรัฐอเมริกา และได้รับตีพิมพ์ใน Proceedings ของการประชุมแล้ว ดังเอกสารที่ได้แนบมาต่อไปนี้

ทั้งนี้ผู้วิจัยยังได้คำเนินการวิจัยต่อให้ละเอียด และสมบูรณ์ขึ้น แล้วนำเขียนขึ้นเป็น paper และ submitted for publication ในวารสาร Mathematical Modelling of Systems แล้ว ดังที่จะสามารถอ่าน ดูรายละเอียดของการวิเคราะห์วิจัยได้ในเอกสารที่แนบมาด้วยนี้เช่นกัน A Singular Perturbation Analysis of a Product Inhibition

Model for Continuous Bio-Reactor

A SINGULAR PERTURBATION ANALYSIS OF A PRODUCT INHIBITION MODEL FOR CONTINUOS BIO-REACTORS

Y. LENBURY Department of Mathematics, Faculty of Science, Mahidol University, Bangkok, Thailand.

N. TUMRASVIN Department of Mathematics, Faculty of Science, Mahidol University, Bangkok, Thailand.

ABSTRACT

A model of a continuous bio-reactor subject to product inhibition is considered where a one hump substrate-limited specific growth rate is used. Analysis of the model is carried out through singular perturbation arguments which allow us to derive explicit conditions on the parameters that identify different dynamic behavior of the system, and specifically ascertain the existence of a limit cycle composed of a concatenation of catastrophic transitions occurring at different speeds. Moreover, the interactions between the limiting substrate and the growing microorganisms can give rise to high-frequency oscillations, which can arise during the transients toward the attractor or during the low-frequency cycle. This periodic burst of high-frequency oscillations develops as a result of the effective product inhibitory mechanisms. The analysis helps us in identifying the safe operating region in which undesirable complexed dynamic behavior may be avoided.

1 INTRODUCTION

Viewing the behavior of microbial cultures within the framework of lumped kinetic models, a multitude of models have been proposed and theoretically studied in diverse ways since the model due to Monod [1] fashioned after Michaelis-Menten kinetics for single enzyme-substrate reactions.

In [2], Yano and Koga made a theoretical study on the behavior of a single-vessel continuous fermentation subject to a growth inhibition at high concentration of the rate limiting substrate S. They used the following expression for their continuous fermentation system:

$$\mu = \frac{\mu_{m}}{(K_{s}/S) + 1 + \sum_{i=1}^{n} (S/K_{j})^{j}}$$
(1)

where μ_m and the K's are positive constants and n is a positive integer. Other workers [3-5] have adopted simpler specific growth rate functions involving less control parameters but exhibiting similar necessary characteristics as the usual substrate inhibition model, for example the one hump substrate inhibition function

$$\mu = kSe^{-S/K_s} \tag{2}$$

where k and K_s are positive constants.

Later, Yano and Koga discussed in [6] the nature of the chemostat in which the specific growth rate depends on the concentrations of both a substrate and an inhibitory product of a microorganism. They assumed the specific growth rate equation as follows;

$$\mu = \frac{\mu_{m}S}{\left(K_{s} + S\right)\left\{1 + \left(\frac{P}{K_{p}}\right)^{n}\right\}}$$
(3)

They showed, with the analog computer, that when the product formation was negatively growth-associated, diverging as well as damped oscillations appeared. No oscillations could be observed, on the other hand, when the product formation was either completely growth-associated, or partially growth-associated. Oscillation phenomena are, however, not unusual in continuous cultures [3]. Since such penchant for periodicity is undesirable from the point of view of process control, it is necessary to identify the safe operating regions in which complexed dynamic behavior may be avoided.

In [4], the dynamic behavior of a chemostat subject to product inhibition was analyzed and classified in terms of multiplicity and stability of steady states and limit cycles. The substrate was assumed to be in sufficient supply so that the model was reduced to a system of two nonlinear differential equations involving only the cells and product concentrations.

In this paper, we consider the full three-variable product inhibition model consisting of the following nonlinear differential equations (described in more detail in [6]):

$$\frac{dS}{dt} = D(S_F - S) - \frac{\mu}{Y}X$$
 (4)

$$\frac{\mathrm{dX}}{\mathrm{dt}} = \mu \mathbf{X} - \mathbf{DX} \tag{5}$$

$$\frac{dP}{dt} = \eta_0 \mu X - DP \tag{6}$$

where X(t) denotes the cells concentration at time t; S(t) the substrate concentration at time t; P(t) the product concentration at time t; S_F the concentration of the feed substrate; Y the cells to substrate yield; P(t) the dilution rate; and P(t) the constant for product formation. Equations (4) and (5) are based on the well known Monod's model for cells and substrate interaction, described in more detail in reference [1]. To take into account the inhibitory effects of the substrate as well as the product increase in the chemostat, however, we adopt the following expression for the specific growth rate function:

$$\mu = \frac{kSe^{-\frac{S}{K_s}}}{1 + \frac{P}{K_P}} \tag{7}$$

Further, the cells to substrate yield Y is assumed to vary linearly with the substrate level at any time t, allowing for the positively-growth associated situation; namely

$$y = AS + B \tag{8}$$

Such substrate dependent yield has been used previously by several other workers in this field [3-5].

Equation (6) describes the change in the product concentration as X and S change. The first term on the right of this equation is the contribution to the rate of change in P, which is assumed to vary directly as the rate at which X increases, η_0 being the positive constant of variation. The cells X, substrate S, and product P are extracted from the chemostat at a constant dilution rate D, and hence the terms -DS, -DX, and -DP in the three model equations (4) through (6).

The analysis of the model is done through a singular perturbation argument, assuming that the substrate concentration exhibits fast dynamics. The time responses of the different components in the system are assumed to decrease dynamically from top to bottom. The structure of the corresponding attractors and the nature of the transients are then analyzed. It is shown that the model system can exhibit low-frequency cycles in which periodic bursts of high-frequency oscillations may develop giving rise to more complexed dynamical behavior for specified ranges of the system parameters.

2 SYSTEM MODEL

In order to analyze the model system of equations (4), (5) and (6), together with (7) and (8) through the singular perturbation technique, we scale the dynamics of the three hierarchical components of the system by means of two small dimensionless positive parameters ε and δ ;

namely, we let
$$x=\frac{S}{S_F}$$
, $y=X$, $z=\frac{P}{\epsilon K_P}$, $d_1=D$, $d_2=\frac{D}{\epsilon}$, $d_3=\frac{D}{\epsilon\delta}$, $\omega=\frac{kS_F}{\epsilon}$,
$$\eta=\frac{\eta_0\omega}{\epsilon\delta K_P}$$
, $\gamma=\frac{k}{AS_F}$, $\beta=\frac{B}{AS_F}$, and $a=\frac{S_F}{K_S}$.

We are led to the following system of differential equations:

$$\frac{dx}{dt} = d_1(1-x) - \frac{\gamma x e^{-ax} y}{(x+\beta)(1+\varepsilon z)} = f(x,y,z)$$
 (9)

$$\frac{\mathrm{d}y}{\mathrm{d}t} = \varepsilon y \left[\frac{\omega x \mathrm{e}^{-\mathrm{a}x}}{1 + \varepsilon z} - \mathrm{d}_2 \right] = \varepsilon \mathrm{g}(x, y, z) \tag{10}$$

$$\frac{dz}{dt} = \varepsilon \delta \left[\frac{\eta x e^{-ax}}{1 + \varepsilon z} y - d_3 z \right] = \varepsilon \delta h(x, y, z)$$
 (11)

Thus, with ε and δ small, the equation of the substrate concentration represents the fast system, while that of the cells and product concentrations represent the intermediate and the slow systems respectively. Under suitable regularity assumptions, the singular perturbation method allows us to approximate the solution of the system (9)-(11) with a sequence of simple dynamic transitions along the various equilibrium manifolds of the system and occurring at different speeds. The resulting path, composed of all such transitions, approximates the solution of the system in the sense that the real trajectory is contained in a tube around these transients, and that the radius of the tube goes to zero with ε and δ . The formal proof of this is not given because it is long and trivial and has already been discussed and extensively used in the literature [7-10].

3 EXISTENCE OF LIMIT CYCLE

We now show that if ε and δ are sufficiently small and

$$a > 1 \tag{12}$$

$$\beta > 1 - \frac{1}{a} - \frac{1}{a^2} \tag{13}$$

$$e^{a} < \frac{\omega}{d_{2}} < ae \left[\frac{\varepsilon \eta d_{1}}{\gamma d_{3}} \left(1 - \frac{1}{a} \right) \left(\frac{1}{a} + \beta \right) + 1 \right]$$
 (14)

$$\frac{\eta d_1 \beta}{\gamma d_3} > \frac{1}{ae} \tag{15}$$

then a limit cycle exists for the model system (9)-(11).

We first prove that inequalities (12)-(15) guarantee that the geometry of the manifolds f = 0, g = 0 and h = 0 is as in Fig. 1.

Manifold f = 0

We observe that this manifold is given by the equation

$$y = \frac{d_1}{\gamma} (1 - x)(x + \beta)(1 + \varepsilon z) \frac{e^{ax}}{x}$$
 (16)

which defines a surface $y = \varphi(x, z)$ which intersects the (x, y) plane along the curve

$$y = \frac{d_1}{\gamma} (1 - x)(x + \beta) \frac{e^{ax}}{x}$$
 (17)

From equation (16), it is seen that the manifold intersects the (x,z) plane along the line x = 1 as shown in Fig. 1.

The slope of the curve in (17) is given by

$$\frac{\mathrm{d}y}{\mathrm{d}x} = \frac{\mathrm{d}_1}{\gamma} \frac{\mathrm{e}^{\mathrm{a}x}}{\mathrm{x}^2} F(x) = \frac{\mathrm{d}_1}{\gamma} \frac{\mathrm{e}^{\mathrm{a}x}}{\mathrm{x}^2} \left[-x^3 + (\mathrm{a} - \mathrm{a}\beta - 1)x^2 + \mathrm{a}\beta x - \beta \right] \tag{18}$$

which may vanish for some values of x < 1.

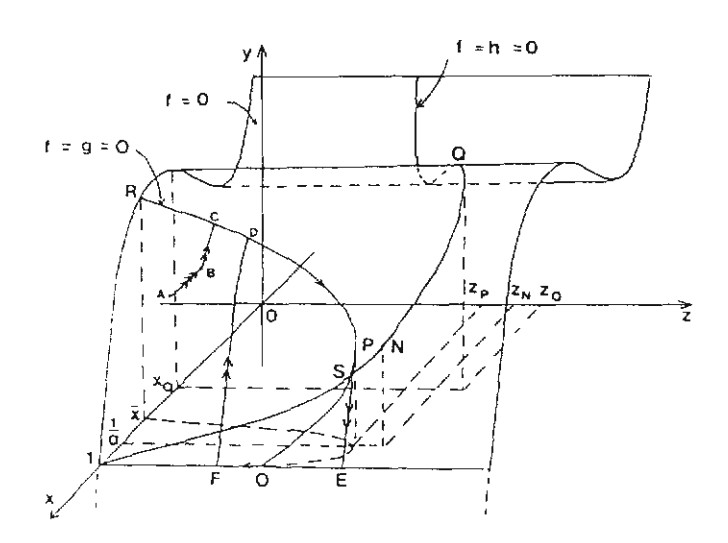


Figure 1 Equilibrium manifolds of the model system (9)-(11). In this case, transitions of different speeds develop into a closed cycle, where one, two and three arrows indicate transitions at low-, intermediate-, and high-speed, respectively.

Manifold g = 0

This manifold consists of 2 parts; the trivial manifold y = 0 and the nontrivial manifold given by the equation

$$\frac{xe^{-ax}}{1+\varepsilon z} = \frac{d_2}{\omega} \tag{19}$$

which defines a surface $z = \psi(x)$. We observe that at $x = \frac{1}{a}$

$$\frac{\mathrm{d}z}{\mathrm{d}x} = 0$$

and so inequality (12) ensures that the point $P(x_p, y_p, z_p)$ in Fig. 1 is located on the manifold f = 0 at the point where $x_p = \frac{1}{2} < 1$.

We also need the point P to be located on the stable part of the manifold f = 0. This is guaranteed by requiring that

$$F\left(\frac{1}{a}\right) < 0 \tag{20}$$

which is equivalent to inequality (13)

The manifolds f = 0 and g = 0 intersect along the curve given by

$$y = \frac{d_1\omega}{d_2\gamma}(1-x)(x+\beta)$$

reaching a maximum at the point $M(x_M, y_M, z_M)$ where

$$x_{M} = \frac{1-\beta}{2}$$

Finally, the curve f = g = 0 intersects the (x,z) plane at the point $O(x_0, y_0, z_0)$ where $x_0 = 1$ and, from (19),

$$z_0 = \frac{1}{\varepsilon} \left(\frac{\omega}{d_2 e^a} - 1 \right) \tag{21}$$

We see, therefore, that the left side of inequality (14) guarantees that $z_0 > 0$.

Thus, the manifold f = g = 0 is shaped as shown in Fig. 1. We note that the point R may be located on the unstable part of the manifold f = 0. However, the transients also develop into a limit cycle in the case that inequalities (12)-(15) are satisfied.

Manifold h = 0

This manifold is given by the equation

$$z = \frac{\eta x y e^{-ax}}{d_3(1 + \varepsilon z)} \tag{22}$$

which defines a surface $z = \rho(x, y)$. This intersects the manifold f = 0 along the curve

$$z = \frac{\eta d_1}{\gamma d_3} (1 - x)(x + \beta) \tag{23}$$

using equation (16). Thus, z reaches a maximum along this curve at the point $Q(x_Q, y_Q, z_Q)$ where $x_Q = \frac{1}{2}(1-\beta) = x_M$

Also, the curve f = h = 0 intersects the (x,z) plane at the point (1,0,0) as seen in Fig. 1. If we let $N(x_N, y_N, z_N)$ be the point on the curve f = h = 0 with $x_N = \frac{1}{a}$, then from equation (23) we find that

$$z_{N} = \frac{\eta d_{1}}{\gamma d_{3}} \left(1 - \frac{1}{a} \right) \left(\frac{1}{a} + \beta \right) \tag{24}$$

while, from equation (19), we find that

$$z_{\mathbf{P}} = \frac{1}{\varepsilon} \left(\frac{\omega}{\text{aed}_2} - 1 \right) \tag{25}$$

Therefore, so that the equilibrium point S where the curves f = g = 0 and f = g = 0 intersect should be located on the unstable part of the manifold f = g = 0, we require

$$Z_p < Z_N$$

which is exactly the right side of inequality (14).

Finally, along this curve f = h = 0 given by equation (23),

$$z = \frac{\eta d_1}{\gamma d_3}$$

when x = 0, and therefore inequality (15) guarantees that the curve f = h = 0 crosses the curve f = g = 0 only once at the point S.

Now, starting from a point A = (x(0), y(0), z(0)) (see Fig. 1 where low-, intermediate-, and high-speed trajectories are indicated, respectively, with one, two, and three arrows) at first a high-speed transition develops at constant y and z while only the fast system

$$\dot{x} = f(x(t), y(0), z(0))$$

is active and the intermediate (y) and slow (z) variables are frozen at their initial values y(0) and z(0). The high speed transition brings the system to the point B on the stable part of the fast manifold f=0, at which point the intermediate system has now become active. A second intermediate-speed transition takes place on the manifold at constant x (segment AB in Fig. 1) until the point C is reached. A slow transition is then made along the curve f=g=0 until the point P is reached where the stability of the equilibrium manifold g=0 is lost and a quick transition then takes the state of the system to the equilibrium point E on the stable trivial manifold y=0. A slow transition then develops along this manifold until a point is reached where the stability is again lost at some point F beyond O (see Fig. 1). The proof of the existence and location of such a point \dot{F} is lengthy and can be found in Schecter and Osipove et al. [11,12]. At this point a quick jump again takes us back to the point D on the stable manifold f=g=0, resulting in a closed cycle DPEF lying on the equilibrium manifold f=0.

Fig. 2 shows numerical simulation of the model equations (9)-(11) with parametric values chosen to satisfy inequalities (12)-(15). The trajectory is seen here to develop into a low-frequency limit cycle as theoretically predicted. The time courses of the three variables in this case are shown in Fig. 3.

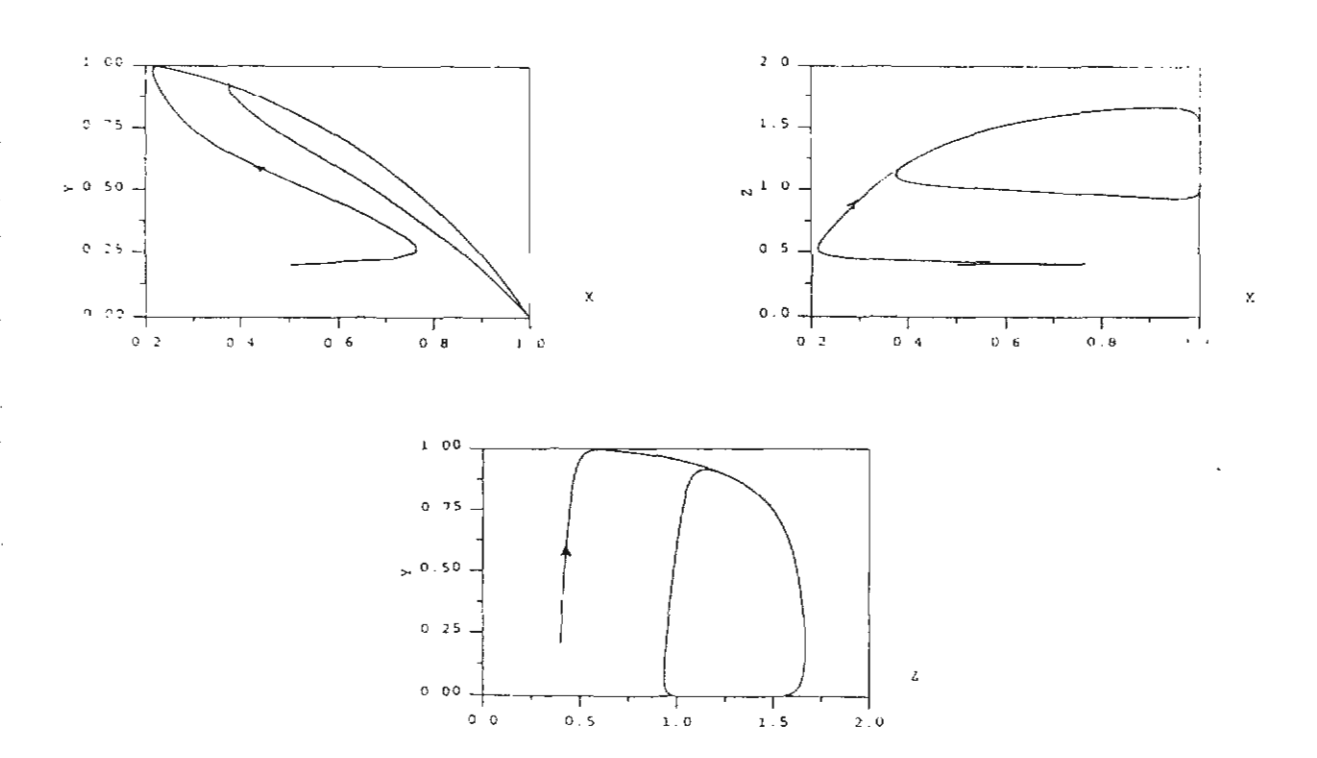
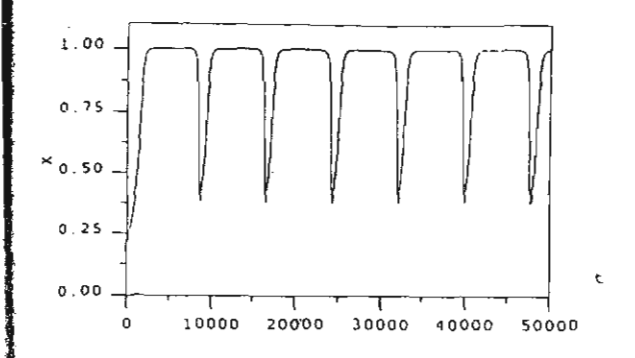
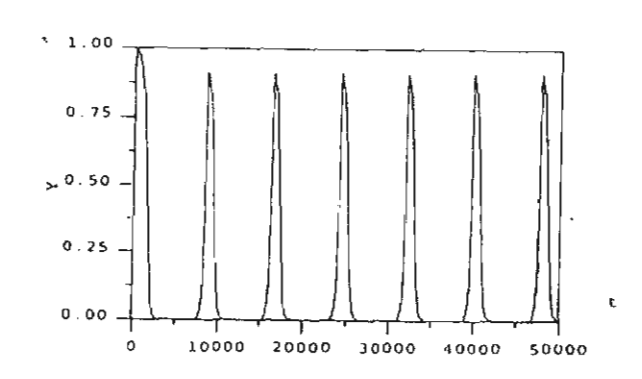


Figure 2 Numerical simulation of the model equations (9)-(11) where the parametric values have been chosen to satisfy inequalities (12)-(15), so that the solution trajectory tends toward a low-frequency limit cycle as theoretically predicted. Here, $\varepsilon = 0.1$, $\delta = 0.01$, $\beta = 0.8$, $\gamma = 2.0$, $\eta = 10.0$, $\omega = 3.0$, $\alpha = 1.5$, $\alpha = 0.25$, $\alpha = 0.3$, $\alpha = 0.1$, $\alpha = 0.25$, $\alpha = 0.3$, $\alpha = 0.1$, $\alpha = 0.25$, $\alpha = 0.3$





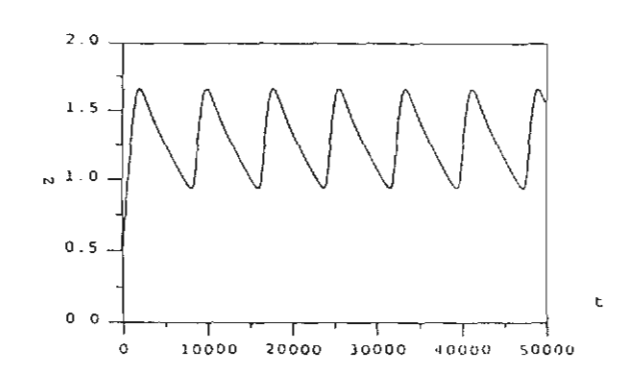


Figure 3 The time courses of the three variables x(t), y(t), and z(t) are shown here corresponding to the case seen in Fig. 2. Here, $\varepsilon = 0.1$, $\delta = 0.01$, $\beta = 0.8$, $\gamma = 2.0$, $\eta = 10.0$, $\omega = 3.0$, $\alpha = 1.5$, $\alpha = 0.25$, $\alpha = 0.3$, $\alpha = 0.1$, $\alpha = 0.1$, $\alpha = 0.25$, $\alpha = 0.25$, $\alpha = 0.3$, $\alpha = 0.1$, $\alpha = 0.1$, $\alpha = 0.25$, $\alpha = 0.3$

4 BURSTS OF HIGH-FREQUENCY OSCILLATIONS

For the occurrence of periodic burst of high-frequency oscillations during each low-frequency cycle, we further require that the manifold f = 0 has an unstable portion. This is equivalent to requiring that the slope given by equation (18) is positive at some value of x < 1, say $x = \frac{1}{3}$.

Letting $x = \frac{1}{3}$ in (18) leads to the following inequality

$$\beta < \frac{3a-4}{27-6a} \tag{26}$$

which ensures that the curve $y = \varphi(x,0)$ has positive slope on some interval containing the point $x = \frac{1}{3}$.

Combining inequalities (13) and (26) leads to the requirement that

$$1 - \frac{1}{a} - \frac{1}{a^2} < \beta < \frac{3a - 4}{27 - 6a} \tag{27}$$

It is also necessary to have

$$F(\overline{x}) > 0 \tag{28}$$

so that the point R should be located now on the unstable branch of the manifold f = 0. This is easily accomplished by letting

$$\bar{\mathbf{x}} = \frac{1}{3} - \theta \tag{29}$$

for a sufficiently small θ , then simply set

$$\frac{d_2}{\omega} = \overline{x}e^{-\overline{x}} = (\frac{1}{3} - \theta)e^{-(1/3 - \theta)}$$
(30)

Finally, in order that the transition goes back into high-frequency oscillations in each low-frequency cycle, we require $z_0 < z_M$, which is equivalent to

$$e^{-a} < \frac{1-\beta}{2} e^{-a(1-\beta)/2}$$
 (31)

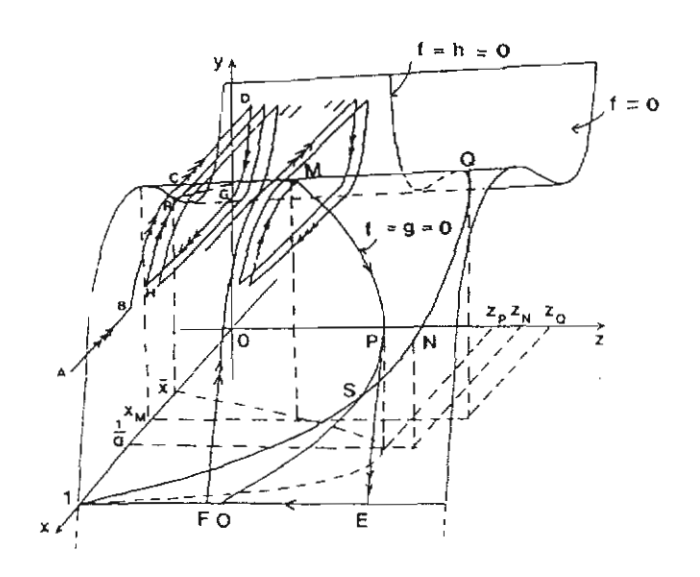


Figure 4 Equilibrium manifolds of the model system (9)-(11). In this case, transitions of different speeds develop into a low-frequency cycle with a period of high-frequency oscillation as identified in the text.

With all the above inequalities being satisfied, the equilibrium manifolds are shaped as shown in Fig. 4. Starting from the point A, a fast transition takes us, as explained earlier, to the point B on f = 0. An intermediate transition develops on this manifold until C is reached where the stability of the equilibrium fast manifold is lost. A fast transition then takes the system to the stable equilibrium point D. An intermediate speed transition is then made along this branch of manifold until G is reached where the stability is again lost and a quick jump brings us to the stable point H. This almost closes up the cycle but just misses the point B. The slow system has become active and z has been slowly increasing since $\dot{z} > 0$ here. Transitions then develop following the same pattern but with slowly varying z as seen in Fig. 4 until M is reached, at which point the trajectory develops into a slow cycle which goes back into the fast cycles since inequality (31) guarantees that $z_F < z_M$.

Thus, we have proved, by the above discussions, the following theorem

THEOREM If inequalities (12), (14), (15), (27), (30) and (31) hold then the system of equations (9)-(11) has a periodic solution which will be a low-frequency limit cycle containing high-frequency oscillations if ε , δ , and θ are sufficiently small.

Fig. 5 shows numerical simulation of the model equations (9)-(11) with parametric values chosen to satisfy all inequalities mentioned in the above theorem. The corresponding time courses of the three variables are shown in Fig. 6, where the burst of high frequency oscillations is observed in each low-frequency cycle.

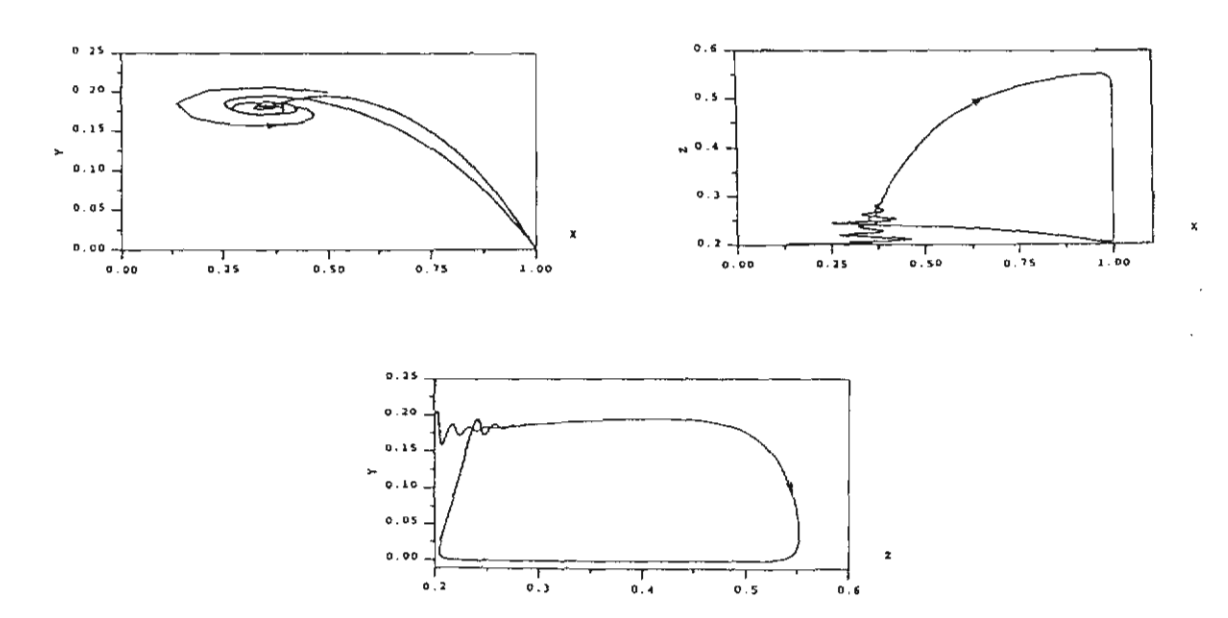


Figure 5 Numerical simulation of the model equations (9)-(11) where the parametric values have been chosen to satisfy all the inequalities set out in the Theorem. The solution trajectory is a low-frequency limit cycle which contains a period of high-frequency oscillations. Here, $\epsilon = 0.1$, $\delta = 0.01$, $\beta = 0.02$, $\gamma = 2.0$, $\eta = 10.0$, $\omega = 3.0$, $\alpha = 1.5$, $\alpha = 0.25$, $\alpha = 0.5$,

 $d_3 = 0.1$, x(0) = 0.5, y(0) = 0.2, and z(0) = 0.2.

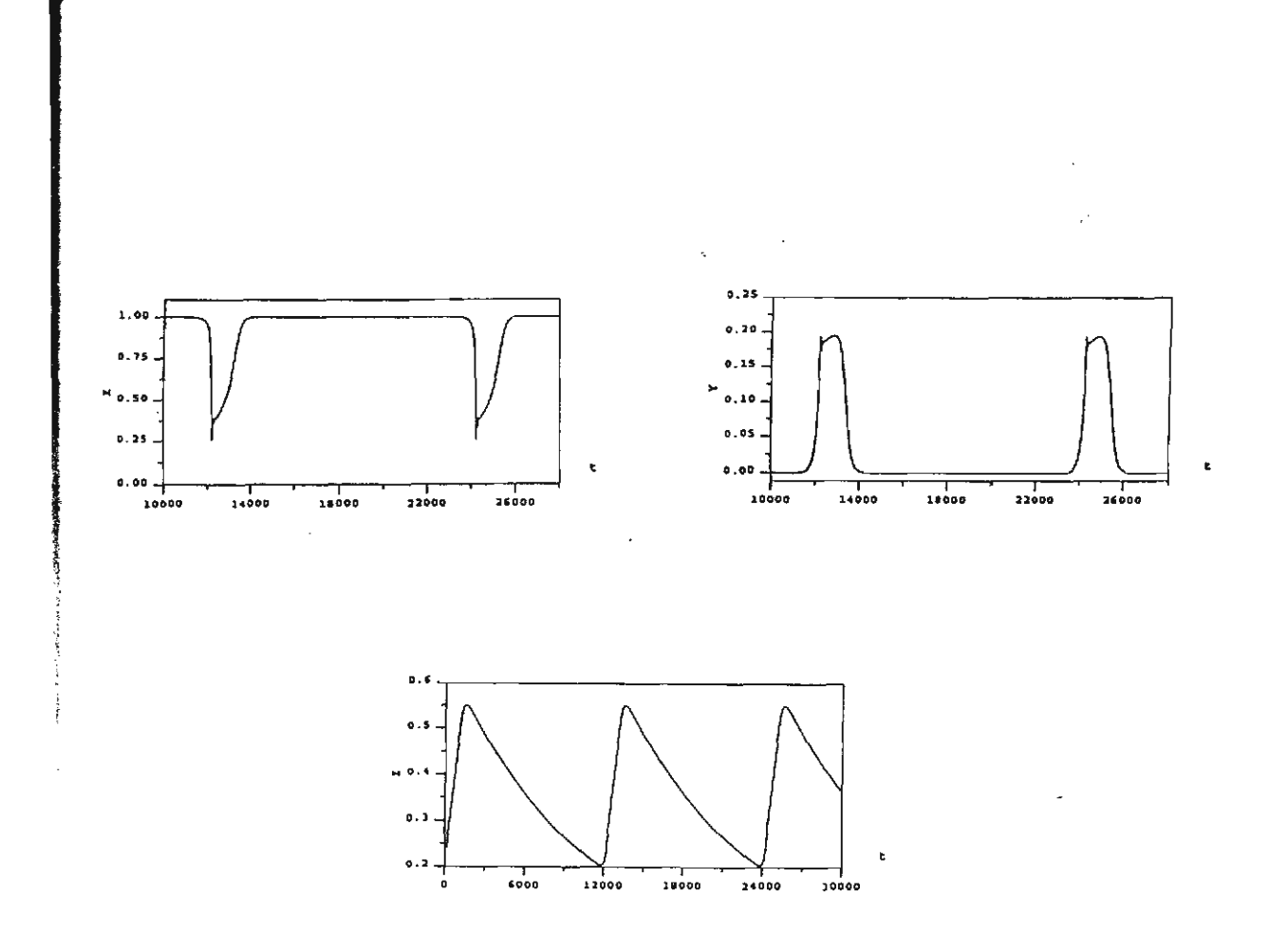


Figure 6 The time courses of the three varibles x(t), y(t), and z(t) corresponding to the case seen in Fig. 4 are shown here, where periodic bursts of high-frequency oscillations are clearly observed. Here, $\epsilon = 0.1$, $\delta = 0.01$, $\beta = 0.02$, $\gamma = 2.0$, $\eta = 10.0$, $\omega = 3.0$, a = 1.5, $d_1 = 0.25$, $d_2 = 0.5$, $d_3 = 0.1$, x(0) = 0.5, y(0) = 0.2, and z(0) = 0.2.

5 CONCLUSION

The dynamic behavior of a continuous bio-reactor described by equations (9)-(11) has been sinvestigated in this paper. Assuming that the time responses of the three components are highly diversified, increasing from bottom to top, we were able to use standard singular perturbation analysis to describe the nature of the transients and the attractors of the system.

Complexed oscillatory behavior is extremely undesirable not only for control and design problems, but also for its potential for dangerous situations which may result in the case where toxic compounds are involved, such as in the operation of toxic waste treatment processes. Insights that can be gained from this type of analysis described above should prove most valuable in the light of such considerations.

ACKNOWLEDGMENT

Appreciation is rendered to the Thailand Research Fund for the financial support which made possible this research project.

REFERENCES

- J. Monod, recherces pur la croessance des cultures bacteriennes, Hermann et Cie, Paris (1942).
- 2. T. Yano. and S. Koga, Dynamic Behavior of the Chemostat Subject to Substrate Inhibition, Biotechnology and Bioengineering. 11: 139-153 (1969).
- 3. P. Agrawal, C. Lee, H.C., Lim and D. Ramkrishna, Theoretical Investigations of Dynamic Behavior of Isothermal Continuous Stirred Tank Biological Reactors, *Chemical Engineering Science*. 37(3): 453-462 (1982).
- Lenbury, Y., Novaprateep, B., and Wiwatpataphee, B., Dynamic Behavior Classification of Model for a Continuous Bio-Reactor Subject to Product Inhibition, Mathl. Comput. Modelling, 19(12): 107-117 (1994).
- 5. J. Cheng-Fu, Existence and uniqueness of limit cycles in continuos cultures of microorganisms with non-constant yield factor, Universita degli studi di Bari, Italy (Preprint).
- 6. T.Yano and S. Koga, Dynamic Behavior of the Chemostat Subject to Product Inhibition, J. Gen. Appl. Microbiol. 19: 97-114 (1973).
- 7. F. Hoppensteadt, Asymptotic stability in singular perturbation problems II: Problems having matched asymptotic expansions, *J. Differential Equations*. 15:510-512 (1974).
- 8. P.S. Crooke, C.J. Wee and R.D. Tanner, Continuous fermentation model, *Chem. Eng. Commun.* 6: 333-347 (1980).
- 9. S. Muratori, An Application of the Separation Principle for Detecting Slow-Fast Limit Cycles in a Three-Dimensional System, *Appl. Math. and Comput.* 43: 1-18 (1991).
- 10. S. Muratori and S. Rinaldi, Remarks on Competitive Coexistence, SIAM J. APPL. MATH. 49 (5): 1462-1472 (1989).
- 11. S. Muratori and S. Rinaldi, Low- and High-frequency Oscillations in Three Dimensional Food Chain Systems, SIAM J. APPL. MATH. 52(6): 1688-1706 (1992).
- 12. S. Schecter, Persistence unstable equilibria and closed orbits of a singularly perturbed equation, *J. Differential Equations*. 60, : 131-141 (1985).
- 13. A.V. Osipove, G. Soderbacka and T. Eirold, On the Existence of Positive Periodic Solutions in Dynamical System of Two Predator-One Prey Type, *Viniti Deponent n.*4305-B86 [In Russian].

Modelling Effects of High Product and Substrate Inhibition on Oscillatory Behavior in Continuous Bioreactors

MODELLING EFFECTS OF HIGH PRODUCT AND SUBSTRATE INHIBITION ON OSCILLATORY BEHAVIOR IN CONTINUOUS BIOREACTORS

Yongwimon Lenbury*

Apichat Neamvong

Somkid Amornsamankul

Pannee Puttapiban

Department of Mathematics

Faculty of Science, Mahidol University

Rama 6 Rd., Bangkok 10400, Thailand

scylb@mahidol.ac.th

^{*} to whom all correspondences should be addressed.

MODELLING EFFECTS OF HIGH PRODUCT AND SUBSTRATE INHIBITION ON OSCILLATORY BEHAVIOR IN CONTINUOUS BIOREACTORS

ABSTRACT

In this study we consider a model for continuos bioreactors which incorporates the effects of high product and substrate inhibition on the kinetics and biomass and product yields. We theoretically investigate the possibility of various dynamic behavior in the bioreactor over different ranges of operating parameters to determine the delineating process conditions which may lead to oscillatory behavior. Application of the singular perturbation technique allows us to derive explicit conditions on the system parameters which specifically ascertain the existence of limit cycles composed of concatenation of catastrophic transitions occurring at different speeds. We discover further that the interactions between the limiting substrate and the growing microorganisms can give rise to high frequency oscillations which can arise during the transients toward the attractor or during the low-frequency cycle. Such study can not only more fully describe the kinetics in a fermentor but also assist in formulating optimum fermentor operating conditions and in developing control strategy for maintaining optimum productivity.

Key words: continuous bioreactors, product inhibition, substrate inhibition, singular perturbation, oscillation.

NOMENCLATURE

- X concentration of cells in bioreactor, g/ℓ
- S concentration of substrate in bioreactor, g/ℓ
- S_F concentration of substrate in the feeding solution, g/ ℓ
- P concentration of product in biorector, g/ℓ
- T time, h
- K_S , K_D positive constants, g/ℓ
- D dilution rate, h-1
- Y yield coefficient, g cell/g substrate
- μ specific growth rate, h-1
- μ_m maximum specific growth rate, h-1

INTRODUCTION

The growth of microorganisms is an unusually complicated phenomenon. Viewing the behavior of microbial cultures within the framework of lumped kinetic models, a multitude of models have been proposed and theoretically studied in diverse ways since the model due to Monod [9] fashioned after Michaelis-Menten kinetics for single enzyme-substrate reactions.

In ethanol fermentation, instantaneous biomass yield of the yeast Saccharomyces cerevisiae was found by Thatipamala et al. in [15] to decrease with the increase in ethanol concentration (P), indicating a definite relationship between biomass yield and product inhibition. It was also found in [15] that substrate inhibition occurs when substrate concentration (S) is above 150 g/ ℓ . Figure 1 shows experimental data taken from the work of Thatipamala et al. [15] indicating the effect of substrate inhibition on the specific growth rate at low ethanol concentrations. Figure 2, on the other hand, shows the effect of product inhibition on the specific growth rate, with data taken from the same source [15].

A number of simple kinetic expressions have been suggested in the literature for specific growth rate μ incorporating product and/or substrate inhibition [2-4,16]. Mainly, four types of inhibition correlations have been suggested based on experimental observations: linear, exponential, hyperbolic, and parabolic. In [16], Yano and Koga made a theoretical study on the behavior of a single-vessel continuous fermentation subject to a growth inhibition at high concentration of the rate limiting substrate S. They used the following expression for their continuous fermentation system:

$$\mu = \frac{\mu_{\rm m}}{(K_{\rm s}/S) + 1 + \sum_{j=1}^{n} (S/K_{j})^{j}}$$
(1)

where μ_m and the K's are positive constants and n is a positive integer. Other workers [1,8] have adopted simpler specific growth rate functions involving less control parameters but exhibiting similar necessary characteristics as the usual substrate inhibition model, for example the one hump substrate inhibition function

$$\mu = kSe^{-S/K_s} \tag{2}$$

where k and K_s are positive constants

Later, Yano and Koga discussed in [17] the nature of the chemostat in which the specific growth rate depends on the concentrations of both a substrate and an inhibitory product of a microorganism. They assumed the specific growth rate equation as follows;

$$\mu = \frac{\mu_{\rm m}S}{(K_{\rm s} + S)\left\{1 + \left(\frac{P}{K_{\rm p}}\right)^{\rm n}\right\}}$$
(3)

They showed, with the analog computer, that when the product formation was negatively growth-associated, in which the rate of product formation decreases with the increase in the cells concentration, diverging as well as damped oscillations appeared. No oscillations could be observed, on the other hand, when the product formation was either completely growth-associated, or partially growth-associated. Oscillation phenomena are, however, not unusual in continuous cultures [1]. Since such penchant for periodicity is undesirable from the point of view of process control, it is necessary to identify the safe operating regions in which complexed dynamic behavior may be avoided.

In [14], Ramkrishna et al. presented a chemostat model which assumed that viable cells (X) interact with a substrate (S) so as to produce the new viable cells and a cell-killing product (P). This product interacts with viable cells to form dead cells, in the process of which the cell-killing product may be released.

In [8], the dynamic behavior of a chemostat subject to product inhibition was analyzed and classified in terms of multiplicity and stability of steady states and limit cycles. The substrate was assumed to be in sufficient supply so that the model was reduced to a system of two nonlinear differential equations involving only the cells and product concentrations.

In this paper, we consider the full three-variable product inhibition model consisting of the following nonlinear differential equations:

$$\frac{\mathrm{dX}}{\mathrm{dt}} = \mu \mathbf{X} - \mathbf{DX} \tag{4}$$

$$\frac{dS}{dt} = D(S_F - S) - \frac{\mu}{Y}X$$
 (5)

$$\frac{dP}{dt} = \eta_0 \mu X + \eta_1 P - DP \tag{6}$$

where X(t) denotes the cells concentration at time t; S(t) the substrate concentration at time t; P(t) the product concentration at time t; S_F the concentration of the feed substrate, while D is the dilution rate at which the feed substrate is being fed into the reactor and the content of the bio-reactor is being removed, and η_0 is the constant for product formation. The term $\eta_1 P$ in equation (6) takes into account the release of the cell-killing product during the product's interaction with viable cells to form dead cells, following the suggestion of Ramkrishna *et al.* in their earlier mentioned paper [14]. Here, we assume that the production rate is directly proportional to the amount of the product present, with $\eta_1 < D$ being the positive constant of variation.

We also adopt the following expression for the specific growth rate function:

$$\mu = \frac{kSe^{-a\frac{S}{S_F}}}{1 + \frac{P}{K_P}} \tag{7}$$

where a and k are positive constants, to take into account the inhibitory effects of both the substrate and the product increase in the chemostat.

Further, the cells to substrate yield Y defined as

$$Y \equiv \frac{\text{amount of cells produced}}{\text{amount of substrate consumed}}$$

is assumed to vary linearly with the substrate level at any time t, allowing for the positively-growth associated situation; namely

$$Y = A + BS \tag{8}$$

Such substrate dependent yield has been used previously by several other workers in this field [1, 8].

The analysis of the model is done through a singular perturbation argument, assuming that the substrate concentration exhibits fast dynamics. The time responses of the different components in the system are assumed to decrease dynamically from top to bottom. The structure of the corresponding attractors and the nature of the transients are then analyzed. It is shown that the model system can exhibit low-frequency cycles in which periodic bursts of high-frequency oscillations may develop giving rise to more complexed dynamical behavior for specified ranges of the system parameters.

SYSTEM MODEL

In order to analyze the model system of equations (4), (5) and (6), together with (7) and (8) through the singular perturbation technique, we assume that the substrate has fast dynamics, while the cells and product have intermediate and slow dynamics respectively, and scale the time responses of the three hierarchical components of the system by means of two small dimensionless positive parameters ϵ and δ ; namely, we let $x=\frac{S}{S_F},\;y=X,\;z=\frac{P}{\epsilon K_P},\;d_1=D,$ $d_2=\frac{D}{\epsilon}$, $d_3=\frac{D-\eta_1}{\epsilon\delta},\;\omega=\frac{kS_F}{\epsilon K_P},\;\eta=\frac{\eta_0\omega}{\epsilon\delta},\;\gamma=\frac{k}{AS_F},$ and $\beta=\frac{A}{BS_F}.$ We are

led to the following system of differential equations:

$$\frac{\mathrm{d}x}{\mathrm{d}t} = \mathrm{d}_1(1-x) - \frac{\gamma x \mathrm{e}^{-ax} y}{(x+\beta)(1+\varepsilon z)} \equiv f(x,y,z) \tag{9}$$

$$\frac{\mathrm{d}y}{\mathrm{d}t} = \varepsilon y \left[\frac{\omega x \mathrm{e}^{-ax}}{1 + \varepsilon z} - \mathrm{d}_2 \right] = \varepsilon \mathrm{g}(x, y, z) \tag{10}$$

$$\frac{\mathrm{d}z}{\mathrm{d}t} = \varepsilon \delta \left[\frac{\eta x \mathrm{e}^{-\mathrm{a}x}}{1 + \varepsilon z} y - \mathrm{d}_3 z \right] = \varepsilon \delta \mathrm{h}(x, y, z) \tag{11}$$

Thus, with ε and δ small, the equation of the substrate concentration represents the fast system, while that of the cells and product concentrations represent the intermediate and the slow systems, respectively. Under suitable regularity assumptions, the singular perturbation method allows us to approximate the solution of the system (9)-(11) with a sequence of simple dynamic transitions along the various equilibrium manifolds of the system and occurring at different speeds. The resulting path, composed of all such transients, approximates the solution of the system in the sense that the real trajectory is contained in a tube around these transients, and that the radius of the tube goes to zero with ε and δ . The formal proof of this is not given because it is long and trivial and has already been discussed and extensively used in the literature [7,10-12].

Two-dimensional dynamics

By means of singular perturbation analysis, the solution of the system of equations (9)-(11) can be approximately found for small values of ε and δ . First, the slow (z) and intermediate (y) variables are frozen at their initial values z(0) and y(0), and the evolution of the fast component of the system is determined by solving the 'fast system' consisting of equation (9) with z set equal to z(0). If, for simplicity of the following analysis, we assume that the starting value of z is comparatively small, since δ is small, the value of z remains small during the initial phase. The evolution of the system components can then be approximately determined by first setting $\delta = 0$ and z = 0 in the equations (9)-(11). Thus, we are led to the following system:

$$\frac{dx}{dt} = d_1(1-x) - \frac{\gamma x e^{-ax}y}{(x+\beta)}$$
(12)

$$\frac{dy}{dt} = \varepsilon y \left[\omega x e^{-ax} - d_2 \right]$$
 (13)

which is a fast-slow second-order system for which the dynamical behavior can be analyzed and existence of limit cycles detected through the singular perturbation principle. The results are summarized in Figure 3, where two cases of interest can be identified. The conditions on the parameters identifying the two cases are as follows.

Case 1

The system (12) has an equilibrium manifold where $\dot{x} = 0$ given by

$$y = (1 - x)(x + \beta) \frac{e^{ax}}{x} \equiv \varphi(x)$$
 (14)

which intersects the x-axis at the point x = 1 as shown in Figure 3. The slope of the curve in (14) is given by

$$\frac{dy}{dx} = \frac{e^{ax}}{x^2} F(x) = \frac{e^{ax}}{x^2} \left[-x^3 + (a - a\beta - 1)x^2 + a\beta x - \beta \right]$$
 (15)

Letting $x = \frac{1}{3}$ in (15) leads to the following inequality

$$\beta < \frac{3a-4}{27-6a} \tag{16}$$

which ensures that the curve $y = \varphi(x)$ has positive slope on some interval containing the point $x = \frac{1}{3}$.

The equilibrium manifold of the intermediate system (13) consists of 2 parts, the trivial manifold y = 0 and the nontrivial manifold given by the equation

$$xe^{-ax} = \frac{d_2}{\omega} \tag{17}$$

In Case 1, the curve (17) intersects the graph of (14) at the point R in the Figure 3 where $x = \overline{x}$ for which

$$F(\bar{x}) > 0 \tag{18}$$

which means that the point R is located on the unstable branch of the manifold f = 0. This is easily accomplished by letting

$$\overline{x} = \frac{1}{3} - \theta \tag{19}$$

for a sufficiently small θ , then simply set

$$\frac{d_2}{\omega} = \bar{x}e^{-\bar{x}} = (\frac{1}{3} - \theta)e^{-(1/3 - \theta)}$$
 (20)

Thus, Case 1 is identified by the inequality (18) with (19) and (20).

Case 2

This case is then identified by the opposite inequality to (18), namely

$$F(\bar{x}) < 0 \tag{21}$$

However, since the nontrivial intermediate manifold is given by (17),

$$\bar{x} > \frac{d_2}{\omega}$$
 (22)

We see that (21) will be satisfied if $\frac{d_2}{\omega}$ is sufficiently large as well as satisfying

$$\frac{d_2}{\omega} < 1 \tag{23}$$

to allow for \bar{x} to be located to the left of the point x = 1 where the fast manifold crosses the x-axis.

Thus, in Figure 3 where transitions of low, intermediate, and high speeds are indicated by one, two, and three arrows, respectively, if we start from the point marked by the number 1 above the curve $\dot{x}=0$, then $\dot{x}<0$ here and a fast transition develops toward the point 2 on the stable manifold (section AB), while y still remains frozen at the initial value y(0). (If we start from the point 1 below the curve $\dot{x}=0$, then $\dot{x}>0$ here and so a fast transition will develop toward point 3 on section CD of the manifold). Since the manifold is stable here, a transition of intermediate speed is made along the curve as the intermediate system becomes active. From point 2, the transition develops along the direction of decreasing y since $\dot{y}<0$ on the left of the curve g=0. Once the point B is reached, the manifold loses its stability and a fast transition is made towards the point D on the stable section CD of the manifold. Transition of intermediate speed upwards along this curve ends if either a stable equilibrium R is reached in Case 2, or a quick jump brings the trajectory back to the section AB completing a closed cycle ABDC in Case 1.

Three-dimensional dynamics

As z increases, the slow system (11) becomes active. We now show that, for suitable values of the parameters and for ε and δ sufficiently small, the system (9)-(11) has a unique attractor that is either a stable equilibrium or a low-

frequency limit cycle which may exhibit high-frequency oscillations during a finite interval of time.

To do this, we observe that the manifold

$$f(x,y,z) = 0 (24)$$

intersects the nontrivial intermediate manifold along the curve

$$f = g = 0 \tag{25}$$

given by the equation

$$\frac{xe^{-ax}}{1+\epsilon z} = \frac{d_2}{\omega} \tag{26}$$

which defines a surface $z = \psi(x)$. We observe that at $x = \frac{1}{a}$

$$\frac{dz}{dx} = 0$$

Thus, to ensure that the point $P(x_P, y_P, z_P)$ in Fig. 4 is located on the stable part of the manifold f = 0 at the point where $x_P = \frac{1}{a} < 1$, we require

$$F\left(\frac{1}{a}\right) < 0 \tag{27}$$

or equivalently,

$$\beta > 1 - \frac{1}{a} - \frac{1}{a^2} \tag{28}$$

and

$$a > 1 \tag{29}$$

Combining the inequalities (16) and (28), we arrive at the requirement that

$$\frac{3a-4}{27-6a} > \beta > 1 - \frac{1}{a} - \frac{1}{a^2} \tag{30}$$

Now, the curve (25) is given by the equation

$$y = \frac{d_2}{\omega}(1-x)(x+\beta)$$

which reaches a maximum at the point $M(x_M, y_M, z_M)$ where

$$x_{M} = \frac{1-\beta}{2}$$

Finally, the curve f = g = 0 intersects the (x,z)-plane at the point $O(x_0,y_0,z_0)$ where $x_0 = 1$ and, from (26),

$$z_{o} = \frac{1}{\varepsilon} \left(\frac{\omega}{d_{2}e^{a}} - 1 \right) \tag{31}$$

We therefore require that

$$e^{a} < \frac{\omega}{d_2} \tag{32}$$

to ensure that $z_0 > 0$.

We now analyze each of the two cases separately.

Case 1

We observe that in this case the point R is located on the unstable part of the manifold f = 0 and the curve f = g = 0 remains on the unstable part, as shown in Figure 4, until the point M is reached. The curve then stretches along the stable part of the manifold f = 0 until either the point S is reached in the cases 1(a) and 1(b), or the point P is reached first in the cases 1(c) and 1(d). Thus, four subcases can be identified as follows.

<u>Casel(a)</u> This case is identified by the inequality

$$a < 1 \tag{33}$$

so that the turning point P is below the (x,z)-plane. Thus, starting from an initial point A in Figure 4, a fast transient takes us to the point B on the stable part of the fast manifold f = 0. Transition of intermediate speed is then made along this manifold in the direction of increasing y until the point C is reached where stability is lost. A fast jump is made to the point D on the other stable branch of the manifold f = 0 from which point a transition of intermediate speed develops until stability is lost again at the point G. A quick jump back to H almost closes up the cycle. However, z has been slowly increasing in the meantime so that the same cycling transitions are repeated in the direction of increasing z, densely covering the surface f = 0, until the point M is reached. The transient now follows the curve f = g = 0 until the point S is reached in the case f = 0. In this case, the point S where f = 0 is on the stable part of the manifold f = 0 and thus the transitions end at this stable equilibrium point.

Case 1(b) This is the case identified by the inequality

$$a > 1 \tag{34}$$

so that the point P is located on f = 0 above the (x,z)-plane as shown in Figure 4 (b). This case is also identified by the fact that the point S, where f = g = h, is located on the stable part of the curve f = g = 0. This situation is guaranteed by requiring that

$$z_{P} > z_{N} \tag{35}$$

where $N(x_N, y_N, z_N)$ is the point on the curve f = h = 0 with $x_N = \frac{1}{a}$. From equating f and h to zero, we find that

$$z_{N} = \frac{\eta d_{1}}{\gamma d_{3}} \left(1 - \frac{1}{a} \right) \left(\frac{1}{a} + \beta \right) \tag{36}$$

while, from equation (26), we have

$$z_{P} = \frac{1}{\varepsilon} \left(\frac{\omega}{\text{aed}_{2}} - 1 \right) \tag{37}$$

Therefore, so that S is located on the stable part of f = g = 0, we require

$$\frac{\omega}{d_2} > ae \left[\frac{\varepsilon \eta d_1}{\gamma d_3} \left(1 - \frac{1}{a} \right) \left(\frac{1}{a} + \beta \right) + 1 \right]$$
 (38)

which guarantees that (35) holds.

In this case 1(b) then, the transition also reaches the point S first and ends there since it is a stable equilibrium point where $\dot{x} = \dot{y} = \dot{z} = 0$. Moreover, along The curve f = h = 0 we have

$$z = \frac{\eta d_1}{\gamma d_3}$$

when x = 0. Therefore we must also require that

$$\frac{\eta d_1 \beta}{\gamma d_3} > \frac{1}{ae} \tag{39}$$

to ensure that the curve f = h = 0 intersects the curve f = g = 0 only once.

Case 1(c) This case is identified by inequality (34) and the opposite inequality to (38), that is

$$\frac{\omega}{d_2} < ae \left[\frac{\varepsilon \eta d_1}{\gamma d_3} \left(1 - \frac{1}{a} \right) \left(\frac{1}{a} + \beta \right) + 1 \right] \tag{40}$$

which guarantees that the point P is reached first during the transition from the point M in Figure 4(c). At the point P, there is a loss of stability and a quick jump to E takes place. A slow transition develops now along this manifold where x = 1 until a point is reached where stability in again lost at some point F. A transition of intermediate speed will develop along the fast manifold f = 0 back to the point L which completes the limit cycle in the case 1(c).

Case 1(d) In order that the transition goes back into high-frequency oscillations in each low-frequency cycle, we need to require that $z_0 < z_M$, which is equivalent to

$$e^{-a} < \frac{1-\beta}{2}e^{-a(1-\beta)/2}$$
 (41)

Thus, starting from the point A in Figure 4(d), a fast transition takes us, as explained earlier, to the point B on f = 0. An intermediate transition develops on this manifold until C is reached where the stability of the equilibrium fast manifold is lost. A fast transition then takes the system to the stable equilibrium point D. An intermediate speed transition is then made along this branch of manifold until G is reached where the stability is again lost and a quick jump brings us to the stable point H. This almost closes up the cycle but just misses the point B. The slow system has becomes active and z has been slowly increasing since $\dot{z} > 0$ here. Transitions then develop following the same pattern but with slowly varying z as seen in Figure 4(d) until M is reached, at which point the trajectory develops into a slow cycle which goes back into the fast cycles since inequality (41) guarantees that $z_0 < z_M$.

Case 2

We observe that in this case the point R is located on the stable part of the fast manifold f = 0 as shown in Figure 5. Mainly 3 subcases can therefore be identified here.

Case 2(a) If (21) as well as (33) hold then starting from the point A in Figure 5(a), a fast transition develops to the point B, followed by a transient of intermediate speed to C, from which point a slow transient takes us to the stable equilibrium point S where the transition ends.

Case 2(b) If (21) holds as well as (38) then, similarly to Case 2(a), transients develop toward the stable equilibrium point S where $\dot{x} = \dot{y} = \dot{z} = 0$ and the transition ends.

Case 2(c) Finally, if (21) holds as well as (40) then, from the point C in Figure 5(c), the point P is reached first where the stability is lost. A quick jump to E, followed by a transition at slow speed from E to F, then at intermediate speed back to D, closes the trajectory up into a low-frequency limit cycle for this case 2(c).

The above analysis can be summarized by the following theorem.

Theorem If ε and δ are sufficiently small, and if (16), (30), (32), and (39) hold, then system (9)-(11) has a global attractor which is a stable equilibrium if (18) and (33) hold, or (18), (34) and (38) hold, or if (21) and (33) or (38) hold. It is a low-frequency limit cycle if (21) and (40) hold, or if (18), (34) and (40) hold. Moreover, if (18), (34) and (40) as well as (41) hold, then the attractor is a low-frequency limit cycle which contains a period of high frequency oscillations.

NUMERICAL RESULTS AND DISCUSSION

Figure 6(a) shows a numerical simulation of the model equations (9)-(11) with parametric values chosen to satisfy inequalities (18), (30), (32), (34), (39) and (40). This is therefore the case 1(c) and the solution trajectory develops into a low-frequency limit cycle as predicted. The corresponding time courses of the three variables are shown in Figure 7(a).

Figure 6(b) shows a numerical simulations of the model equations (9)-(11) with parametric values chosen to satisfy inequalities (18), (30), (32), (34), (39), (40) as well as (41). This is therefore Case 1(d). The solution trajectory develops into a low-frequency limit cycle which contains high frequency oscillations as predicted in the above theorem. The corresponding time courses of the three variables are shown in Figure 7(b). Such underlying high frequency cycles in the biomass concentration profile have frequently been observed by a number of investigators [16-18]. In [16], the total budding cells count in their bioreactor data shows oscillatory behavior closely resembling our result of case 1(d) shown in Figure 7(b). Experimenting with different values for the system parameters such as β ,d₃, a, and so on, shows that the frequencies and amplitude of oscillations can be appropriately adjusted to fit different chemostat conditions.

We observe that the constant a plays an important role in the kinetics of the chemostat under study. Considering the model in equation (7), a is in fact an indicator of how late or how soon the substrate inhibition sets in. In Figure 1, substrate inhibition seems to set in approximately half way to the maximum substrate level, suggesting that a should by around 2. Thus, the numerical results presented in Figures 6(a) and 6(b) can be considered as corresponding to the case where substrate inhibition is late in setting in (a < 2). In Figure 6(c), we present a numerical simulation of equations (9)-(11) in which a = 2.5, thus corresponding to the situation where the inhibition sets in rather early (a > 2). With this value of a, inequality (32) is violated and $z_0 < 0$. Therefore, the transition develops from the

point E (in Figure 4(c) or 5(c)) all the way to the point (1, 0, 0) on the x-axis which is a stable washout steady state of the system. Figure 7(c) shows the corresponding time courses of the state variables in this case, where both the cells and product levels are seen to decrease toward zero, while the substrate level tends toward the maximum level $(S = S_F)$.

Also, it is numerically found that solution trajectories can still develop as theoretically predicted even though the values of ε and δ are not so small, and the assumption that the three components of the system carry highly diversified dynamics can be relaxed to a certain extent.

CONCLUSION

The appearance of sustained oscillations in bioreactor variables in continuous cultures indicates the complex nature of microbial systems, and the difficulties which may arise in bioprocess control and optimization.

In this paper, the dynamic behavior of a continuous bioreactor described by equations (9)-(11) has been investigated, incorporating the inhibitory effect at high levels of product and substrate concentrations. Assuming that the time responses of the three components are highly diversified, increasing from bottom to top, we were able to use standard singular perturbation analysis to describe the nature of the transients and the attractors of the system.

Complexed oscillatory behavior is extremely undesirable not only for control and design problems, but also for its potential for dangerous situations which may result in the case where toxic compounds are involved, such as in the operation of toxic waste treatment processes. Insights that can be gained from this type of analysis described above should prove most valuable in the light of such considerations.

ACKNOWLEDGMENT

Appreciation is rendered to the topland Research Fund for the financial support which made possible this research project.

FIGURE CAPTIONS

- FIGURE 1. Effect of substrate inhibition on specific growth rate at low ethanol concentration. (Data points taken from reference [15]).
- FIGURE 2. Effect of product inhibition on specific growth rate. (Data points taken from reference [15]).
- FIGURE 3. Two possible cases of trajectory development for the two dimensional fast-slow system (12), (13). Trajectories go toward a limit cycle ABDC in Case 1, and toward a stable equilibrium point R in Case 2.
- FIGURE 4. Trajectories of the model system (9)-(11) in Case 1 exhibiting four possible subcases 1(a), 1(b), and 1(c) identified in the text.
- FIGURE 5. Trajectories of the model system (9)-(11) in Case 2 exhibiting three possible subcases 2(a), 2(b), and 2(c) identified in the text.
- FIGURE 6. Numerical simulation of the model equations (9)-(11). Here, $\epsilon=0.1$, $\delta=0.01$, $\gamma=2.0$, $\eta=10.0$, $\omega=3.0$, $d_1=0.25$, $d_2=0.25$, and $d_3=0.1$. In 6(a), the parametric values satisfy the inequalities of Case 1(c), with $\beta=0.8$, a=1.5, and the solution trajectory tends toward a low-frequency limit cycle as theoretically predicted. In 6(b), the parametric values satisfy the inequalities of Case 1(d), with $\beta=0.2$, a=1.5, and the solution trajectory tends toward a low-frequency limit cycle which contains a period of high-frequency oscillations. In 6(c), $\beta=0.2$, and a=2.5 which corresponds to the situation where substrate inhibition is early in setting in.
- FIGURE 7. The time courses of the state variables x(t), y(t) and z(t) are shown here corresponding to the three respective cases seen in Figure 6.

 represents x(t) + 2.2 in 7(a), x(t) + 0.4 in 7(b), and x(t) in 7(c).

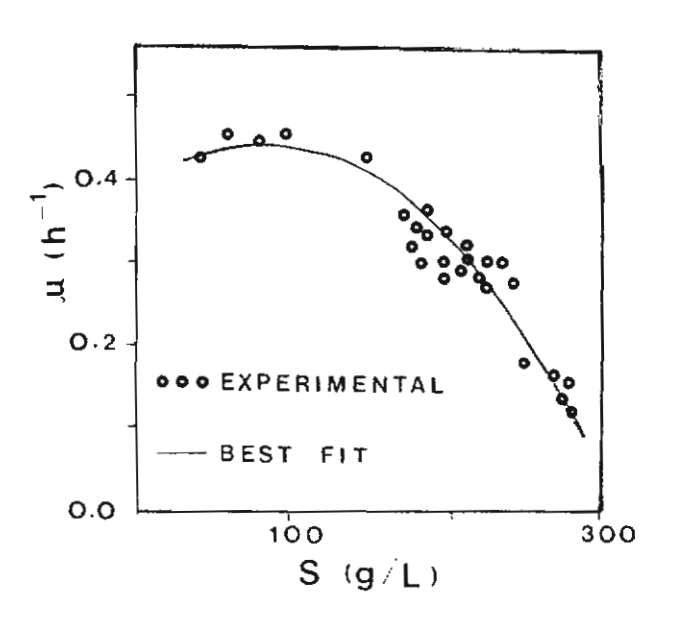
 o—o represents y(t).

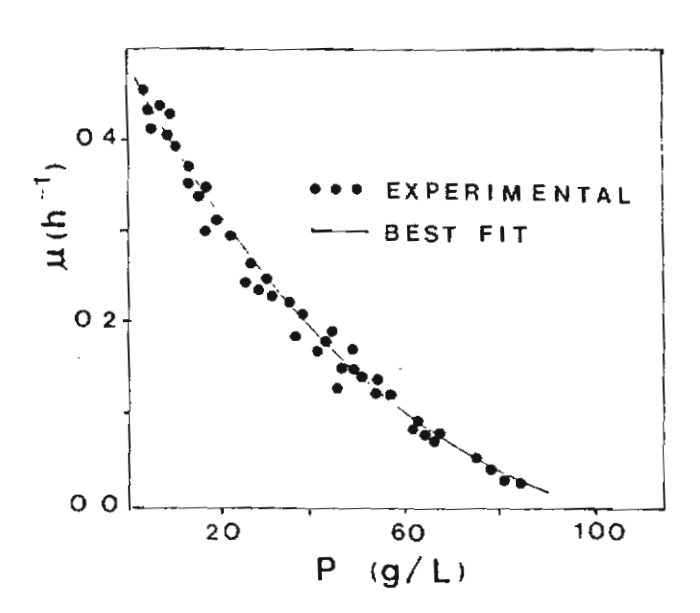
 ×—× represents z(t) + 0.3 in 7(a), and z(t) in 7(b) and 7(c).

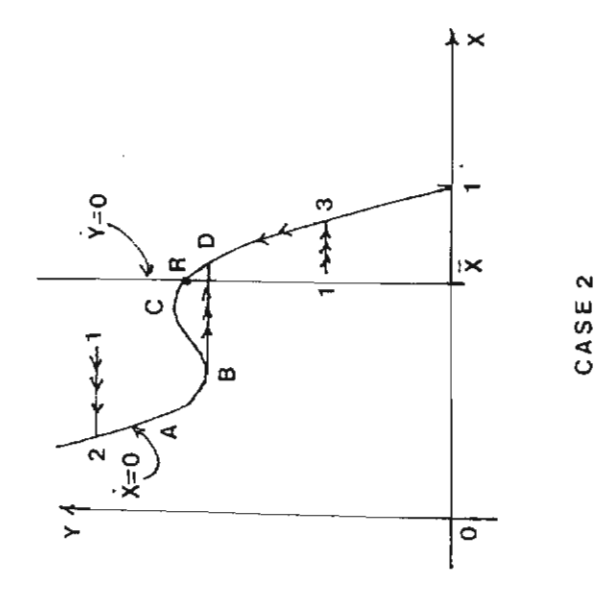
REFERENCES

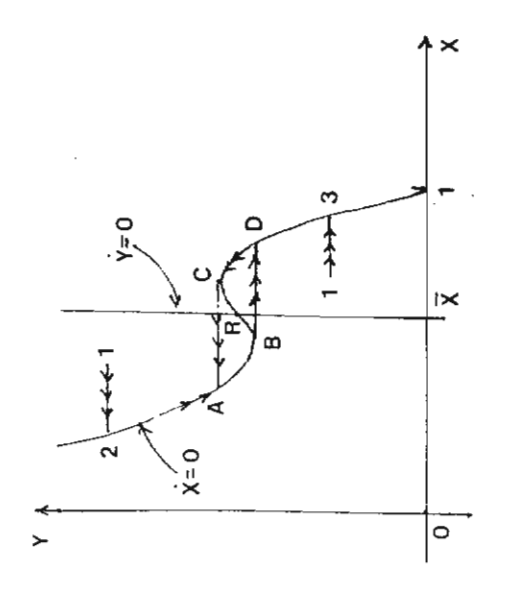
- 1. Agrawal, P., Lee, C., and Lim, H.C.: and Ramkrishna, D., Theoretical Investigations of Dynamic Behavior of Isothermal Continuous Stirred Tank Biological Reactors. *Chemical Engineering Science*. 37 (1982)3, pp. 453-462.
- 2. Aiba, S., and Shoda, M.: Reassesment of the product inhibition of alcohol fermentation. J. Ferment. Technol. 47 (1969) pp. 790-799.
- 3. Andrews, J. F.: A mathematical model for the continuous culture of microorgnisms utilizing inhibitory substrates. *Biotechnology and Bioengineering*. 10 (1968) pp. 707-723.
- 4. Bazua, C. D., and Wilke, C. R.: Ethanol effects on the kinetics of a continuous fermentation with Saccharomyces cerevisiae. Biotechnology and Bioengineering Symp. 7 (1977) pp. 105-118.
- Ching-I Chen, and McDonald, K. A.: Oscillatory Behavior of Saccharomyces cerevisiae in Continuous Culture: I Effects of pH and Nitrogen Levels. Biotechnology and Bioengineering. 36 (1990) pp. 19-27.
- Ching-I Chen, and McDonald, K. A.: Oscillatory Behavior of Saccharomyces cerevisiae in Continuous Culture: II Analysis of Cell Synchronization and Metabolism. Biotechnology and Bioengineering. 36 (1990) pp. 28-38.
- 7. Hoppensteadt, F.: Asymptotic stability in singular perturbation problems II: Problems having matched asymptotic expansions. J. Differential Equations. 15 (1974) pp. 510-512.
- 8. Lenbury, Y., Novaprateep, B. and Wiwatpataphee, B.: Dynamic Behavior Classification of a Model for a Continuous Bio-Reactor Subject to Product Inhibition. *Mathl. Comput. Modelling.* 19 (1994) 12, pp. 107-117.
- 9. Monod, J.: recherces pur la croessance des cultures bacteriennes, Hermann et Cie, Paris, 1942.

- Muratori, S.: An Application of the Separation Principle for Detecting Slow-Fast Limit Cycles in a Three-Dimensional System. Applied Mathematics and Computation. 43 (1991) pp. 1-18.
- 11. Muratori, S. and Rinaldi, S.: Remarks on Competitive Coexistence, SIAM J. APPL. MATH. 49 (1989) 5, pp. 1462-1472.
- Muratori, S. and Rinaldi, S.: Low- and High-frequency Oscillations in Three Dimensional Food Chain Systems. SIAM J. APPL. MATH. 52 (1992) 6, pp. 1688-1706.
- Olsvik, E. S., and Kristiansen, B.: Influence of Oxygen Tension, Biomass Concentration, and Specific Growth Rate on the Rheological Properties of a Filamentous Fermentation Broth. *Biotechnology and Bioengineering*. 40 (1992) pp. 1293-1299.
- Ramkrishna, D., Fredrickson, A.G., and Tsuchiya, H.M.: Dynamics of Microbial Propagation: Models Considering Inhibitors and Variable Cell Composition, Biotech. Bioeng. 9 (1967) p. 129-170.
- Thatipamala, R., Rohani, S., and Hill, G. A., Effects of High Product and Substrate Inhibitions on the Kinetics and Biomass and Product Yields During Ethanol Batch Fermentation, *Biotechnology and Bioengineering*. 40 (1992) pp. 289-297.
- Yano, T., and Koga, S.: Dynamic Behavior of the Chemostat Subject to Substrate Inhibition. Biotechnology and Bioengineering. 11 (1969) pp. 139-153.
- 17. Yano, T. and Koga, S.: Dynamic Behavior of the Chemostat Subject to Product Inhibition. J. Gen. Appl. Microbiol. 19 (1973) pp. 97-114.









CASE 1